Synthesis-Structure-Property Relations of TiAlN Based Hard Coatings

by

Martin Pfeiler

Leoben, December 2008

being a thesis in partial fulfillment of the requirements for the degree of a

Doctor of Montanistic Sciences (Dr.mont.)

This thesis was supported by the Austrian Federal Government and the Styrian Provincial Government under the frame of the Austrian COMET Competence Center program and was conducted at the Department of Physical Metallurgy and Materials Testing at the Montanuniversität Leoben, Austria in cooperation with the Materials Center Leoben Forschung G.m.b.H. in Leoben, Austria, CERATIZIT Austria G.m.b.H. in Reutte, Austria and CERATIZIT Luxembourg S.á.r.l. in Mamer, Luxembourg.

Affidavit

I declare in lieu of oath that I did the PhD thesis by myself using only literature cited in this volume.

Leoben, December 2008

Acknowledgements

My sincerest gratitude and appreciation is due to my supervisor Christian Mitterer, Head of the Thin Film Group for having trust in me, for his help, patience and endless kindness and most of all for being a wonderful teacher and a friend in innumerable aspects during the last 5 years. Danke Christian, für alles was ich von dir lernen durfte.

Special thanks to the people who decided to support me and the project experimentally. Your work is an important part of this thesis. In particular I would like to thank my diploma students Jürgen Wagner, Johannes Zechner and Jörg Radanitsch as well as my student co-workers Thomas Weirather, Markus Pohler and Richard Rachbauer for their great support and the fun we had during and besides work.

I also want to express my gratitude to Kerstin Kutschej for supporting me whenever and wherever she could and her endless patience and kindness.

I would also like to thank Helmut Clemens, Head of the Department of Physical Metallurgy and Materials Testing (DMW), for giving me the opportunity to carry out this work at his institute. I am also very grateful to my employer, the Materials Center Leoben (MCL) especially to Reinhold Ebner, Managing Director of the MCL for giving me the opportunity to carry out my PhD within an MCL-project. Special thanks to Hilde Stopar at the DMW and Ulrike Egger, Simone Fink and Elisabeth Wolkenstein at the MCL for the perfect cooperation.

Furthermore, I would like to thank Martin Kathrein from CERATIZIT Austria as well as Claude Michotte and Marianne Penoy from CERATIZIT Luxembourg for their perfect support, their interest in my and the projects progress and the valuable advices and discussions. It was a pleasure to work with you.

Ten out of ten points for my colleagues at the Department and in the Thin Film Group who made my life here so enjoyable and work so much fun. Special thanks to my office mates Josef Wagner, Kerstin Kutschej and David Hochauer for countless chats about literally every aspect of life, to Nazanin Fateh, Claudia Walter, Marisa Figueiredo, Robert Franz, Rostislav Daniel for answering thousands of stupid questions about their home countries and listening to my endless explanations about Austrians and to Martin Moser, Florian Rovere, Svea Mayer, Gerardo Fontalvo, Paul Mayrhofer, Christian Mitterer, Michael Schober, Rainer Hochfellner and Herbert Willmann for countless great moments. Special thanks to Jörg Paulitsch who taught me that the almost complete absence of shared interests can still build an excellent friendship.

Danksagung

Ein besonderer Dank gilt meinen Freunden abseits der Uni, meiner Familie und meiner Lebensgefährtin Irene für die bedingungslose Unterstützung und weil sie alle immer dafür sorgen, dass ich den Boden unter den Füßen nicht verliere.

The most exciting phrase to hear in science, the one that heralds new discoveries, is not "Eureka!" (I found it!) but "That's funny ..."
(Isaac Asimov)

I hate quotations.
(Ralph Waldo Emerson)

Contents

Introduction

The relevance of materials science and engineering can be seen by the fact, that many epochs of mankind are termed after the predominant class of material in use. For instance the term "stone age" reveals that the tools of these ancient humans mainly consisted of rock, broken into useful shape. As a daily look at the news reveals, mankind itself has not really developed any further since that times, however the materials in use certainly have. Moreover, technological progress and the realisation of new ideas often depend on the availability of the proper material suitable to fulfil the demands required. The surface of a material is of special importance since any interaction between two bodies occurs via their surfaces. The importance of surface science and engineering has its origins also in the fact, that nowadays technical applications often exhibit demands a single bulk material cannot fulfil. This has led to the development of composite materials, which are a combination of at least two materials with the aim of combining the benefits of both materials while avoiding their respective disadvantages. One possibility is the deposition of films and coatings on so-called substrate materials. There, the technical requirements are split between the surface and the substrate. The applications in that field range from selective transmission films for architectural glass to diffusion barriers for integrated circuits and wear resistant hard coatings for cutting tools, to name just some of the possibilities. Thin films for cutting tools are very successful examples for such composites, because the use of hard coatings has expanded the life time of the tools and the efficiency of the machining process by orders of magnitude. The substrate material is mostly high speed steel or cemented carbide and provides the shape, strength, toughness and transport of heat, while the surface provides hardness, resistance against high temperature, wear and corrosion and sometimes even the proper colour.

Most of these hard coatings are produced via condensation from the vapour phase. Chemical vapour deposition (CVD) gains the vapour by gaseous precursors and is conducted typically at high temperatures, where these precursors react and form the chemical compound of the coating. The high temperatures limit the possible substrate materials mainly to cemented carbide. CVD processes are suitable to coat parts with complex geometries and can reach coating thicknesses of up to 20 μm. Furthermore, the deposition

of oxide coatings is still a domain of CVD. Physical vapour deposition (PVD) processes generate the vapour from a solid source by physical methods and are conducted at lower temperatures, which enables also the use of steels as substrate materials. The high possible ionisation of the film-forming species and the low temperatures enable the deposition of metastable coatings far from the thermodynamic equilibrium, which is one of the main reasons for the broad variety of the producible coatings and the high flexibility of this method.

The first hard coatings where developed, some 30 years ago and are based on binary carbides and nitrides of transition metals, namely TiC, TiN and CrN. Although, these coatings are still applied successfully in certain fields, the demand of industry to higher cutting speed and higher feed rates in combination of longer service times of the tools is beyond the possibilities of these coating systems because of their low resistance to oxidation. This has lead to the development of TiAlN and CrAlN coatings which exhibit higher oxidation resistance.

However, the developments in machining technology have led to an enormous variety of different requirements for cutting tools. This makes it impossible to provide one single solution or the "ultimate hard coating" for all purposes. The current trend in thin film technology is the development of hard coatings with exactly tailored properties for the respective application. Therefore, a basic understanding on the relation between the deposition process, the structure and morphology of the coating and the resulting mechanical, tribological, physical and chemical properties is needed. This is far from being a simple task since process parameters like gas flow, electrical current and voltage, alloying elements and alternating layer architectures can have a dramatic influence on the nucleation and growth conditions and thus on the coatings´ structure, properties and the cutting performance. In addition, findings and relations developed on lab-scale facilities are not necessarily directly applicable on industrial production plants, which adds the issue of upscaling to industrial conditions to the challenges mentioned before. In total, all these effects make it scientificly and technically demanding to elucidate principle relations in hard coating deposition, or, according to Mr. Fred Sinowatz: "Das ist alles sehr kompliziert" ("everything is very complicated", Fred Sinowatz, 1929-2008, former Austrian chancellor from 1983-1986).

The focus of this work is the correlation between synthesis, the resulting structure and the properties of TiAlN-based hard coatings. Various coatings were deposited by cathodic arc evaporation on an industrial production plant. Based on TiAlN reference materials with Al/Ti ratios of 1.5 and 2, four different alloying elements were added. Vanadium, to generate self-lubrication effects based on the formation of lubricious V-oxides, the so-called Magnéli-phases. Tantalum should work as solid solution hardener and improve the

hot hardness of the coating. Si and B are added in small doses in order to fill voids and vacancies left after segregation of V to the surface and improve mechanical properties. Although all alloying elements were proven to be highly beneficial, it will be shown that the origin of their potential for improvements is sometimes unexpected. Furthermore, the process parameter bias voltage was intensively studied and optimized between voltages from -40 to -160V. Based on these results, the most promising candidates were deposited in multilayered structures and evaluated in cutting tests. In total, this thesis represents the concentrate of 71 different coating systems deposited onto more than 2500 samples and cutting inserts.

The first part of this thesis gives a comprehensive overview on the theoretical background of the most important issues concerning the topic. Subsequent to a short summary of the most important results, the scientific output of the findings is presented in six publications, where the investigated phenomena and relations are comprehensively discussed.

Part I.

Theoretical background

1. Synthesis

The general principles of physical vapour deposition (PVD) processes are simple. In a reduced pressure environment, a vapour of the so-called target, acting as the material source for the coating is produced by physical mechanisms (evaporation or collisional impact). This is followed by transportation of the vapour to the substrate, where it condenses and forms a solid film. This simple setup enables one of the major benefits of PVD processes, which is the high flexibility. The application of reactive gases in the working chamber fosters reactions between the vapour and the reactive gas and enables the deposition of compounds like nitrides, carbides and oxides. Also the methods how the vapour is generated, transported to the substrate and the conditions of condensation can be varied and modified in a broad range, giving rise to the possibility of tailoring the coatings to the respective application and desired properties. This has led to an extremely wide field of process modifications in the field of PVD [1]. Within this thesis, the cathodic arc evaporation (CAE) technique has been used to deposit the investigated materials. Thus, the most important issues of this technique will be discussed.

1.1. Cathodic arc evaporation

The CAE technique uses a vacuum arc to generate the vapour to be deposited. A vacuum arc is a high current - low voltage electrical discharge between two electrodes. The term "vacuum arc" is misleading since a vacuum obviously cannot provide the conducting species. According to Lafferty a vacuum arc burns in an enclosed volume, that prior to ignition (e.g. by a mechanical igniter) is a high vacuum [2]. The point of contact between the arc and the cathodic target is called arc spot. There is a certain degree of controversy in literature about the processes within this arc spot, mainly because the extreme conditions present in the spot makes it a challenge to study these processes. However there is general agreement that the arc spot is small (10^{-8}-10^{-6} m in diameter), thus the current density is very high (10^{6}-10^{12} A/m^2) and that the arc moves rapidly over the surface of the cathode (100 m/s), which means that the lifetime of a single arc spot is very short. Fig. 1.1 shows the principal setup of an arc source and the arc spot [3].

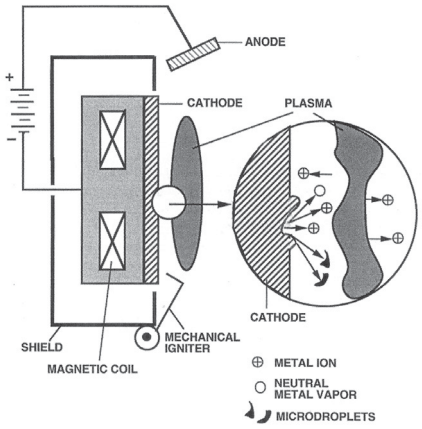

Figure 1.1.: Schematic of cathodic arc source and the arc spot [1].

The life cycle of an arc spot is displayed in Fig. 1.2. The high current density, concentrated on a random roughness tip causes rapid heating of the tip (Fig. 1.2a) and its vicinity which leads to an explosion like evaporation and melting of the surrounding material. The high pressure in the arc spot leads to the ejection of the plasma towards the recipient, the so-called plasma jet. In addition, the molten material is pushed out of the arc spot which leads to the generation of liquid droplets and the formation of a new tip (Fig. 1.2b-d). This is followed by migration of the arc spot to this new location, where the process is repeated (Fig. 1.2e) [4].

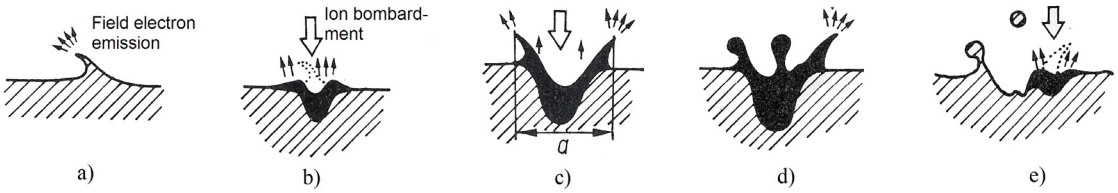

Figure 1.2.: Life cycle of a cathodic arc spot (modified after [4]).

Thus, the arc which produces the vapour by erosion of the target moves at random over the surface of target. This mode of operation is called *random arc*. It has the advantage of a good utilisation rate of the target material but has also the possibility, that the arc is concentrated on a small area, followed by melting of the target and damage of the cooling system located behind the target. Furthermore, special isolation rings are needed to make sure, that the arc can not leave the target and damage the vicinity. This can be avoided by use of magnetic systems, placed behind the target, which force the arc onto a wanted, mostly circular track. This mode of operation is then termed *steered arc*. [5]. The differences between the two modes in operation can be seen in Fig. 1.3.

The produced metal vapour in the plasma jet is highly ionized (up to 100%), with

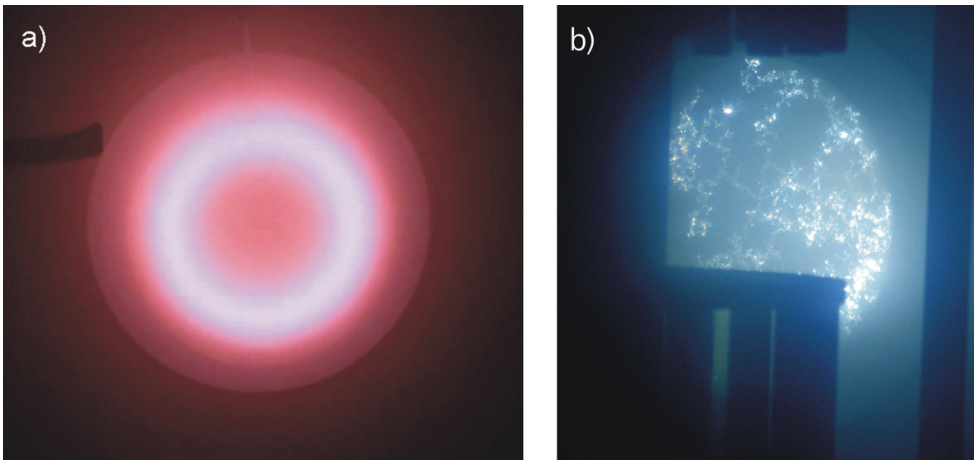

Figure 1.3.: (a) steered arc mode, (b) random arc mode (Photos by J. Radanitsch).

multiply charged ions and a kinetic energy of 50-150 eV [2][3]. This gives rise to the application of a bias voltage, a negative potenial between the cathodic substrate and the positive cations. With the bias voltage the energy of a large fraction of the arriving particles can be controlled, which enables the modification of growth conditions and thus film properties.

Fig. 1.1 shows that, additionally to the plasma jet, droplets of molten target material are ejected from the arc spot and end up as defects in the coating [6]. Droplets are mainly emitted at low angles (0° - 30°), while the plasma jet, i.e. the ions are predominantly ejected perpendicular to the substrate [3]. This offers the chance of shielding the droplets from the plasma flux. However, if the droplets reach the substrate, they are incorporated into the coating. The curved surface of solidified droplets on the growing film acts as new nucleation site which leads to the growth of defective and voided cauliflower structures (see Fig. 1.4a,c). These structures represent mechanical weak spots which might easily break out, if loaded. Furthermore, these voided and less dense structures represent quick paths for diffusion, especially out-diffusion of coating elements or substrate material is observed (see paper V and [7]).

Droplets are also the main reason for surface roughness of arced coatings (see Fig. 1.4b), which makes coatings produced by CAE less applicable for decorative purposes if the majority of the droplets are not removed from the vapour flux. The hard and sharp surface tips, caused by droplets, also influence the behaviour in tribological tests. The droplet generated surface roughness can lead to massive abrasion of the counter body material in early stages of the tribo-test, which results in more wear debris in the contact and thus changes the tribosystem. The thereby increased area of contact also changes the loading conditions, i.e. the Hertzian contact pressure during the test, which influences the test results (see paper I and IV). The amount of droplets can be reduced by suitable

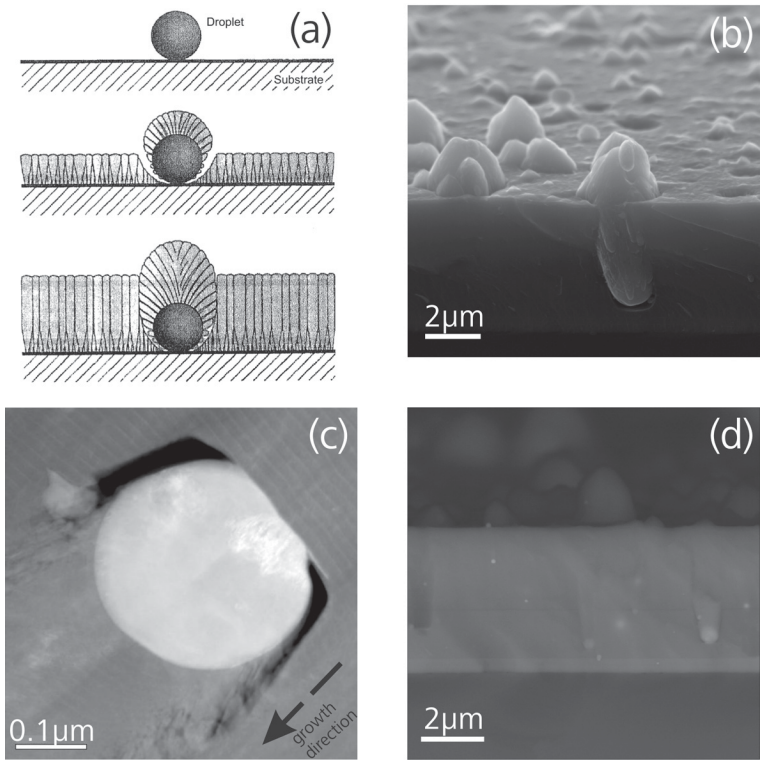

Figure 1.4.: (a)modification of layer growth by droplets according to Petrov et al. [9], (b) SEM image of droplet generated surface roughness, (c) HAADF-STEM image of a droplet, (d) back scattered SEM image of an arced coatings´ fracture surface showing droplets of various size and position in the coating (Fig. 1.4b-c own work).

shielding or filter systems. Various filter systems have been discussed in a review by Sanders and Anders [6]. Furthermore, the application of a steered arc instead of random arc mode is also reported to be beneficial, but droplets remain one of the major drawbacks of cathodic arc evaporation [8].

1.2. Growth

1.2.1. The basic modes of layer growth

After an atom hits the surface of the substrate, this atom might be either reflected by or loosely bonded to the substrate. If the atom transfers sufficient energy to the surface it is bonded in a weakly adsorbed state, known as physisorption and becoming a so-called adatom. These adatoms may diffuse at the surface and desorb after a while or initiate the formation of a cluster of supercritical size, called nucleus. After nucleation, the film grows by coalescence of the surface nuclei to form a continuous layer and develops ”structure”,

which means crystallography and topography [4][10]. Within this process, the surface energy γ plays a determinant role in early growth stages. In particular, the relation between the surface energy of substrate free surface γ_s, of the film free surface γ_f and of the film-surface interface γ_i defines the three modes of growth (Fig. 1.5).

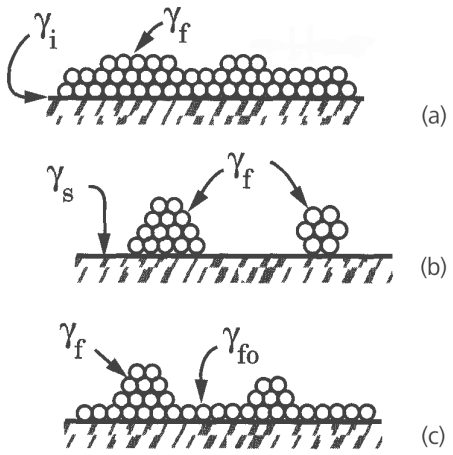

Figure 1.5.: Film growth modes: (a) Frank-van der Merwe (layer), (b) Volmer-Weber (island), (c) Stranski-Krastanov [10].

For $\gamma_f + \gamma_i < \gamma_s$ the total surface energy can be decreased if the substrate is evenly covered by the film. This is called *Frank-van der Merve* growth and requires a strong bonding between substrate and film. On the contrary, in absence of such bonding, the relation would be $\gamma_f = \gamma_i + \gamma_s$. Thus, the formation of a layer on the substrate would always increase the total surface energy which favors the formation of 3D islands. This is called *Volmer-Weber* growth. The third mode is a mixture of the first two modes and occurs if the growth changes from initial layer to island growth, which is then referred to as *Stranski-Krastanov* growth [10].

1.2.2. Structural development

The model described above is valid in the ideal case that sufficient surface diffusion of the adatoms is possible so they can rearrange to minimize γ, nucleation is not kinetically limited and the equilibrium state can be reached. The other extremum is the so-called quenched growth, where every adatom sticks where it lands [10]. For most of the cases, the real growth conditions are somewhere between these two extremes. Then the important parameters which influence the growth are the initial surface roughness, the activation energy of surface and bulk diffusion and the bonding energy between adatom and substrate. The surface roughness of the substrate causes *shadowing*, which is a geometric interaction between the surface topography and the angle of incidence of the "line-of-sight" vapour

flux. This effect prevents a homogeneous supply of all positions of the coatings surface. To balance the inhomogeneous supply of the surface, the adatoms need sufficient mobility. If the energy of the adatoms is high enough, adatoms can fill up the voids caused by shadowing by surface diffusion. At even higher energies, bulk diffusion is possible which enables recrystallisation of the coating and thus the equilibrium state [5][11].

Since adatom mobility is related to the melting point of the material, it can be expected that every parameter is dominant in a certain range of T/T_m where T is the substrate temperature and T_m the melting point of the coating. This relation between a certain "degree of mobility" of the adatom and the temperature is the basis of the so-called structure zone models (SZM)[4][11]. These models, based on observations by Movchan and Demchishin, [12] consist of basically three zones (zone 1-3). Thornton connected every zone with a predominant phenomenon controlling the mobility of adatoms in the growing film [13]. In *zone 1*, the temperature is too low for surface diffusion, thus shadowing can not be balanced and the formation of fine columnar grains with open boundaries is the result. The transition *zone T* is located between zone 1 and zone 2. It is characterised by a higher density and fine fibrous grains, caused by limited surface diffusion. In *zone 2*, surface diffusion can balance the effects of shadowing which leads to columnar growth and low porosity. With increasing T, the diameter of the columns increases. In *zone 3*, bulk diffusion is possible, which results in recrystallisation and dense structures with equiaxed grains.

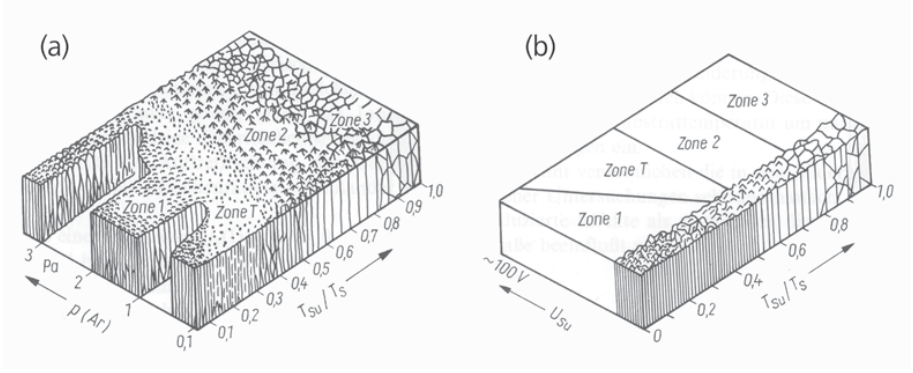

Figure 1.6.: Structure zone models: (a) after Thornton [13], (b) after Messier et al. [14].

Additionally to the relations mentioned above, also process parameters influence the energy of the arriving particles and thus the mobility of adatoms. With increasing gas pressure (Fig. 1.6a), the mean free path for the atoms decreases and thus, interactions between vapour flux and working gas atoms increase. This effect is called gas scattering and it reduces the energy of the arriving particles, which consequently decreases the mobility of the adatoms on the surface [1]. Thus, the transition between *zone 1* and *zone T* is shifted to higher temperatures with increasing Ar pressure. This effect has no

influence at higher temperatures, when the mobility of the adatoms is thermally activated, therefore, the transitions to *zone 2* and *zone 3* remain unaltered.

The influence of the bias voltage on the SZM has been reported by Messier et al. [14], shown in Fig. 1.6b. Increasing bias voltage increases the energy of the ion bombardment, which leads to higher mobility of the adatoms. Consequently, the transition from *zone 1* to *zone T* is shifted to lower temperatures if the bias voltage is increased [1]. Without bias voltage, the *zone T* is very narrow, or does not even exist. This already indicates the strong influence of the bias voltage on growth conditions and thus coating properties, especially in cathodic arc evaporation, with its high degree of ionisation of the produced vapour. A detailed discussion is provided in the following section.

1.2.3. Preferential growth and ion bombardment

Preferential growth of certain crystallographic orientation is widely observed in thin films. The grain structure of coatings develop from fine grains at the interface which are topped with columnar, conical grains. Similar effects are observed in the solidification of casted metals which develops elongated grains which follow the main heat flow. Both structures exhibit the phenomenon of preferred grain growth along certain crystallographic orientations, which is also refereed to as texture. Columnar structures are observed when the mobility of deposited atoms is limited. Depending on the angle of incidence of the vapour flux, tilting of the columns towards the vapour flux can be observed. Sufficiently high ion bombardment, which leads to increased mobility of the adatoms, eliminates the phenomenon [1]. This indicates that improved mobility of the adatoms modifies the growth conditions and thus the morphology of the coating.

According to Knuyt et al. the driving force for texture evolution in a growing film is the trend to lowest possible surface energy. Even if the orientation of the nuclei is randomly distributed, with increasing film thickness the texture evolution proceeds until only the lowest energy orientation survives [15]. But this is only valid under certain circumstances. Gall et al. [16] reported on ab initio studies of TiN growth. They reported that the surface energy for TiN (001) is less than for TiN (111) which suggests (001) as the dominant orientation if thermodynamics rather than kinetics control the growth of the coating (which is the case for high growth temperatures). Since PVD processes mostly work at low temperature ($\leq$450°C) kinetics are expected to control the growth. According to Gall et al. texture evolution can also be determined by the different surface diffusion energies of adatoms on, in that case TiN (100) and TiN (111) lattice sites. This would favor the preferential growth of orientations where adatoms are stronger bonded and surface diffusion is hindered.

In a review by Petrov et al. [17] it is reported that the nucleation barrier is gener-

ally expected to be low, thus randomly oriented nuclei can be assumed in early stages of growth. During island coalescence, the island with the lower energy per atom transfers its orientation on the other island, which is consumed. So coarsening is the first phenomenon leading to preferred orientation during growth. This is followed by processes where different surface diffusivity and adatom potential energies control the preferential growth of the grains. If the surface diffusivity and the potential energy of an orientation is low, the mean residence time of an adatom at its adsorption site is high, which increases the probability of incorporation of this respective adatom in the lattice. Consequently, grains with this orientation grow faster and overgrow the slower orientations [17].

Ionbombardment during thin film growth has a significant impact on the growth conditions and thus has the potential to influence preferential growth and the resulting properties of the film. At "low energy, low ion flux" - conditions the growth is still determined by adatom diffusivities and potential energies of the respective lattice sites. With increasing energy (and low flux) of the bombardment, so-called linear cascade effects come into play. The high energy of the impacting ions causes increased defect density, which can destroy the local epitaxial growth of columns and cause continuous renucleation [17]. The texture is controlled by collision cascade effects as described by Dobrev [18]. According to his report, grains with open channel direction have a higher survival possibility and grow preferentially. If the impacting ion can penetrate deeper into lattice, the kinetic energy of the ion is distributed over a larger volume, which causes lower sputter yields and lattice distortion compared to orientation where the ion energy is dissipated in the first few, topmost layers (Fig. 1.7).

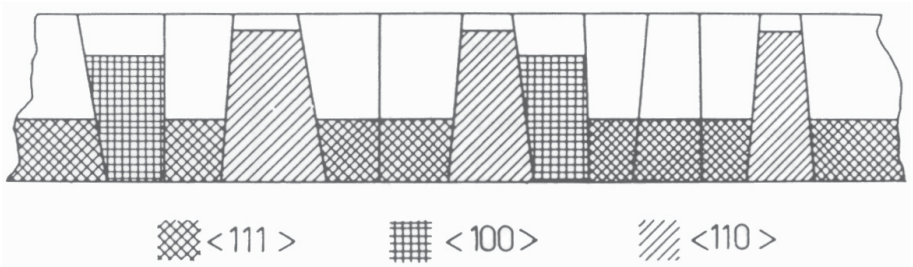

Figure 1.7.: Different sputter yields of polycrystalline silver films caused by collision cascade effects [18].

Finally, high flux, low energy bombardment also leads to altered growth conditions and thus texture. In case of transition metal nitrides with NaCl structure (e.g. TiN) it was reported that the (001) lattice plane exhibits both, metal and nitrogen bonds, which is referred to as non-polar direction. On the contrary, the (111) plane is either metal or nitrogen determined, i.e. a polar direction. The high flux bombardment increases the

dissociation of N_2 and provides an increased supply of atomic N for the (100) grains, while for the N-terminated (111) grains, the additional atomic N can not be utilized. The better supply with atomic N lowers the diffusivity of metal cations for the (100) lattice sites and thus improves the growth of (100) grains which results in a switch of the film texture from (111) to (100) if the N supply is rate limiting [17].

Cathodic arc evaporation, as mentioned before exhibits a high ionization rate up to 100%, thus a high flux ion bombardment is certain. This fosters the application of **bias voltage** as a powerful tool for growth modification due to the high energies of the impacting ions. As mentioned above, high energy ion bombardment leads to collision cascade effects. Thus, with increasing bias voltage collision cascade effects gain importance during growth, which results in changes in predominant texture and the distribution of orientations (see Fig. 1.8 and Publications I and IV).

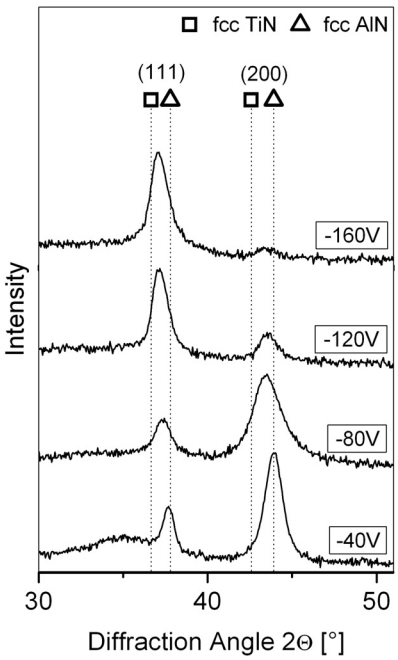

Figure 1.8.: Texture crossover of TiAlTaN from (200) to (111) with increasing bias voltage (from publication IV)

In addition, the higher defect density caused by the ion bombardment influences the stresses in the coating as reported by Ljungcrantz et al. [19]. Two concurrent effects can be distinguished. First, the increase of the defect density increases the residual compressive stresses. This process is found dominant at low bias voltages. Second, the ion bombardment increases adatom mobility and diffusivity which supports the annihilation

of defects, which can be observed at bias voltages exceeding -150V. Similar results were obtained within this work (see publication I) and by other authors [20][21].

For multicomponent systems, like TiAlN, the ionisation rate and the degree of ionisation are not evenly distributed between Ti and Al. In particular, Ti has a higher degree of ionisation, which fosters the predominant attraction of Ti to the substrate. Furthermore, the ion bombardment causes back-sputtering of already deposited material. The back-sputter rates of different elements are not necessarily the same. Both effects lead to deviations between the target composition and the composition of the coating. In arc evaporated TiAlN coatings a loss of Al and vice versa an enrichment of Ti compared to the target composition can be observed [22].

Increased bias voltage was also found to yield reduced surface roughness, which can be seen in Fig. 1.9. Decreased surface roughness was detected by scanning electron microscopy (SEM) and atomic force microscopy (AFM).

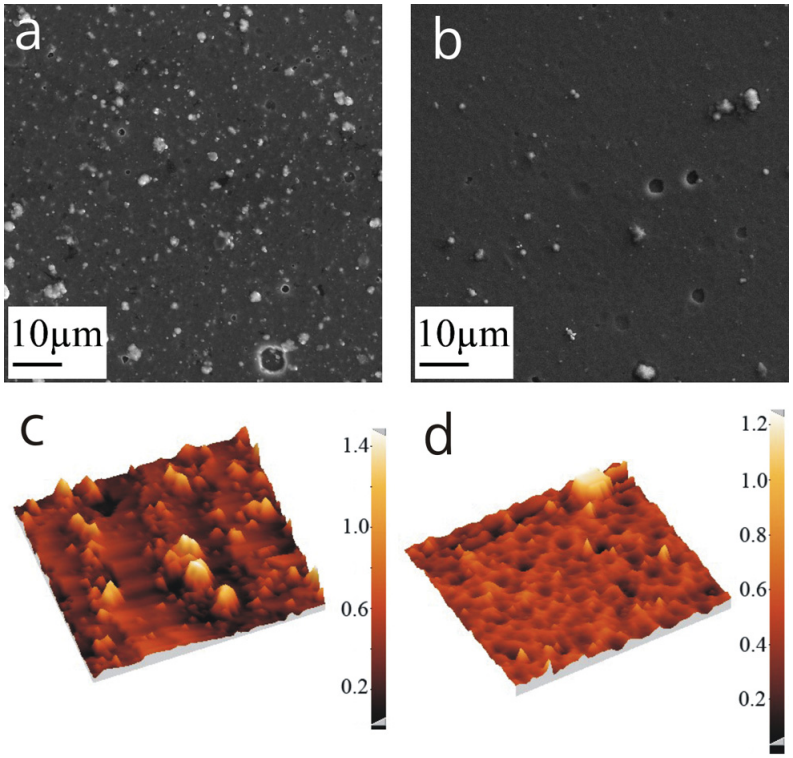

Figure 1.9.: Surface roughness after deposition due to droplets: (a) SEM topview -40V bias (b) SEM topview -160V bias (c) AFM -40V bias (d) AFM -160V bias (own work)

As mentioned before, the main reason for surface roughness in CAE are droplets, which represent curved nucleation sites and cause cauliflower like growth through the whole coating and consequently surface roughness peaks. As described above, bias and ion

bombardment have a significant influence on the growth conditions and the adatom mobility. If the mobility is limited, shadowing and the thereby preferred supply of elevated positions on the surface (like droplets) cause the conical and pyramidal-toped structures which can be seen in Fig. 1.9b,c. These structures can be observed to grow through the whole coating, even if the droplets are formed in early stages of the deposition process. The formed peaks are never flattened during the growth of the coating, so every droplet results in a surface peak and contributes to the surface roughness. High energetic ion bombardment increases adatom mobility and enable to balance the inhomogeneous supply of higher and lower position on the surface. Thus, the cauliflower structure may be flattened after a certain time and only droplets formed at the end of the deposition run can contribute to the surface roughness.

A second possibility would be that the bias voltage influences the formation or the transport of droplets to the substrate. Droplets are formed in the cathodic arc spot and are generally uncharged. Even if surface charges on the liquid particle may exists, the momentum of the ejected droplet should be too high to be influenced by an electric field, provided by the bias voltage. Therefore, it is unlikely that bias voltage influences the generation, size or transport of the droplets. Further investigations are needed to clarify the issue.

In dual phase structures, like TiAlN with high Al content, the bias voltage was also found to influence the fraction of hexagonal close packed (hcp) and face centered cubic (fcc) phases. In particular, a preferred formation of fcc phases was detected in case the bias voltage was increased. This effect is of huge importance for several other film properties and will be described in detail in section 2.2.

2. Structure

2.1. Crystallography of TiAlN

TiAlN is an evolutionary development based on TiN coatings. TiN together with TiC and TiCN was highly successful as wear resistant coating during the 1980´s. Starting from first publications in 1986, TiN coatings have been widely replaced by TiAlN in the last 20 years, due to its higher wear and oxidation resistance [23][24]. In thermodynamic equilibrium, TiN crystallizes in the face centered cubic (fcc) B1 rocksalt structure, while for AlN, the hexagoal close packed (hcp) B4 wurtzite structure is the stable one. Concerning the character of chemical bonding, transition metal nitrides like TiN are metallic materials, while nitrides, carbides and borides of aluminium exhibit a covalent bonding nature. Due to these different characteristics, the combination of TiN and AlN in a single phase material is not possible in equilibrium, i.e. the solubility of Al in the TiN crystal is extremely low and vice versa (see Fig. 2.1a) [25]. The application of PVD processes enables the formation of metastable multicomponent coatings with high Al contents in the TiN lattice. Cremer et al. [26] developed a modified phase diagram for PVD processes which shows the stability of fcc TiAlN up to high Al contents and also indicates the presence of a transition zone where both phases are present (see Fig. 2.1b).

According to Mayrhofer et al. [27], the phase stability of fcc TiAlN is determined by the distribution of Al atoms in the TiN lattice, i.e. the number of Ti-Al bonds. The energy of formation is lowest if the number of Ti-Al bonds is also low. This is the case if Ti and Al rich zones within the same fcc lattice are formed. The formation of such a low-energy configuration might be connected with the mobility of the atoms, which as mentioned before, can be widely influenced by the process parameters, especially by the bias voltage and the related ion bombardment. Consequently, the solubility limit of Al in TiN is highly influenced by the process conditions used. This has led to a broad variety of experimentally obtained solubility limits between 52% to 70% published in literature [7][29][30][31][32]. Calculations by Makino on the solubility limit of various fcc transition metal nitrides for Al indicate a solubility limit for Al in TiN to be around 65 at% [33].

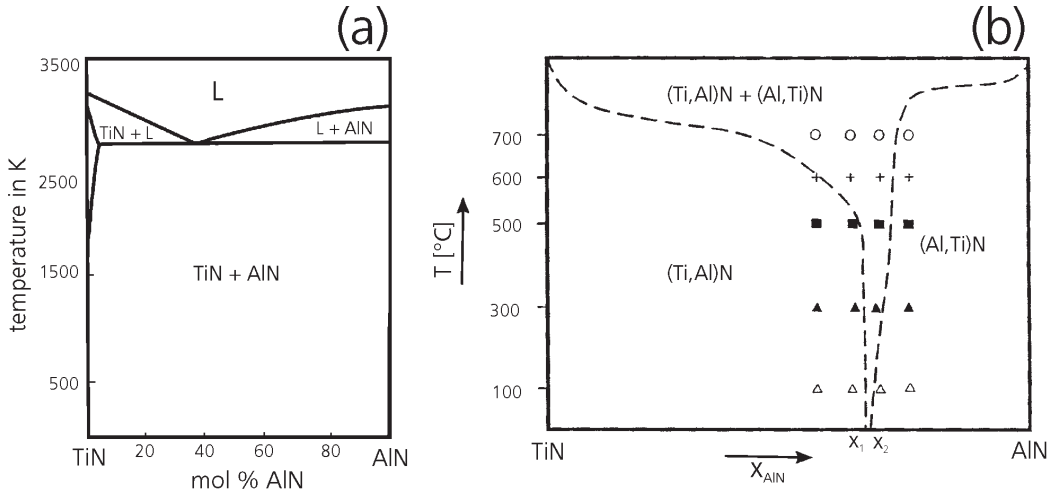

Figure 2.1.: (a) Binary phase diagram TiN-AlN after Holleck [25], (b) Modified metastable phase diagram TiAlN after Cremer et al. [26].

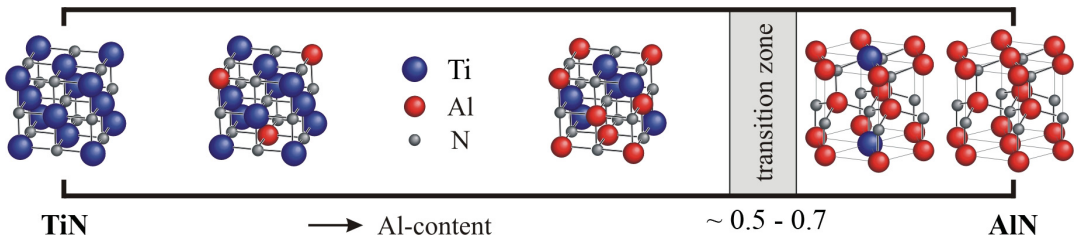

Figure 2.2.: Stability range of fcc and hcp TiAlN (modified after [28]).

Fig. 2.2 shows this variety of solubility limits reported in literature; thus, a fcc structure can roughly be expected up to 50 at% Al. At Al contents exceeding the solubility limit of Al in TiN a dual phase structure is present with fcc and hcp TiAlN phases (also indicated by Cremer et al., Fig.2.1b). With further increasing Al content, the fraction of fcc phases decreases until a single phase hcp structure is present. Within the experimental work for this thesis, TiAlN coatings were deposited with atomic ratios of Al/Ti of 1, 1.5 and 2. With the standard process parameters, an fcc single phase structure was only obtained for the coating with an Al/Ti ratio of 1, i.e. $Ti_{50}Al_{50}N$. That is, in the work being basis of this thesis and by application of the standard process (without modifications), the solubility limit of Al in TiN was between 50 and 60 at%.

However, as mentioned before, the solution of Al in TiN is metastable. That means under suitable conditions, i.e. sufficient temperature and time, decomposition of TiAlN into fcc TiN and hcp AlN takes place. The process of decomposition is accompanied by the important phenomenon of age hardening by spinodal composition. Generally, the hardening effect of age hardening is connected with coherency stresses between matrix and small coherent domains which are formed during annealing. For TiAlN coatings, between 850 and 900°C cubic domains are formed during annealing which could be identified as fcc AlN. The precipitation of fcc AlN is accompanied by a significant increase in hardness. This is explained by Mayrhofer et al. by spinodal decomposition of fcc TiAlN into fcc TiN and hcp AlN via an intermediate step by formation of fcc AlN [34][35]. Consequently, the total reaction of decomposition can be written as follows:

$$\textbf{fcc TiAlN} \rightarrow \textbf{fcc TiN} + \textbf{fcc AlN} \rightarrow \textbf{fcc TiN} + \textbf{hcp AlN}$$

2.2. The influence of bias voltage

Fig. 2.3 shows the results of XRD investigations of Ti-Al-V-N coatings. At -40V bias, a dual phase structure with fcc and hcp TiAlN phases can be observed. The peaks are shifted from the standard positions of fcc TiN and hcp AlN due to the solid solution of Ti in AlN and vice versa. Since Ti incorporation in the hcp AlN lattice causes lattice expansion and therefore a larger lattice spacing, the hcp peaks appear at lower diffraction angles. The bias voltage is found to have a strong influence on the presence of hcp phases. With increasing bias voltage, the hcp phase fraction decreases, which can be seen by decreased hcp peak intensities between 32 and 35°. Thus it is possible, to transfer a dual phase fcc + hcp structure into a single phase fcc structure by high bias voltages (see also publication I and IV).

There a several possibilities to explain this effect. The higher mobility of the adatoms, caused by the intense ion bombardment might be able to support a low-energy config-

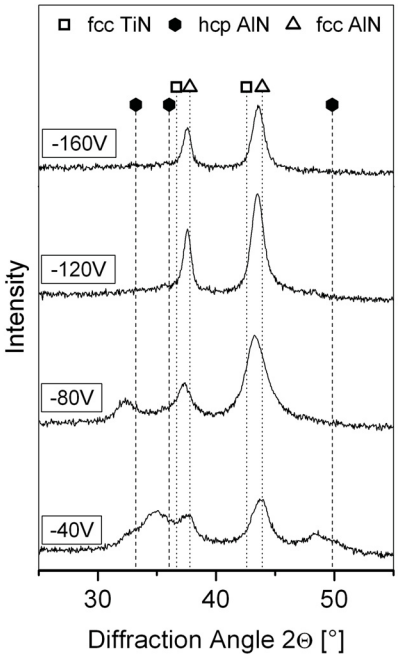

Figure 2.3.: Influence of bias on fraction of hcp phases in Ti-Al-V-N coatings (own work).

uration, as reported by Mayrhofer et al. [27]. In addition, collision cascade effects, as described in detail in section 1.2.3, could lower the survival rate of hcp nuclei which would lead to preferred growth of fcc grains. Since the higher bias voltage can also result in higher compressive stresses [19][36], these stresses might also contribute to the preferential growth of the denser fcc phase and might hinder the formation of the less dense hcp phase. A correlation between stresses and the presence of hcp phase has also been reported by Zhou et al. [29]. Furthermore, the effect of ion bombardment on selective back-sputtering must also be considered. As reported by Coll et al. [22], the ion bombardment leads to a loss of Al with respect to the target composition which is related to differences in the ionisation rate and the back-sputtering properties of Al, compared to Ti. Increased bias voltage could thus lead to further loss of Al and the tendency to form hcp phases would be reduced. Similar observations have also been reported by Sato et al. [37] on cathodic arc evaporated TiAlN and recently by Moser et al. [38] who reported on Ti-Al-Y-N deposited by bipolar pulsed DC magnetron sputtering.

2.3. The influence of alloying elements

Further improvement of TiAlN-based coatings by a so-called multicomponent approach is widely used and reported in literature [39]. The reason for the selection of a specific alloying element mostly aims at the improvement of mechanical properties or the resistance to oxidation or corrosion. However, apart from the original purpose, the incorporation of a new element can foster side effects on growth and the phase composition of the coatings. That is, the addition of further elements mostly promotes the formation of either the fcc or the hcp phase, which consequently can have a big impact on other properties of the coating.

Within the project being the basis for this thesis several multi-component systems were investigated. In particular, vanadium, tantalum, silicon and boron were used as alloying element in powder metallurgically produced compound targets in various contents. The influence of these elements on the formation of hcp phases are shown in Fig. 2.4. All coatings shown exhibit a dual phase structure with peaks from hcp phases at 32.5, 34.3 and 48°, while fcc phases appear at around 37, 43, 63 and 69°.

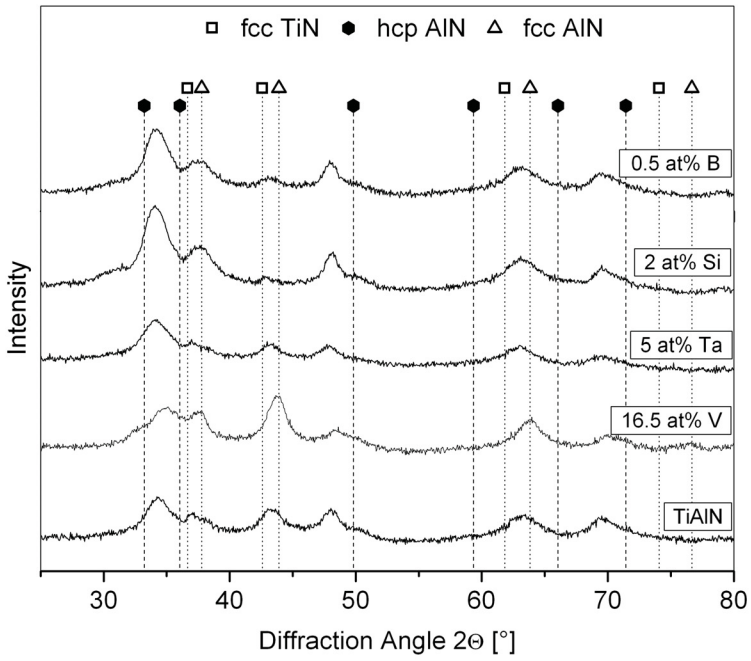

Figure 2.4.: Influence of alloying elements on fraction of hcp phases in Ti-Al-X-N coatings (X = V, Ta, Si, B)(own work).

The effect of alloying elements on the fraction of hcp and fcc phases is discussed in details in various publications included in this thesis (see publication I-IV). However, a

brief summary is also presented here. In general, if the alloying element also forms a fcc nitride, a promoting effect for the fcc phase is likely; if the respective nitride forms complicated or various crystal structures, a prediction of the impact on the phase fractions is much more difficult.

Alloying with V leads to decreased formation of hcp phase, thus V stabilizes the fcc phase. This can be observed by decreased intensity of the hcp peaks in comparison to the neighboring fcc peaks (see publication I and II) and is in good agreement with results published by Kutschej et al. [40]. At high V contents which replace Ti, as investigated within this thesis (up to 25 at% V), a suitable explanation is also that, according to Makino [33], the solubility of Al in VN is higher than in TiN. So, the replacement of Ti by V should also foster a higher solubility of Al in Ti-Al-V-N coatings.

Alloying with Ta does not seem to promote or hinder any of the two phases. However, a more detailed study (publication IV) revealed that Ta can also be considered as a fcc promoting element. The alloying content of Si and B was very low. Both elements seem to form amorphous tissue phases if a certain content is exceeded (see also chapter 3.1). Despite the low content, it was clearly seen that alloying (doping) with Si and B promotes the formation of hcp phase which can be seen by the significant increase of the intensity of the hcp peak around 34°, compared to unalloyed TiAlN. Similar results were also published by others [41][42][43]. As mentioned before, for higher contents of B and Si, the structure of Ti-Al-(Si,B)-N coatings changes dramatically and consists of small, nano-sized TiAlN crystallites surrounded by an amorphous Si_3N_4 or BN tissue phase. This structure is called nano composite and exhibits extremely high hardness, thus called superhard coatings (see [44] and references therein).

3. Property relations

3.1. Mechanical properties

In general, the term "mechanical properties" of a material is a selection of elastic parameters like stress, strain and elasticity and values which define the plastic behaviour of a material like yield strength, elongation to failure or hardness. Contrary to bulk materials, the mechanical properties defined for thin films and hard coatings are limited. Here, the "mechanical properties" are described taking only stresses in films, elasticity, i.e. the Young´s modulus, and the hardness into account, which are also the parameters which are widely published and discussed in literature [1].

For thin films the hardness and Young´s modulus are often evaluated by nano indentation, which is simply an indentation test in which the length scale of penetration is measured in nanometers. These low indentation depths are necessary because otherwise the evaluated hardness would represent the hardness of the substrate instead of the hardness of the coating. Recording of the load-displacement curve enables the automatic calculation of the created surface of the indent and thus a hardness value. Fig. 3.1 shows such a curve and the measured values. Due to low loads applied (in the range of mN) and the thus low penetration depth this necessarily includes the correction of several effects like initial penetration, the compliance of the system and deviations of the indenter from the ideal shape (for details see [45][46]).

Residual stresses in the coatings are often measured by the so-called stress-curvature method. The stresses in the coating cause the bending of a sufficiently thin substrate (mostly a thin Si wafer of defined shape), which can be measured by a laser beam. The stresses are then calculated by the modified Stoney equation [47].

Hardness is commonly defined as the resistance of a material to its plastic deformation [1]. On a more detailed scale, hardness not only depends on interatomic forces (intrinsic hardness), but also on impurities, the dislocation structure, the grain size and texture [49][50]. High intrinsic hardness is related to high cohesive energy, short bond length and a high degree of covalent bonding. This can be seen by comparing TiC with TiN. TiC

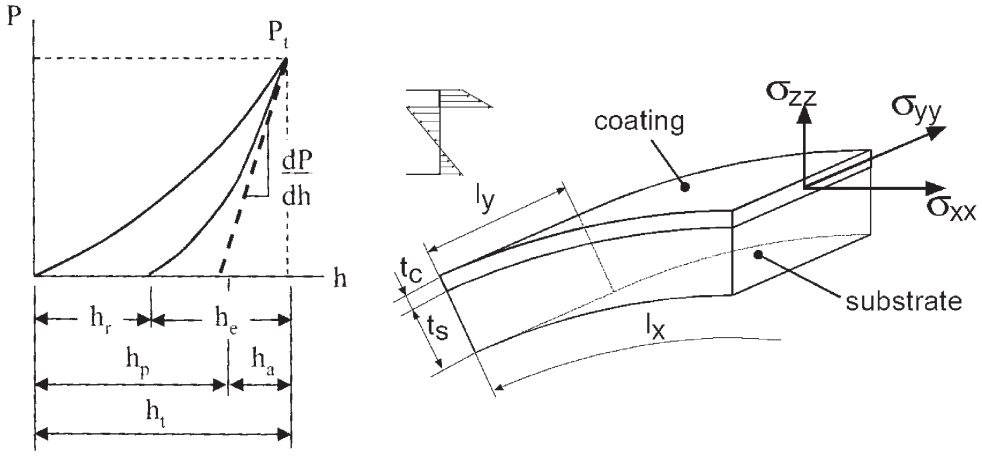

Figure 3.1.: Left: load-displacement curve of a nano indentation experiment with maximum load P_t and depth at maximum load h_t. The depth of the contact circle h_p and dP/dh allow the calculation of modulus and hardness. h_r is the depth of residual impression, h_e the elastic recovery during unloading [45]. right: bended coating-substrate composite due to residual stress, the detail shows the stress distribution over the cross section (length l_x, width l_y, thickness of coating t_c and substrate t_s and stress components in x, y and z direction $\sigma_{xx}, \sigma_{yy}, \sigma_{zz}$) [48].

has a higher degree of covalent bonding, while TiN as mentioned before has a metallic nature. Thus, TiC has a higher intrinsic hardness. The easiest way to increase strength and thereby hardness is to make the material impure, also referred to as solid solution hardening. These impurities can be an alloying element, a residual gas atom from the deposition process or point defects caused by ion bombardment. Such defects introduce an elastic strain field in the surrounding of their lattice sites, because their size deviates from the size of the atoms of the host lattice. Furthermore, the impurity can be an interstitial. The elastic strain fields hinder dislocation movement, which results in a remarkable increase in strength and hardness [51]. Smaller grains also lead to higher hardness because the higher content of grain boundaries hinders the dislocation movement and thus plastic deformation. The influence of grain size is related to the well known Hall-Petch relation [49]:

$$H = H_0 + kd^{-1/2}$$

where H is the hardness, H_0 is the intrinsic hardness for a single crystal, d the grain size and k a material constant. In case of thin films with columnar growth, the important parameter is often the diameter of the columns. So, with decreasing column diameter, the so-called domain size, the hardness increases. The growth conditions of thin films are

also the reason why PVD coatings often exhibit a strong preferred orientation, which can lead to different hardness values of different orientations due to hardness anisotropy of the material. In case of TiN it was found that the (111) orientation exhibits 15% higher hardness in comparision to (110) oriented TiN [49][52].

Young´s modulus is the resistance of a material to elastic deformation. It is defined as the slope of the stress-strain line, given by Hooke´s law or in other words it is the theoretical stress required for 100% elastic strain. The Young´s modulus is related to the atomic bonding strength or the stiffness of bonds which can be assumed as homogenous if the stretching is small [51]. Young´s modulus is also sensitiv to changes of texture. Since the strength of atomic bonds is also anisotropic with respect to various crystallographic orientations, so is the Young´s modulus. A good example is again TiN, but also pure metals like ferritic iron show a significant difference of Young´s modulus between (111) and (100) [53]. The Young´s modulus is also measured by nano indentation, where in particular the unloading part of the load-displacement curve is evaluated.

Residual stresses in thin films are an unavoidable consequence of depositing a film at one temperature and using it in another. One source of stresses is the mismatch in thermal expansion and the lattice mismatch between film and substrate. That is, the film cannot be considered without taking the substrate into account the film is deposited on [1]. Furthermore, stresses can also origin from the deposition process. Ion bombardment of the growing film can cause excess interstitials and defects which can not anneal during the growth process and thus remain in the deposited film and cause high compressive stresses. The mentioned effects occur simultaneously and can be additive or competing, depending on the deposition process, the deposition temperature and the film-substrate pair. Cemented carbide and silicon have a lower coefficient of thermal expansion than most nitrides, thus one would expect tensile stresses in the film after deposition. However, the influence of the ion bombardment determines the cumulated stress state, which leads to compressive stresses for most PVD hard coatings [19][54]. High compressive stresses in the coating hinder the penetration of the indenter while nano indentation, thus compressive stresses increase hardness and Young´s modulus. On the contrary, CVD coatings are deposited at much higher temperatures, which rises the influence of thermal mismatch and enables the annealing of defects. Tensile stresses after deposition are the consequence.

The mechanical properties of TiAlN based hard coatings are determined by the interplay of the Al content and the phase fraction of fcc and hcp phases. As mentioned before, especially the fraction of hcp phase can be adjusted by the deposition process

which enables also tailoring the mechanical properties. According to results published by Zhou et al. [29], hardness and Young´s modulus increase with increasing Al content, which is related to solid solution hardening. This is also indicated by decreasing lattice parameters, caused by incorporation of the smaller Al atom at Ti sites in the fcc TiN lattice. The maximum values are reached at 50 mol% AlN and coincide with maximum residual compressive stress. If the Al content is further increased, a rapid drop of hardness, Young´s modulus and stress can be observed which is connected with the transition from a fcc single phase to a fcc+hcp dual phase structure. That is, the presence of hcp phases has a detrimental effect on mechanical properties, as reported also by other authors [29][30][55][56][57]. Hardness and Young´s modulus are often found to exhibit the same trend. According to calculations by Mayrhofer et al. [27], the elastic moduli for the hcp phase are significantely lower compared to the fcc phase. Thus, at appearance of hcp phases, the Young´s modulus decreases.

The bias voltage influences the mechanical properties in various aspects. As mentioned before, increased bias voltage is a suitable tool to prevent the formation of hcp phases. Therefore, in dual phase fcc+hcp systems, the hardness and the Young´s modulus increase with increasing bias voltage. A second contribution, independent from the phase fractions, is the relation between bias voltage, compressive stresses and hardness. Increasing bias voltage leads to higher compressive stresses caused by increased ion bombardment and defect density. As a consequence, the resistance of the material to plastic and elastic deformation also increases which results in higher hardness and Young´s modulus. The vanishing of the hcp phase and increased compressive stress are additive factors, which both enhance hardness and Young´s modulus (see also publication I). However, the main contribution is suspected to be provided by the presence/absence of the hcp phase (compare paper VI).

The influence of alloying elements depends on the alloying element itself and its nature and of course on the alloying content. If the alloying content of Si and B is sufficiently high, it can lead to the formation of a completely different structure. This structure consists of an amorphous Si_3N_4 or BN tissue phase surrounding small nanocrystalline TiAlN grains and forming so-called nano composites [44]. Carvalho et al. reported on a Ti-Al-Si-N nano composite containing up to 18 at% Si with enhanced mechanical properties [58][59]. Likewise, also the addition of B was found to cause significant improvement of the mechanical properties [60][61]. The hardness enhancement of these structures exceeds the mentioned Hall-Petch effect. Thus another powerful mechanism must be present. According to Rafaja et al. [62] the improved hardness of nano composites is connected

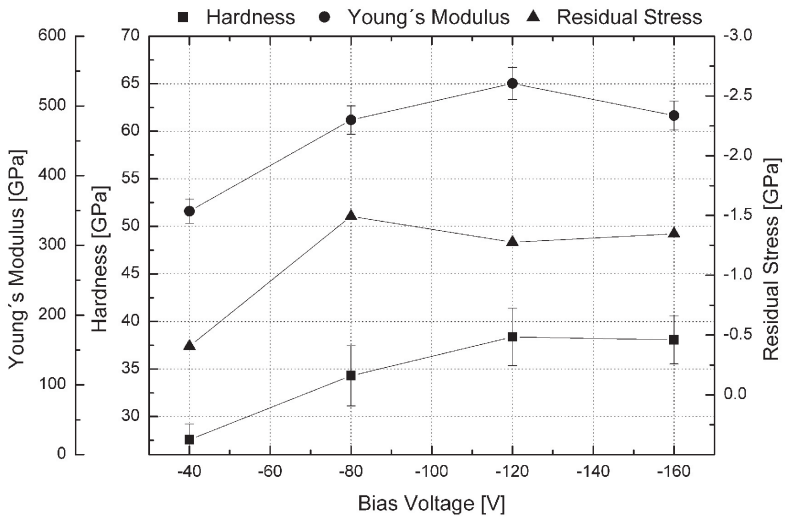

Figure 3.2.: Young´s modulus, hardness and residual compressive stress of Ti-Al-V-N coatings vs. bias voltage (from publication I).

with coherency stresses, i.e. intrinsic stresses at the crystallite boundaries. However, if a certain thickness of the amorphous tissue phase (i.e. a certain content of B or Si) is exceeded, the crystallites become non-coherent and the hardness increase vanishes due to lack of these beneficial coherency stresses [63]. Within this thesis, the used contents of B and Si were to small to form a nano composite (see publication III). Even if the formation of hcp phase was increased by B and Si doping, which would suggest a decrease in hardness, the mechanical propterties remained more or less unchanged. This can be understood by the fact that significant changes of the mechanical properties are only observed if a phase transition from single phase fcc to dual phase fcc+hcp can be achieved. Since already the unalloyed TiAlN exhibits a dual phase structure, the increase of hcp phase is not strong enough. Contrary to the bias voltage, the influence of such small amount of alloying elements on the hcp phase fraction is too small, thus a significant change of hardness or Young´s modulus is not observed.

In contrast to Si and B, the literature concerning Ta alloyed TiAlN is limited. Kutschej et al. reported on Ta to be a fcc promoting element to the expense of hcp phase. This is connected to an increase of mechanical properties and wear resistance [41]. However, within this work, no change in hardness or Young´s modulus was observed up to contents of 5 at% Ta in the target.

According to reports by Knotek et al., single phase Ti-Al-V-N coatings show decreasing hardness values with increasing V contents [64][65]. This is in contrast to reports by Kutschej et al. who reported that V acts as a solid solution hardener for TiAlN based

hard coatings [40]. Due to the high V contents investigated in this thesis (up to 25 at% V) for V-alloyed TiAlN coatings a significant enhancement for hardness and Young´s modulus as well as decreased residual stresses were found. The high V contents lead to a significant reduction of hcp phases, which results in the observed hardness and Young´s modulus increase. In contrast, the residual compressive stresses are significantly reduced. This is attributed to the difference in lattice mismatch between fcc TiN, VN and AlN. While the lattice mismatch between TiN and AlN is approximately 3%, it is only 0.5% between VN and AlN. Thus, with increasing V content to the expense of Ti, the average lattice mitmatch decreases, which results in lower compressive stresses. As mentioned before, this has also a decreasing impact on the hardness values. Thus, V alloying represents a competition between hardness enhancement due to reduced hcp phase and hardness decrease due to lower compressive stress (see Fig. 3.3 and publication II).

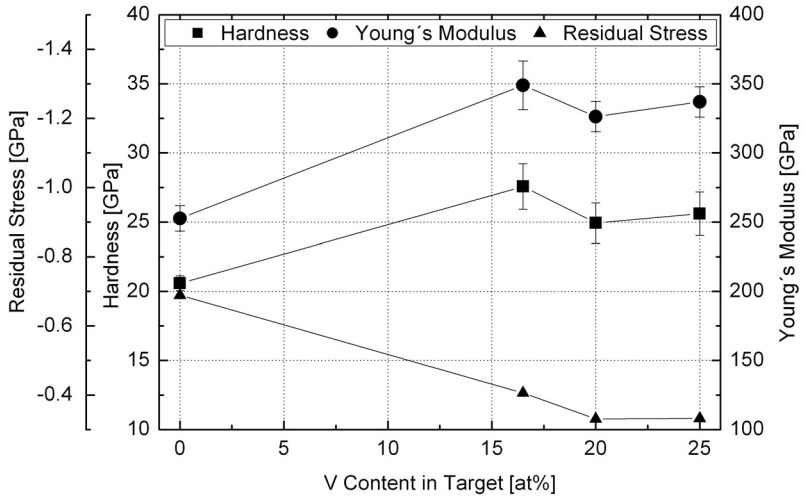

Figure 3.3.: Young´s modulus, hardness and residual compressive stress of Ti-Al-V-N coatings vs. V content (from publication II).

3.2. High temperature oxidation

3.2.1. General

The oxidation of an atom is equal to the loss of an electron which results in the increase of the oxidation number of the atom. That does not necessarily include chemical reactions with oxygen [66]. However, if exposed to the atmosphere, most technically applied materials are unstable to a certain degree at both high and low temperatures. That means that

deterioration by corrosion or high temperature oxidation is a daily challenge in technical applications. Therefore, the following section will concentrate on phenomena between metal and oxygen following the principal equation [67]:

$$Me(s) + 1/2O_2(g) \leftrightarrow MeO(s)$$

The reaction reveals that the formation of a solid oxide scale $MeO(s)$ leads to a separation of the reactants $Me(s)$ and $O_2(g)$. This highlights the importance of transport phenomena for oxidation since either oxygen must be transported to the oxide-metal interface or metal to the free surface for the oxidation reaction to proceed. This is especially valid at elevated temperatures, where diffusion is supported by high thermal energy. Furthermore, metal oxides exhibit a ionic nature, so the transport of *ions* through the oxide layer must be considered instead of transport of neutral atoms. For electrical neutrality, this automatically involves also the transport of negative (electrons) and positive charge carriers (cation vacancies) [67]. A schematic of the involved transport phenomena and the related reactions can be seen in Fig. 3.4.

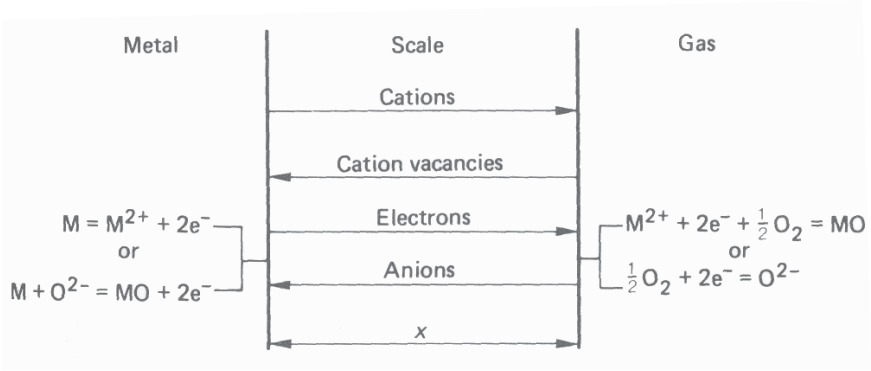

Figure 3.4.: Transport phenomena during diffusion controlled oxidation [67].

The initial formation of an oxide scale is divided into several steps which include the adsorption of oxygen at the surface and the chemical reaction including the transfer of electrons. This is followed by nucleation of the oxide, lateral growth into a continuous film and finally growth in thickness (see Fig. 3.5a). The rate of these individual steps depend on the material, the atmosphere, the temperature and the oxide scale itself, since some oxides form a so-called protective film, but others do not [68]. Of special importance is the ratio between molar volume between metal and metal oxide. To form a dense and protective oxide scale, a larger molar volume of the oxide is needed. But due to this volume mismatch between the metal and the oxide, stresses are generated, which increase with increasing oxide scale thickness. These stresses, if sufficiently high can cause cracking

or spalling of the oxide scale, which exposes unoxidized metal to the atmosphere and leads to an instant acceleration of the oxidation rate. If this process repeats periodically, it is called *break away oxidation* [67][68].

The oxidation rate, by which the growth of the oxide scale proceeds can be described by three different rate laws, which are displayed in Fig. 3.5b. The *parabolic rate law* is found if diffusion of the species through the oxide is rate limiting and a perfect adhering and compact scale is assumed. It is the most common relation between weight gain and time experimentally found. A *linear rate law* indicates that the oxide scale is not protective but porous. Furthermore, it is found at the beginning of oxidation where the scale is not fully developed yet. Finally a logarithmic rate low is often observed at low temperatures and exhibits rapid layer growth at early stages of oxidation which almost comes to a hold after a certain oxide layer thickness is reached [67][68][69].

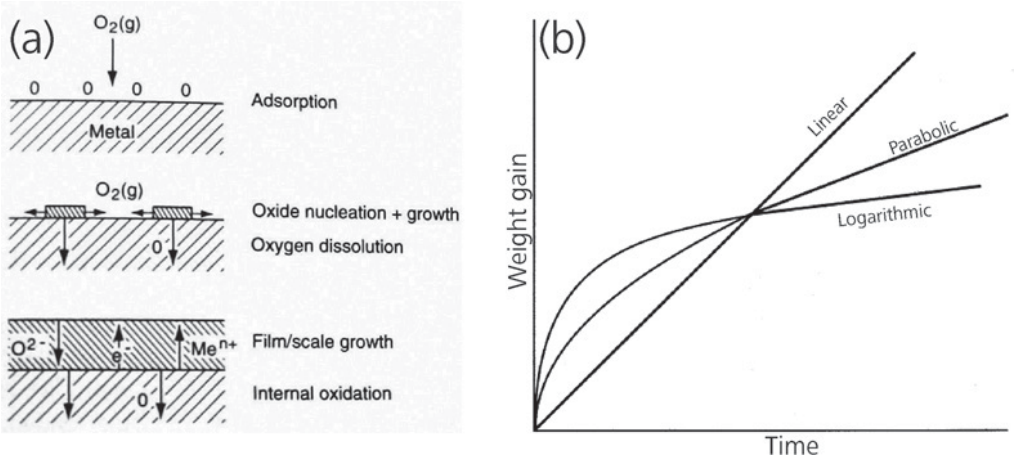

Figure 3.5.: (a) Initial stages of oxide scale formation [68], (b) Oxidation rate laws [68].

3.2.2. High temperature oxidation of TiAlN

The main benefit of TiAlN over TiN coatings is its superior resistance to oxidation which results in significantly higher wear resistance [23][24][70]. The oxidation of TiAlN and TiN is well reported in literature. The oxidation of TiAlN starts at 700 to 800°C, while TiN starts to oxidize between 500 and 600°C [70][71]. The oxidation of TiN to TiO_2 rutile is accompanied by spalling of the oxide scale due to stresses caused by a mismatch in molar volume [72]. According to McIntyre et al. [73], the oxidation of TiAlN coatings leads to the formation of a layered oxide scale with an Al-rich top-layer and a Ti-rich sub-layer. Similar observations are also reported by others [74][75]. According to Hofmann, the formation of the Al-rich top-layer can be explained by its higher oxide formation free enthalpy [76]. McIntyre et al. attributed the superior oxidation resistance compared

to TiN to the upper dense Al_2O_3 top-layer, which is expected to hinder in-diffusion of oxygen. Inert marker experiments revealed that the mobile species are Al and O, which means that the oxidation of TiAlN proceeds via out-diffusion of Al which forms the Al_2O_3 top-layer and the indiffusion of O to the oxide-nitride interface, where Ti is oxidized [73] (see Fig. 3.6).

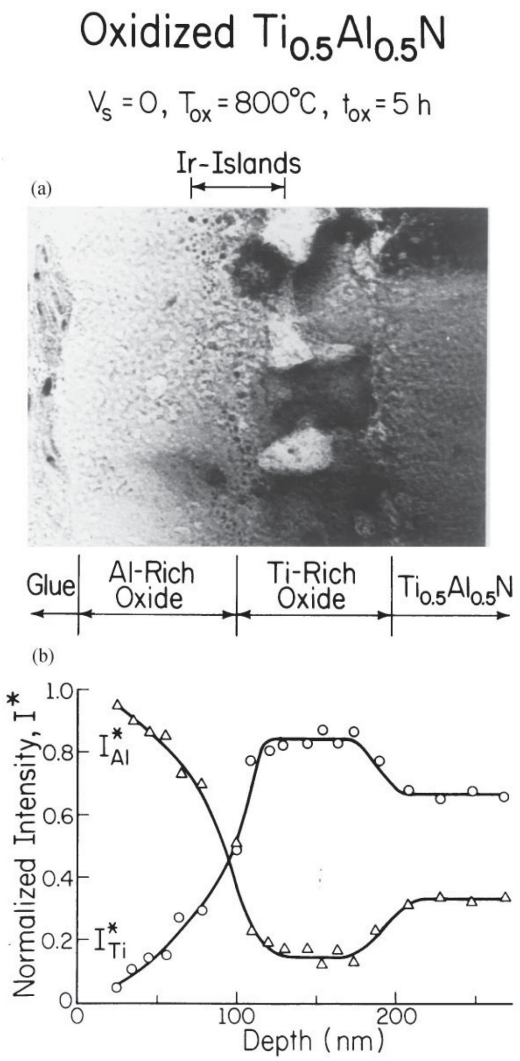

Figure 3.6.: (a) Cross-sectional transmission electron micrograph (TEM) of the oxide overlayer formed on a $Ti_{50}Al_{50}N$ film after oxidation at 800°C for 5h. Ir diffusion markers were deposited on the film surface prior to oxidation. (b) Normalized Ti and Al signal intensities obtained from scanning transmission electron microscopy (STEM)-generated energy dispersive X-ray (EDX) spectra, are plotted as a function of depth from the oxide surface [72][73].

However, Joshi et al. reported that the formation of this protective layered oxide scale is not generally observed but requires a sufficiently high oxidation temperature. At tempera-

tures below 700°C, the oxide scale consists of a mixed Ti-Al-oxide. At high temperatures, exceeding 800°C a layered structure, as mentioned above, is formed [77]. Similar results were also published by Vaz et al. [78]. Furthermore, Vaz et al. reported that as the oxidation proceeds, the increased thickness of the TiO_2 sub-layer is accompanied by the development of compressive stress which may lead to cracks and consequently faster oxidation. With increasing Al content in the coating, the Ti-rich sub-layer was found to grow slower. Thus, the authors attributed the better performance of Al-rich coatings to the slower growth of rutile and not exclusively to the Al-rich top-layer, acting as a diffusion barrier [78]. The results by Vaz are in good agreement with observation by McIntyre et al. who reported on a crack network at the surface in late stages of the oxidation experiments and the occurrence of TiO_2 rutile crystals in these cracks. The crack formation was postponed if a bias voltage was applied during deposition [73]. The mentioned model is also only valid up to a certain Al content. Vaz et al. reported that at very high Al contents, the oxidation resistance deteriorates and becomes similar to that of hcp AlN. The critical concentration coincides with the transition from the fcc single phase to fcc+hcp dual phase structure [78]. Consequently, three different fields can be defined in order to improve the resistance of TiAlN to oxidation further. First, the function of Al_2O_3 as diffusion barrier for oxygen. Second, the oxidation of Ti at the oxide nitride interface and the accompanied generation of stresses in the TiO_2 sub-layer. Third, the presence of hcp TiAlN phases in the nitride coating.

Improvement of the Al_2O_3 diffusion barrier is possible by alloying with Y. Lembke et al. [79] reported that Y preferentially diffuses to column boundaries where it blocks diffusion paths. Rovere et al. [80] identified Y in CrAlYN as a so-called reactive element which provides additional sites for heterogeneous nucleation of Al_2O_3. According to Jedlinsky [81] this accelerates the formation of dense α-Al_2O_3. The formation of TiO_2 rutile occurs via nucleation of metastable anatase type TiO_2 and a following phase transition to rutile type TiO_2 which is accompanied by rapid coarsening of the freshly formed rutile grains [82][83][84][85]. Within this work, doping of TiAlN with small contents of Si and B was found to delay or hinder the anatase-rutile phase transformation in the TiO_2 sublayer. This was indicated by a significantly higher amount of anatase type TiO_2 detected in oxidized coatings in comparison to undoped TiAlN (see Fig. 3.7b) This results in improved resistance to oxidation, where especially Si is found to be highly effective (see publication III). Similar observations have also been published for TiSiN [86][87]. The reduced efficiency of B in comparison to Si (see Fig. 3.7a) is probably connected to a loss of B due to the formation and sublimation of BO_x suboxides [88].

Also alloying with Ta has shown to be highly efficient in order to improve the resis-

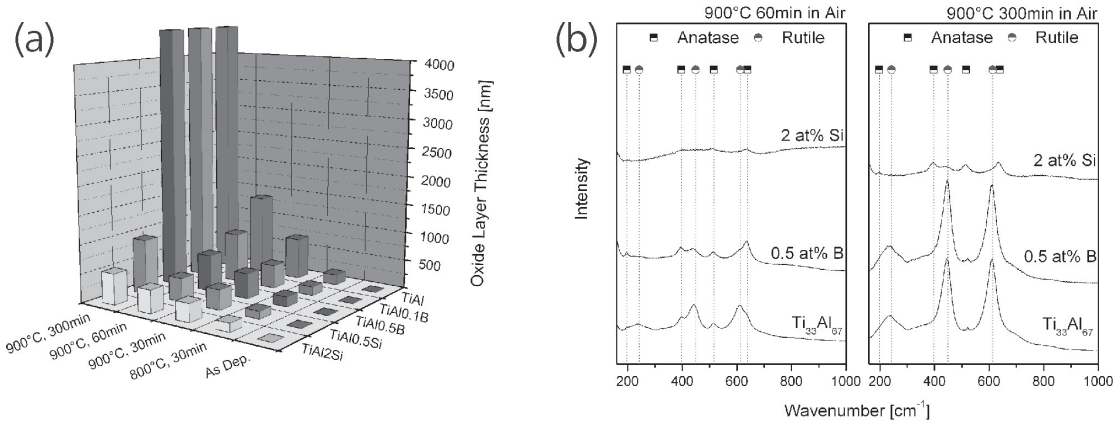

Figure 3.7.: (a) Oxide layer thickness for various coatings and oxidation conditions (publication III) (b) Raman shifts of TiAlN, Ti-Al-B-N and Ti-Al-Si-N after oxidation at 900°C for 60 and 300 min in air (from publication III).

tance of TiAlN to oxidation which results in significantly better high temperature wear resistance (see publication IV and V). Ta also acts as alloying element mainly in the TiO_2 sub-layer but is not found to modify the oxidation sequence of Ti, i.e. the anatase-rutile phase transformation, which is in contrast to observations made for Si and B. Instead it is concluded that Ta substitutes Ti in the rutile type TiO_2 lattice. The higher valency of Ta^{5+} compared to Ti^{4+} leads to a decreased concentration of O-vacancies. This might hinder the O mass transport in TiO_2 to the oxide-nitride interface and retard the oxidation of Ti (publication V). Similar models are also published for bulk TiAl alloys for Ta and other elements of the same valency (5+) [89][90]. Both, Ta and Si lead to an improved oxidation resistance, but seem to generate this improvement via different paths. Thus it can be suspected that Si *and* Ta might act additively and Ti-Al-Ta-Si-N coatings could exhibit an even higher resistance to oxidation.

The oxidation resistance of dual phase fcc+hcp TiAlN can be increased if the bias voltage during deposition is increased and hcp phase formation is hindered. This has been shown for Ti-Al-Ta-N (see Fig 3.8), where the oxide layer thickness after an oxidation treatment at 900°C in ambient air was decreased if the bias voltage was increased from -40 (a) to -80V (b) (see also publication IV). However, for even higher bias voltages, the effect is reversed and higher oxide scale thickness is observed for -160V bias. This is probably related to the higher defect density and smaller grains, enabling easier diffusion or cracking due to the high stresses [69].

The addition of V, as alloying element for TiAlN is reported to lower the coatings resistance to oxidation. Gassner et al. [91] reported that at 520°C the onset of oxidation of VN occurs. Mayrhofer et al. [92] detected rapid oxidation of TiAlN/VN multilayers

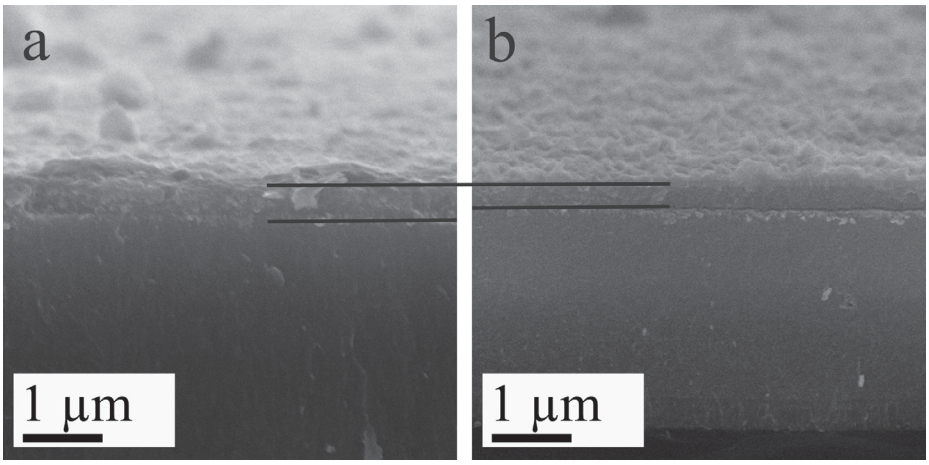

Figure 3.8.: (a) Oxide layer thickness of Ti-Al-Ta-N after oxidation at 900°C for 300 min. Guide lines indicate the position of the surface and the oxide-nitride interface. The coatings were deposited at (a) -40V and (b) -80V bias voltage (from publication IV).

by differential scanning calorimetry at around 550°C. Thus the onset of oxidation of Ti-Al-V-N coatings by V-oxide formation can also be expected in this temperature range.

3.3. Tribology

3.3.1. General

Tribology is the science of interacting surfaces in relative motion. In technical applications, tribology means the understanding, modification and control over friction, wear and lubrication [93]. Friction is the resistance to the relative motion of two bodies with their surface in contact. This resistance leads to energy consumption which is mainly dissipated as heat and energy for plastic deformation. There are three quantitative laws that describe the magnitude of the friction force in relation to the three macroscopic observable variables, namely the applied load, the area of contact and the sliding velocity [93][94][95]:

1. The friction force F_f is proportional to normal force F_N following:$F_\mathrm{f} = \mu F_\mathrm{N}$ with μ being the so-called coefficient of friction (COF).
2. The friction force is independent of the apparent area of contact. Thus there is no difference in COF for small or large objects.
3. The friction force is independent of the sliding velocity.

Concerning the second law, it should be mentioned that the true area of contact is significantly smaller, because contact between two surfaces occurs only where asperities touch. Thus, the true area of contact is the sum of the individual asperity contact areas [95]. There are three basic mechanisms behind the phenomenon of friction. These mechanisms are the deformation of surface asperities, plowing by wear particles and hard asperities and adhesion of the flat portions of the sliding surface [96].

Lubrication is mostly used to reduce the frictional force between sliding surfaces. In general, the lubricant has a lower shear strength in comparison to the sliding surfaces and provides a layer in between those surfaces, thus separating the two surfaces to a certain degree. Lubricants can completely prevent the contact of asperities, reduce the number of contacts or decrease the strength of temporary junctions between asperities. Since contact of the sliding surfaces is also a prerequisite for wear, lubrication also reduces the rate of sliding wear [95].

Wear is the removal of material from solid surfaces as a result of mechanical action. There are many ways to further distinguish types of wear, like for instance, lubricated versus dry sliding wear, although dry sliding wear usually occurs in the ambient atmosphere which means that there is considerable amount of humidity present [95]. It will be shown later on, that this can have an enormous impact on the wear properties. However, the most common classification of wear is to distinguish *adhesion*, *abrasion*, *surface fatigue* and *corrosive wear*. Adhesive wear occurs when two surfaces slide over each other and fragments of one surface are removed and adhere to the other surface. These fragments might stay where they are, be back transfered to the original surface or form free wear debris. Abrasion is defined as material removal due to ploughing, wedge formation and cutting. The generated wear particles are generally loose. Surface fatigue is observed during repeated sliding or rolling which might cause cracks and finally generation of wear particles. Finally, corrosive wear takes place if tribological processes foster chemical reactions in corrosive environments. In absence of sliding, the corrosion product might form a layer which hinders further corrosion. However, sliding removes these protective films and exposes virgin material to the corrosive environment again, which causes further corrosion. The most common example is oxidation wear [94][95].

Within this thesis, wear was measured by so-called ball-on-disc tests in the temperature range between room temperature and 900°C in ambient air as well as in dry and inert atmosphere. Thereby a static alumina ball was pressed onto a rotating disc being the coated substrate. The test results in wear tracks whose volume can be determined using optical methods. From the total volume V of the removed material, the applied load F_{N} and the sliding distance s, a so-called wear coefficient K can be calculated following equation $K = \frac{V}{F_{\mathrm{N}} \times s}$ [97][98].

3.3.2. Wear of TiAlN based coatings

Wear of TiAlN at room temperature (RT) is mainly determined by two parameters. First, the Ti-content and the related tribo-oxidation of Ti at RT and second the surface roughness. The dominant wear mechanism at RT for Ti-based coatings like TiN and TiAlN is reported to be tribo-chemical TiO_2 (rutile) formation. A thin oxide layer, formed in the tribological contact can be easily removed by sliding and exposes virgin material to the atmosphere again. According to Meier zu Köcker et al. who investigated wear of TiAlN against TiAlN, the wear debris consist of TiO_2 and Al_2O_3 [99]. Similar results were also obtained by Vancoille et al. who reported of wear debris of a mixed Al-Ti-oxide [100][101] and Hsieh et al. [102]. This tribo-chemical rutile formation is highly sensitive on the presence of humidity. Moisture accelerates the reaction of Ti and TiN to TiO_2 where in particular the rate constant of oxidation is found to be increased. The result is a higher amount of wear debris formed in humid in comparison to dry atmospheres [104][105]. Furthermore, also the formation of Al_2O_3 as wear debris has been observed and this is also found to be influenced by moisture. Olefjord and Nylund [103] reported on hydration of Al_2O_3 in humid environments. They found that pre-oxidized Al continues to oxidize if exposed to humid atmospheres due to hydration effects. Thus, the formation of oxides in the tribological contact is likely to be promoted by moisture and could enable the easy removal of material by abrasion. This explains the presence of Ti and Al oxides after triblogical tests of TiAlN against TiAlN. However, within this study, it was found that the tribochemical oxidation of Ti is the predominant mechanism of wear at RT. This process has also shown to be extremely sensitive on the presence of moisture which is displayed in Fig. 3.9. The cross sections of wear tracks after tribological tests of a $Ti_{33}Al_{67}N$ hard coating, tested in ambient air can be seen in Fig 3.9a. Increasing the Ti content by testing a $Ti_{40}Al_{60}N$ hard coating leads to increased wear, due to stronger tribo-oxidation of Ti to rutile type TiO_2. The replacement of Ti by 25 at% V (resulting in a $Ti_8Al_{67}V_{25}N$ coating) results in significantly reduced wear (Fig 3.9b). Further reduction of wear can be achieved if oxygen and moisture is removed from the tribo-system by purging with Ar prior and during the tribological test. Detailed studies on that effect by tribological investigations of Ti-Al-Ta-N coatings in ambient air (contains oxygen and humidity), synthetic air (contains oxygen but no humidity) and Ar (no oxygen, no humidity) revealed that especially the presence of moisture is determinant for wear at room temperature (see publication IV). This is in good agreement with already mentioned publications by Konca et al. and others [104][105].

While the Ti content depends only to a minor extent on the deposition parameters, the surface roughness is found strongly dependent on the bias voltage used (see chapter 1). As described earlier, the droplets formed during the deposition cause a cauliflower

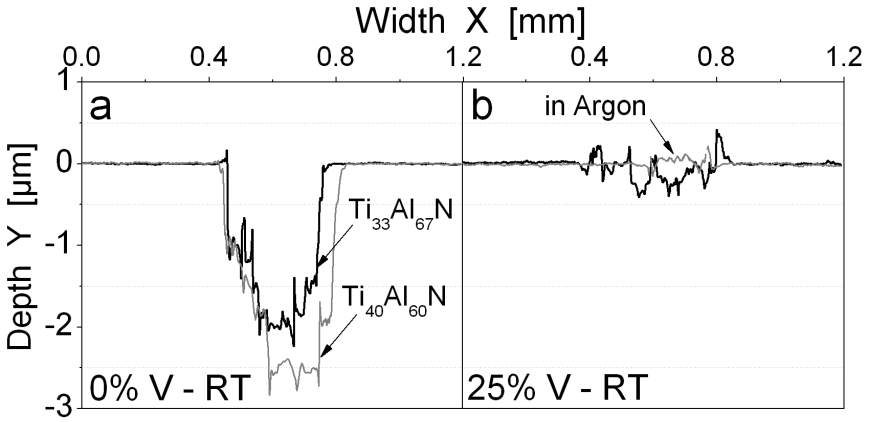

Figure 3.9.: 2D cross-sections of wear tracks of Ti-Al-V-N coatings (V replacing Ti only) plus additional tests in argon atmosphere (from publication II).

like growth structures which leads to sharp, hard surface roughness tips. In early stages of the ball on disc test, these tips act as small cutting edges for the alumina counter material. This leads to significantly higher abrasion of the counter body until the initial surface roughness is removed or flattened. Short-distance experiments revealed that after 20 m sliding the lost volume of the counter body against a rough coating (-40V bias) is increased by factor of 5 in comparison to smoother coatings deposited at higher bias voltages. This higher wear of the counter body has several consequences. First, the area of contact is larger, thus decreasing the Hertzian contact pressure in the tribological contact. Second, the amount of alumina debris in the contact is higher. Thus, the applied load is distributed over more load bearing particles on a larger area of contact. The thereby completely different loading conditions influence the tribological response of the coating. In particular, regardless of differences in mechanical properties (like lower hardness due to lower bias voltage), the rougher coatings shows significantly lower wear after tests at room temperature (see Fig. 3.10 and publication I).

Wear of TiAlN at elevated temperatures In the range up to 500°C, wear is generally found to be very low, which has been published by various authors. For details see also publications I, II and IV and [56][57][107][108]. There are various explanations discussed in literature. One possibility is the change of the ambient atmosphere. Especially the reduced amount of humidity at higher temperatures might play an important role, as described above. In addition, higher toughness and thus reduced fracture probability of

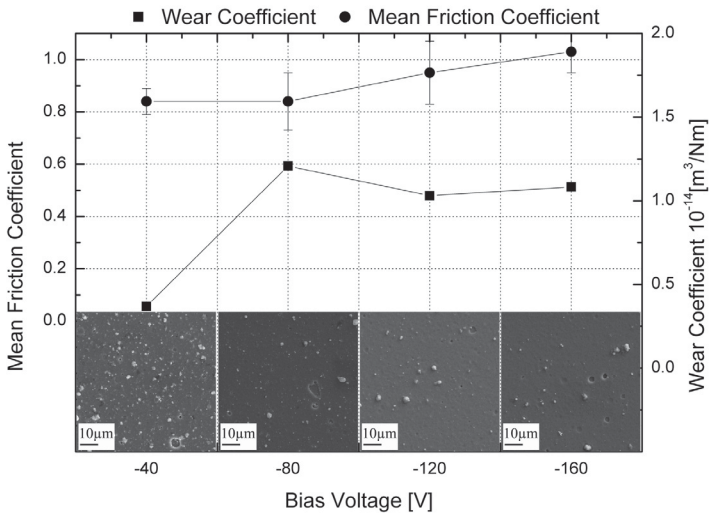

Figure 3.10.: Increased wear of Ti-Al-V-N coatings at room temperature due to surface roughness. Inserts: SEM micrographs of the respective coating surfaces evidencing the different surface roughness (from publication I).

the coatings, as proposed by Beake et al. [106], or the formation of a protective oxide scale in the contact as suggested by Vaz et al. [43] might contribute to the low wear. The surface roughness was found to be an influential parameter on the tribological response of the coatings at 500°C. The already described effect of abrasion of the counter body by surface roughness peaks leads to remarkable changes in the width of the wear tracks, although the wear tracks remain very shallow (see publication I and IV). Furthermore, the coatings resistance to oxidation can play a determinant role for wear at high temperatures. In particular, the temperature where high temperature oxidation begins to govern the wear behaviour depends on the alloying elements and the presence of hcp phases. For instance, the addition of V increases wear already at a temperature range above 500°C. As described before, the onset of oxidation of V containing coatings is reported to be between 520 and 550°C [91][92] and these temperatures are very likely to be exceeded in the tribological contact due to frictional heating and local flash temperatures. Since wear increases with increasing V content, while the friction coefficient remains high (see publication II) it can be assumed that the formed V-rich oxides are neither protective nor lubricating, which is in contrast to reports by others [40][91][92][109]. For TiAlN it was found that in the ranges around 700°C, the presence of hcp phases is governing wear properties, since dual phase structures exhibit a lower resistance to oxidation [43] (see also publication IV). At 900°C rapid oxidation of TiAlN and failure of the coating during the test occurs (see Fig. 3.11). This is not observed for Ti-Al-Ta-N coatings, which exhibit a very high resistance

to oxidation, evidencing that wear at high temperatures is determined mostly by the coatings resistance to oxidation (see publication IV and V).

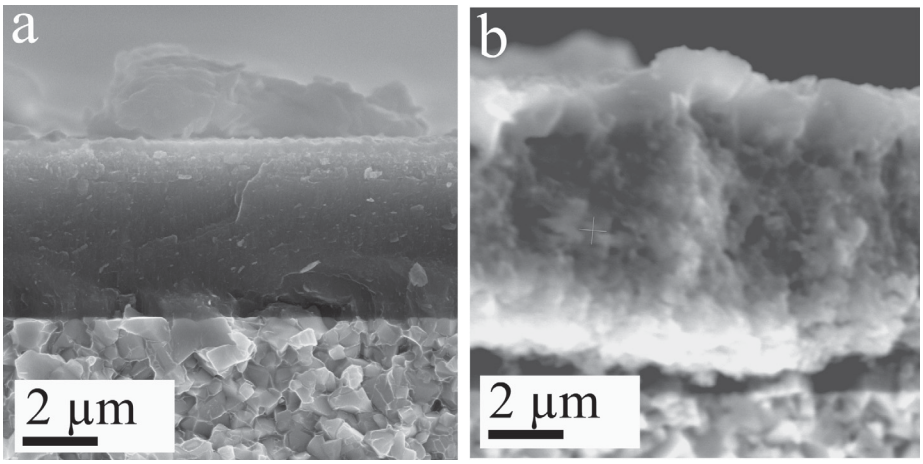

Figure 3.11.: Scanning electron micrographs of (a) Ti-Al-Ta-N and (b) TiAlN coatings after tribological tests at 900°C. TiAlN failed after 20% of the sliding distance (from publication IV).

4. The multilayer approach

4.1. Epitaxy

Epitaxy is the extended growth of a single crystal film on a single crystalline substrate. If the film and the substrate are the same material, it is referred to as *homoepitaxy*. The second type is *heteroepitaxy*, which means that film and substrate are composed of different materials. Except the important case of homoepitaxial growth of Si on a Si substrate, heteroepitaxy is the more common phenomenon in thin film technology. Since in heteroepitaxy, film and substrate are different materials, the respective lattices exhibit a lattice mismatch. Three different cases, referring to the structure of the interface between film and substrate can be distinguished, depending on the extent of lattice mismatch (see Fig. 4.1) [1].

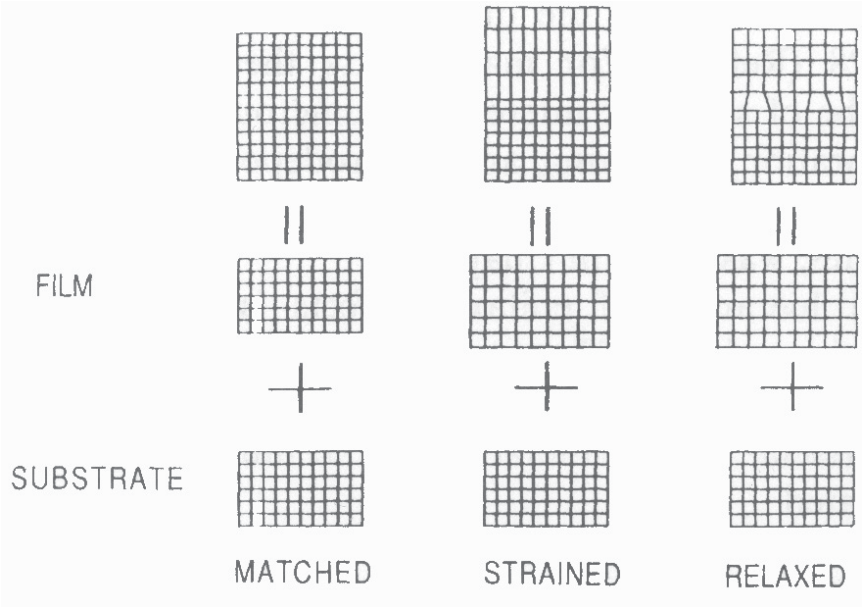

Figure 4.1.: Schematic of lattice-matched, strained and relaxed heteroepitaxial structures. Lattice-matched is structural equal to homoepitaxy [1].

A very small lattice misfit leads to a lattice-matched structure, which becomes a ho-

moepitaxial interface in absence of lattice misfit. If a remarkable misfit is present, there are two possibilities to create a dense interface. First, the lattice parameters are strained in both lattices to accommodate the misfit, leading to a strained structure. Second, if the strained structure cannot be stabilized, misfit dislocation are used to form the interface, which is then referred to as relaxed structure. Strained-layer epitaxy occurs if different materials with the same crystal structure grow on each other. However, the first few layers of the interface normally consist of strained layers in order to match the crystallographic structure of the substrate. This is called pseudomorphic growth and is the reason for the existence of coherent epilayers [1]. This phenomenon can also be observed in multilayered hard coatings and will be discussed in the following section.

4.2. Multilayered hard coatings

The combination of different materials and their beneficial properties in alternating layered structures is a current trend in the industrial application of hard coatings. Multilayers exhibit higher density and finer grains, compared to single layer coatings because the columnar growth is interrupted by the nucleation of the second phase. The higher amount of phase boundaries and interfacial area exhibits the chance for higher hardness and wear resistance [39]. Furthermore, the so-called superlattice effect can lead to a significant hardness enhancement. According to Helmersson et al. [110], hardness of a TiN/VN multilayer increases as the multilayer wavelength is decreased, with a maximum at a multilayer wavelength of 10 nm. Further reduction of the wavelength resulted in loss of hardness. This hardening effect was attributed to differences in the shear modulus between the layer materials due to difference in the dislocation line energy $\sim Gb^2$, where G is the shear modulus and b is the *Burgers vector*. Increasing hardness with decreasing modulation period was also reported by Li et al. [111]. However, according to Long et al. this effect is not generally observed and huge hardness increase is not consistent with the idea of increased dislocation line energy [112]. This is supported by results published by Ljungcrantz et al. [113] who investigated TiN/NbN multilayers with various wavelength by nanoindentation and found no significant influence on hardness or wear resistance.

The growth of multilayered structures can also be used to deposit material with epitaxially stabilized phases. Madan et al. [114] reported on stabilization of fcc AlN in epitaxial TiN/AlN superlattices. Although hcp in the stable configuration and fcc AlN is normally unstable at pressures below 22 bar, it was reported to be possible to stabilize fcc AlN to thicknesses of up to 2 nm. Also Li et al. [111] reported on stabilization of fcc AlN in VN/AlN superlattices up to AlN layer thicknesses of 4 nm. VN acts as a better template layer due to a lower lattice mismatch between VN and AlN in comparison to TiN and

AlN. This so-called *template effect* was also reported by Li et al. [115] on TiN/AlN, by Nordin and Ericson [116] on TiN/TaN multilayers and Larsson et al. [117] on TiN/NbN multilayers.

As a consequence, the utilization of the template effect for TiAlN-based coatings offers another possibility to decrease the fraction of hcp phases by epitaxial stabilization of fcc TiAlN phases. As mentioned before, this only works until a certain thickness of the second layer is reached. This critical thickness depends on the lattice mismatch between the fcc stabilizing layer and the second material. In order to reduce the strain energy between the individual layers, the lattice of the fcc template should exhibit high similarity to the second material. TiAlN with a sufficiently low Al content crystallizes as a single phase fcc structure and has necessarily a high similarity to other TiAlN-based layer materials. Thus, it can act as the perfect fcc-stabilizing template layer for the following, initially dual phase structured, layer (see Fig. 4.2). The substrate rotation during the coating process enables the subsequent alternating deposition of fcc stabilization layers and the second layer. Adjusting the rotation speed allows the generation of sufficiently thin individual layers so that the template effect is not destroyed.

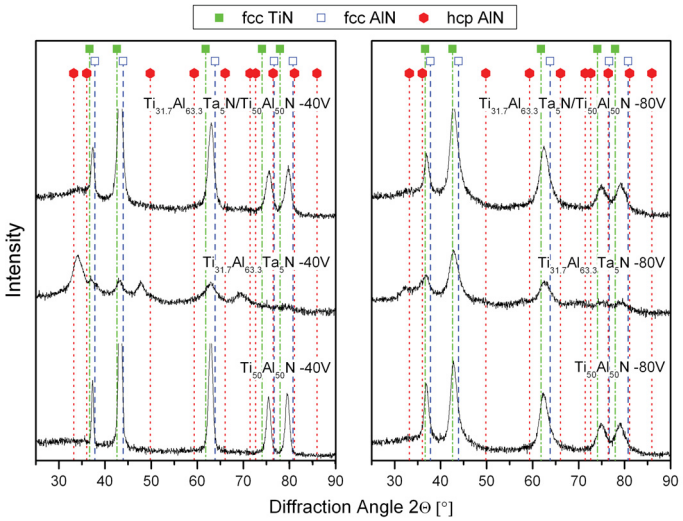

Figure 4.2.: XRD patterns of TiAlN, TiAlTaN and combinations of both in multilayered structures, deposited at -40 V (left) and -80 V (right) bias voltage (own work).

Within this thesis, initially dual phase Ti-Al-V-N has been stabilized by template effect by a $Ti_{50}Al_{50}N$ template up to multilayer wavelengths of 20 nm (see publication VI). Thus, it is possible to hinder the formation of hcp phases with all the related benefits mentioned earlier but without the need of application of higher bias voltage, which has the disadvantage of higher stresses. However, in case the second layer has a high Al content

or hcp promoting alloying elements (e.g. Si or B), the template effect and increased bias voltage can act additively, which means by utilization of the template effect a single phase fcc structure can be reached at lower bias voltages and consequently lower residual stresses. Fig. 4.2 shows the influence of the template effect and the bias voltage for TiAlN/Ti-Al-Ta-N multilayers, investigated by XRD. The left box shows the XRD patterns after depositing at a bias voltage of -40 V, while in the right box, the bias voltage was -80 V. On each side, the two individual layers, i.e. $Ti_{50}Al_{50}N$ and Ti-Al-Ta-N deposited as single layer coatings are shown. The topmost pattern shows the result of the TiAlN/Ti-Al-Ta-N multilayer. The multilayer shows significantly reduced amount of hcp phase. The reduction due to the template effect is also found stronger as the effect of increased bias voltage (compare Ti-Al-Ta-N single layers at -40 and -80V bias). The reduction of hcp phases by the template/multilayer approach was found to be highly beneficial for the mechanical and tribological properties as well as the resistance to oxidation. A detailed discussion can be found in [118].

5. Summary

TiAlN hard coatings for cutting applications are an evolutionary product from TiN and were developed to overcome the shortcomings of its origin. In order to design the next generation of TiAlN based hard coatings, a wide spread approach was conducted within this thesis, including three different fields of optimization. First, the deposition process was optimized by varying the bias voltage during deposition, one of the most influential parameters in PVD processes. Second, the chemical composition was modified by forming the quaternary systems Ti-Al-V-N with high contents of V, Ti-Al-Ta-N with moderate contents of Ta and Ti-Al-B-N and Ti-Al-Si-N with very small amounts of Si and B, respectively. And finally third, the architecture of the hard coating was modified by the deposition of multilayered coatings with the ultimate goal of combining the most beneficial properties, while avoiding the respective weaknesses of the individual layers in one coating. All these aims were conducted in the frame of an industrial scale cathodic arc evaporation process, making the results also directly applicable for the cutting tool industry.

The investigated coatings exhibit a columnar, dense morphology in all cases. If the bias voltage is increased from -40 to -80 V, a significant reduction of surface roughness can be observed. Since the surface roughness is also found an important parameter in early stages of tribological tests, the bias voltage influences the tribological response of the coatings by changing the surface roughness. The solubility limit of Al in TiN for unalloyed TiAlN was found between 50 and 60 at% Al in the target, since $Ti_{40}Al_{60}N$ has a dual phase fcc+hcp structure while $Ti_{50}Al_{50}N$ is single phase fcc. However, the bias voltage offers the possibility to modify the phase composition, i.e. the presence of hcp phases in a wide range from hcp dominated dual phase structures for low bias voltages of -40V to balanced or fcc determined dual phase structures for -80V to fcc single phase structures for -120 to -160V bias voltage. This effects are accompanied by a significant increase in residual compressive stress, hardness and Young´s modulus. Since the hcp phase also exhibits worse resistance to oxidation in comparision to the fcc phase, the overall oxidation resistance is also improved if the bias voltage is increased to -80V. However, it was also observed that the resistance to oxidation deteriorates for the highest bias voltages of -120

and -160 V. The higher defect density or early cracking or delamination due to the higher stresses could be a possible explanation. The tribological response from RT to 500°C is influenced by bias voltage also via the modified surface roughness. Higher surface roughness lead to abrasive wear on the counter body at the very beginning of the test and thus milder loading conditions for the following test. Thus, as a consequence rougher coatings seem to perform better in tribological tests. At high temperatures, higher bias improved the tribological performance of the coatings due to lower content of hcp phases and thus better oxidation resistance.

The crystallographic structure and the related properties are found strongly affected by the addition of alloying elements. Addition of V leads to predominant formation of fcc phases. Furthermore, hardness and Young´s modulus are found increased while the residual stresses decrease. Thus, high V containing Ti-Al-V-N coating offer high mechanical strength combined with low residual stresses. The tribological response at RT is found significantly improved with increasing V content, which might also be connected to the mechanical benefits, but more important is the higher resistance of V to tribo-chemical oxidation in comparison to Ti. So if Ti is replaced by V, mechanical and tribological benefits can be observed. However, at high temperatures Ti-Al-V-N coatings start to oxidize, which is in this thesis not found accompanied by the formation of lubricious oxides. Thus, the friction remains high and rapid decay of the coating is observed in tribological tests at 700°C, which worsens with increasing V content. This limits the applicability of high V containing coatings at elevated temperatures. Ti-Al-Ta-N coatings exhibit comparable mechanical properties as unalloyed TiAlN, although a fcc promoting effect of Ta can be detected. Obviously, the content of Ta is not high enough to foster improvements of the mechanical properties. The same is valid for the tribological response of the coatings up to temperatures of 700°C. However, at 900°C a significantly improved tribological performance can be observed. This is connected to the excellent resistance of this material to high temperature oxidation. Similar observations can also be made for Ti-Al-Si-N and Ti-Al-B-N coatings. The contents of Si and B were low, thus the columnar structure was maintained and the formation of amorphous tissue phases and thus nanocomposites was not observed. Although Si and B promote the formation of the generally undesired hcp TiAlN phase, the mechanical properties do not deteriorate to the extent expected. The reason might be the low content of B and Si, making it more appropriate to speak about Si and B - doped coatings, instead of alloyed ones. However, Si and B are found highly effective elements to improve the high temperature oxidation resistance. The same mechanisms are acting for both elements, however Si-doping is superior over B due to a better stability of the doping effect. In the investigated range, Si-doping leads to comparable results to Ta-alloyed coatings. Consequently it can be said, that Ta and Si alloyed TiAlN

coatings are promising candidates for cutting under severe conditions, where high temperature oxidation governs the wear behaviour. Since both elements improve the oxidation resistance but seem to act via different mechanisms, there is the potential for even higher oxidation resistance by combining both effects in a Ti-Al-Ta-Si-N coating.

The deposition of multilayered coatings was achieved by substrate rotation during the deposition process. Due to the rotation, the substrates are subsequently moved from one target to the other. If the targets differ in composition, a structure with alternating compositions can be deposited. The application of $Ti_{50}Al_{50}N$ as single phase fcc template layer enables the epitaxial stabilization of fcc phases in the second layer and hinders the formation of hcp phases at moderate bias voltages. It has been observed that this template layer has to be a pure single phase structure, since already small amounts of hcp phases in the template layer destroy the desired fcc stabilizing template effect. Thus it was possible to deposit originally dual phase hcp+fcc coatings as single phase fcc or with significantly reduced hcp content which improves the mechanical, tribological and oxidation properties. Furthermore, the template layer can be used as a diffusion barrier, especially for V-containing coatings, where the rapid out-diffusion and oxidation of V destroys the structural integrity of the coating. The TiAlN template layers can act as diffusion barrier which leads to higher resistance to oxidation. This results in a remarkable improvement of the tribological performance of Ti-Al-V-N and widens the temperature range, where V-containing coatings can be applied.

It has been shown, that even if TiAlN-based coatings are well investigated, the field of further development is wide and remarkable improvements can be achieved concerning the composition of the coating and the process it is produced with. Various film properties can be beneficially combined in multilayers under optimized process conditions. Furthermore, the understanding of the role of phases, alloying elements and process parameters enables the production of coatings tailored to a certain application with its specific demands concerning mechanical and tribological properties and oxidation resistance. As a consequence of the observations made and based on the results obtained, two model systems can be suggested which should exhibit significantly higher performance.

1. $Ti_{50}Al_{50}N$ / $Ti_{16.5}Al_{67}V_{16.5}N$

for applications which exhibit moderate thermal loading, because it combines a single phase fcc structure and high mechanical strength with low stresses and the harmful V-outdiffusion is efficiently hindered by a diffusion barrier layer.

2. $Ti_{50}Al_{50}N$ / $Ti_{38}Al_{56}Ta_5Si_1N$

which should exhibit a single phase fcc structure due to reduced Al content with excellent resistance to high temperature oxidation in combination with good mechanical properties. This might be a suitable coating for severe cutting conditions like high speed or dry cutting applications, where high performance materials are needed.

6. The proof of concept

In order to evaluate the application potential of the investigated hard coatings, dry face milling tests were conducted. The results are summarized in Fig. 6.1 and show the performance of different coatings investigated in this thesis. The multilayered systems consist of a $Ti_{50}Al_{50}N$ template layer and a second layer based on alloyed $Ti_{33}Al_{67}N$ or $Ti_{40}Al_{60}N$ (for Ta). The respective compositions are given in at% of the target. The tests were performed with coated SEKN cemented carbide cutting inserts in face milling of steel (DIN 1.7225, 42CrMo4) in dry conditions. The cutting speed was 230 m/min, the feed rate was 0.3 mm and the milling depth was 2 mm. The life time criterion was 0.3 mm wear at the tool flank.

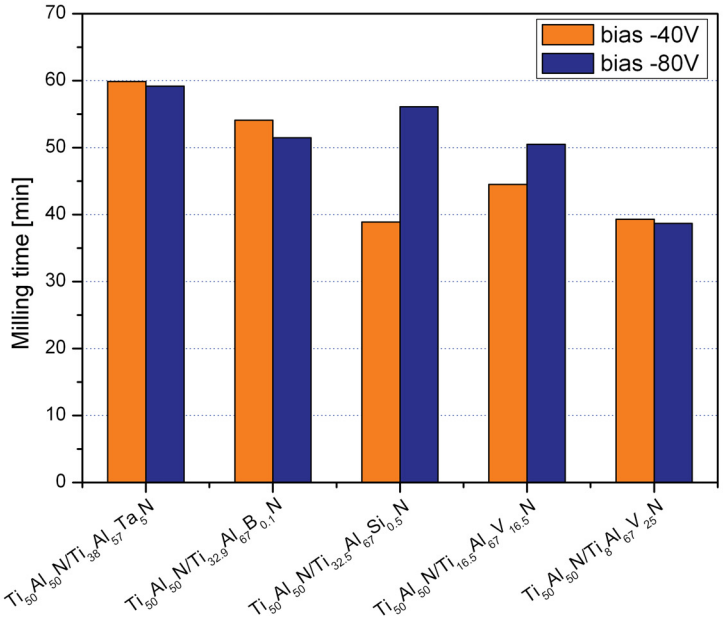

Figure 6.1.: Results of dry face milling tests against steel of various multilayered coatings deposited on SEKN cemented carbide cutting inserts.

The results show that the coatings with the higher resistance to high temperature oxidation (Ta and Si alloyed TiAlN) perform better and in particular the inferior performance of V-containing coatings emphasize the relevance of oxidation resistance. This suggests that the chosen cutting conditions are rather severe and high thermal and oxidative loads are present in the cutting process. Furthermore, the performance of coatings deposited at -40 V bias show that single phase fcc structures (Ta, Si and low V content) are superior compared to dual phase structures. The influence of bias voltage can be interpreted considering the phase composition and residual compressive stresses. Generally, a single phase fcc structure shows superior performance in comparison to dual phase structures. Furthermore, low residual stresses seem to be beneficial for cutting performance in milling as an intermitted process. Thus, for single phase coatings, an increase in bias voltage leads to lower performance because of the higher residual stresses. This can be seen for Ta, Si and high V containing coatings, which are single phase fcc at -40V bias. The low V-content and B-doped TiAlN hard coatings exhibit a dual phase structure at -40V which results in low wear resistance. Increased bias voltage enables a single phase fcc structure with significantly better cutting performance. For those coatings, the benefit of single phase fcc structure overcomes the disadvantage of higher stresses.

Based on these results and conclusions made in the previous chapters, the following criteria should lead to maximum performance for this particular application:

- The template layer must be a fcc single phase structure with good mechanical properties. A good oxidation resistance by alloying is recommended, as long as the single phase fcc structure can be maintained.
- The second layer should exhibit excellent oxidation resistance and good mechanical properties. The composition must be chosen so that epitaxial fcc stabilization by the template layer is possible.
- The bias voltage should be as low as possible to keep the residual stresses low.

Based on these criteria and the results discussed before, the following coating system is suggested for the applied cutting conditions:

$$\mathbf{Ti_{49}Al_{49}Ta_2N\ /\ Ti_{38}Al_{56}Ta_5Si_1N}$$

deposited at -20 V bias voltage.

Bibliography

[1] M. Ohring, *The Materials Science of Thin Films - Deposition and Structure*, 2nd Edition Academic Press, San Diego (2002).

[2] J.M Lafferty in *Handbook of vacuum arc science and technology* edited by R.L. Boxman, D.M. Sanders, P.J. Martin, Noyes Publication, Park Ridge, New Jersey, USA (1995).

[3] J.L. Vossen, W. Kern, Editors, *Thin Film Processes II*, Academic Press, San Diego (1991).

[4] B. Rother, J. Vetter, *Plasma-Beschichtungsverfahren und Hartstoffschichten*, Dt. Ver. für die Grundstoffindustrie, Leipzig (1992).

[5] Fr.-W. Bach, T. Duda, *Moderne Beschichtungsverfahren*, Wiley-VCH, Weinheim (2000).

[6] D. M. Sanders, A. Anders, Surf. Coat. Technol. 133-134 (2000) 78-90.

[7] A. Hörling, L. Hultman, M. Oden, J. Sjölen, L. Karlsson, J. Vac. Sci. Technol. A 20 (5) (2002) 1815-1823.

[8] R.F. Bunshah, Editor, *Handbook of Hard Coatings*, Noyes Publications, Park Ridge, New Jersey (2001).

[9] I. Petrov, P. Losbichler, D. Bergstrom, J.E. Greene, W.-D. Münz et al., Thin Solid Films 302 (1997) 179-192.

[10] D.L. Smith, *Thin-Film Deposition*, McGraw-Hill Inc., (1995).

[11] R. A. Haefer, *Oberflächen und Dünnschicht-Technologie, Teil I*, Springer Verlag Berlin (1987).

[12] B.A. Movchan, A.V. Demchishin, Phys. Met. Metallogr. 28 (1969) 83-90.

[13] J. A. Thornton, Ann. Rev. Mater. Sci. 7 (1977) 239-260.

[14] R. Messier, A.P. Giri, R.A. Roy, J. Vac. Sci. Technol. A 2 (1984) 500-503.

[15] G. Knuyt, C. Quaeyhaegens, J. D´Haen, L.M. Stals, Surf. Coat. Technol. 76-77 (1995) 311-315.

[16] D. Gall, S. Kodambaka, M.A. Wall, I. Petrov, J.E. Greene, J. Appl. Phys. 93 (11) (2003) 9086-9094.

[17] I. Petrov, P.B. Barna, L. Hultman, J.E. Greene, J. Vac. Sci. Technol. A 21 (5) (2003) 117-128.

[18] D. Dobrev, Thin Solid Films 92 (1982) 41-53.

[19] H. Ljungcrantz, L. Hultman, J.-E. Sundgren, J. Appl. Phys. 78 (1995) 832.

[20] A.C. Vlasveld, S.G. Harris, E.D. Doyle, D.B. Lewis, W.-D. Münz, Surf. Coat. Technol. 149 (2002) 217.

[21] M. Odén, J. Almer, G. Håkanson, Surf. Coat. Technol. 120-121 (1999) 272.

[22] B.F. Coll, R. Fontana, A. Gates, P. Sathrum, Mat. Sci. Eng. A140 (1991) 816-824.

[23] W.-D. Münz, J. Vac. Sci. Technol. A 4(6) (1986) 2717-2725.

[24] O. Knotek, M. Böhmer, T. Leyendecker, J. Vac. Sci. Technol. A 4(6) (1986) 2695-2700.

[25] H. Holleck, Surf. Coat. Technol. 36 (1988) 151-159.

[26] R. Cremer, M. Witthaut, D. Neuschütz in Value-Addition *Metallurgy*, The Minerals, Metals & Materials Society, Warrendale (1998) 249-258.

[27] P.H. Mayrhofer, D. Music, J.M. Schneider, J. Appl. Phys. 100 (2006) 1.

[28] H. Willmann, *Al-Cr-N thin film design for high temperature applications*, PhD thesis, Montanuniversität Leoben (2007).

[29] M. Zhou, Y. Makino, M. Nose, K. Nogi, Thin Solid Films 339 (1999) 203-208.

[30] A. Kimura, H. Hasegawa, K. Yamada, T. Suzuki, Surf. Coat. Technol. 120-121 (1999) 438-441.

[31] J. Musil, H. Hruby, Thin Solid Films 365 (2000) 104-109.

[32] J.Y. Rauch, C. Rousselot, N. Martin, Surf. Coat. Technol. 157 (2002) 138-143.

[33] Y. Makino, Surf. Coat. Technol. 193 (2005) 185-191.

[34] P.H. Mayrhofer, A. Hörling, L. Karlsson, J. Sjölén, T. Larsson, C. Mitterer, L. Hultman, Appl. Phys. Lett. 83(10) (2003) 2049-2051.

[35] P.H. Mayrhofer, F.D. Fischer, H.J. Böhm, C. Mitterer, J.M. Schneider, Acta Mat. 55 (2007) 1441-1446.

[36] M. Ahlgren, H. Blomqvist, Surf. Coat. Technol. 200 (2005) 157-160.

[37] K. Sato, N. Ichimiya, A. Kondo, Y. Tanaka, Surf. Coat. Technol. 163-164 (2003) 135-143.

[38] M. Moser, P.H. Mayrhofer, L. Székely, G. Sáfrán, P.B. Barna, Surf. Coat. Technol. 203 (2008) 148-155.

[39] S. PalDey, S.C. Deevi, Mat. Sci. Eng. A342 (2003) 58-79.

[40] K. Kutschej, P.H. Mayrhofer, M. Kathrein, P. Polcik, C. Mitterer, Surf. Coat. Technol. 188-189 (2004) 358-363.

[41] K. Kutschej, P.H. Mayrhofer, M. Kathrein, C. Michotte, P. Polcik, C. Mitterer, in: Kneringer, G., Rödhammer, P., Wildner, H. (eds.) Proceedings of the 16th International Plansee Seminar 2005, vol. 2, pp. 774-788. Plansee Holding AG, Reutte, Tyrol, Austria (2005).

[42] K. Kutschej, N. Fateh, P.H. Mayrhofer, M. Kathrein, P. Polcik, C. Mitterer, Surf. Coat. Technol. 200 (2005) 113-117.

[43] F. Vaz, L. Rebouta, M. Andritschky, M.F. da Silva, J.C. Soares, Surf. Coat. Technol. 98 (1998) 912-917.

[44] S. Veprek, M.J.G. Veprek-Heijman, Surf. Coat. Technol. 202 (2008) 5063-5073.

[45] A.C. Fischer-Cripps, *Nanoindentation* 2nd Edition, Springer, New York (2004).

[46] A.C. Fischer-Cripps, *Introduction to Contact Mechanics*, Springer, New York (2000).

[47] J. Gunnars, U. Wiklund, Mat. Sci. Eng. A336 (2002) 7-21.

[48] P.H. Mayrhofer, *Material science aspects of nanocrystallinge pvd hard coatings* PhD thesis, Montanuniversität Leoben (2001).

[49] J.E. Sundgren, H.T.G. Hentzell, J. Vac. Sci. Technol. A 4 (5) (1986) 2259-2279.

[50] P.J. Burnett, D.S. Rickerby, Thin Solid Films 148 (1987) 515-65.

[51] M.F. Ashby, D.R.H. Jones, *Key Engineering Materials 1* 2nd Edition, Butterworth Heinemann, Oxford, (1996).

[52] J. Wagner, *Chemical vapor deposition of titanium nitride based hard coatings*, PhD thesis, Montanuniversität Leoben (2007).

[53] G. Gottstein, *Physikalische Grundlagen der Materialkunde* Springer, Berlin (2007).

[54] J.A. Thornton, D.W. Hoffman, Thin Solid Films 171 (1989) 5-31.

[55] Y. Tanaka, T.M. Gür, M. Kelly, S.B. Hagstrom, T. Ikeda, K. Wakihira, H. Satoh, J. Vac. Sci. Technol. A 10 (4) 1749-1756.

[56] K. Kutschej, P.H. Mayrhofer, M. Kathrein, P. Polcik, R. Tessadri, C. Mitterer, Surf. Coat. Technol. 200 (2005) 2358-2365.

[57] M. Pfeiler, C. Mitterer, P.H. Mayrhofer, D. Caliskanoglu, W. Kölker, R. Pitonak, in N. Rosso, M. Actis Grande, D. Ugues (Eds.), Tooling Materials and their Application from Research to Market, vol. 1, Politecnico di Torino, Italy, 2006, p.411.

[58] S. Carvalho, L. Rebouta, E. Ribeiro, F. Vaz, M.F. Denannot, J. Pacaud, J.P. Riviere, F. Paumier, R.J. Gaboriaud, E. Alves, Surf. Coat. Technol. 177-178 (2004) 369-375.

[59] S. Carvalho, E. Ribeiro, L. Rebouta, C. Tavares, J.P. Mendonca, A. Caetano Monteiro, N.J.M. Carvalho, J.Th.M. De Hosson, A. Cavaleiro, Surf. Coat. Technol. 177-178 (2004) 459-468.

[60] M.A. Baker, S. Klose, C. Rebholz, A. Leyland, A. Matthews, Surf. Coat. Technol. 151-152 (2002) 338-343.

[61] C. Rebholz, J.M. Schneider, A.A. Voevodin, J. Steinebrunner, C. Charitidis, S. Logothetidis, A. Leyland, A. Matthews, Surf. Coat. Technol. 113 (1999) 126-133.

[62] D. Rafaja, A. Poklad, V. Klemm, G. Schreiber, D. Heger, M. Sima, M. Dopita, Thin Solid Films 514 (2006) 240-249.

[63] D. Rafaja, A. Poklad, V. Klemm, G. Schreiber, D. Heger, M Sima, Mat. Sci. Eng. A462 (2007) 279-282.

[64] O. Knotek, T. Leyendecker, F. Jungblut, Thin Solid Films 153 (1987) 83-90.

[65] O. Knotek, M. Böhmer, T. Leyendecker, F. Jungblut, Mat. Sci. Eng. A 105-106 (1988) 481-488.

[66] P.W. Atkins, J.A. Beran, *General Chemistry*, Scientific American Books, New York, (1992).

[67] N. Birks, G.H. Meier, *Introduction to High Temperature Oxidation of Metals*, Edward Arnold Ltd, London, (1983).

[68] D.A. Jones, *Principles and Prevention of Corrosion*, Prentice Hall, Upper Saddle River, New Jersey, (1996).

[69] J. Zechner, *Oxidation Behavior of Ti-Al-Si-N and Ti-Al-B-N Coatings*, diploma thesis, Montanuniversität Leoben (2008).

[70] O. Knotek, W.D. Münz, T. Leyendecker, J. Vac. Sci. Technol. A 5 (4) (1987) 2173-2179.

[71] M. Wittmer, J. Noser, H. Melchior, J. Appl. Phys. 52 (11) (1981) 6659-6664.

[72] L. Hultman, Vacuum 57 (2000) 1-30.

[73] D. McIntyre, J.E. Greene, G. Håkansson, J.-E. Sundgren, W.-D. Münz, J. Appl. Phys. 67 (3) (1990) 1542-1553.

[74] H. Ichimura, A. Kawana, J. Mater. Res. 8 (5) (1993) 1093-1100.

[75] S. Inoue, H. Uchida, Y. Yoshnaga, K. Koterazawa, Thin Solid Films 300 (1997)171-176.

[76] S. Hofmann, Thin Solid Films 193-194 (1990) 648-664.

[77] A. Joshi, H.S. Hu, Surf. Coat. Techol. 76-77 (1995) 499-507.

[78] F. Vaz, L. Rebouta, M. Andritschky, M.F. da Silva, J.C. Soares, J. Europ. Cer. Soc. 17 (1997) 1971-1977.

[79] M.I. Lembke, D.B. Lewis, W.D. Münz, J.M. Titchmarsh, Surf. Eng. 17 (2) (2001) 153-158.

[80] F. Rovere, P.H. Mayrhofer, A. Reinholdt, J. Mayer, J.M. Schneider, Surf. Coat. Technol. 202 (24) (2008) 5870-5875.

[81] J. Jedlinski, Oxid. Met. 39 (1/2) (1993) 55-60.

[82] G. He, Q. Fang, L. Zhu, M. Liu, L. Zhang, Chem. Phys. Lett 395 (2004) 259-263.

[83] S.X. Wu, Y.J. Liu, X.J. Xing, X.L. Yu, L.M. Xu, Y.P. Yu, S.W. Li, J. Appl. Phys. 103 (2008) 063517.

[84] A.A. Gribb, J.F. Banfield, Am. Mineral. 82 (1997) 717-728.

[85] H. Zhang, J.F. Banfield, J. Mater. Chem. 8 (9) (1998) 2073-2076.

[86] P. Steyer, D. Pilloud, J.F. Pierson, J.-P. Millet, M. Charnay, B. Stauder, P. Jacqout, Surf. Coat. Technol. 201 (2006) 4158-4162.

[87] D. Pilloud, J.F. Pierson, M.C. Marco de Lucas, A. Cavaleiro, Surf. Coat. Technol. 202 (2008) 2413-2417.

[88] S. Veprek, M.G.J. Veprek-Heijman, P. Karvankova, J. Prochazka, Thin Solid Films 476 (2005) 1-29.

[89] R.G. Reddy, Y. Li, M.F. Arenas, High Temperture Materials and Processes 21 (4) (2002) 195-205.

[90] C. Leyens, Oxidation behaviour of titanium alloys and titanium aluminides, in *Titanium and Titanium Alloys*, C. Leyens, M. Peters, Wiley-VCH (2003) 207-209.

[91] G. Gassner, P.H. Mayrhofer, K. Kutschej, C. Mitterer, M. Kathrein, Tribol. Lett. 17 (2004) 751-756.

[92] P.H. Mayrhofer, P.Eh. Hovsepian, C. Mitterer, W.-D. Münz, Surf. Coat. Technol. 177-178 (2004) 1731-1737.

[93] G.W. Stachowiak, A.W. Batchelor, *Engineering Tribology*, 2nd Edition, Butterworth-Heinemann, Boston (2001).

[94] E. Rabinovicz, *Friction and Wear of Materials*, John Wiley and Sons, Inc., New York (1965).

[95] I.M. Hutchings, *Tribology: Friction and Wear of Engineering Materials* Edward Arnold, London (1992).

[96] N.P. Suh, H.-C. Sin, Wear 69 (1981) 91-114.

[97] K. Holmberg, A. Matthews, *Coatings Tribology: Properties, Techniques and Applications in Surface Engineering*, vol. 28 of Tribology Series, Elsevier, Amsterdam, (1994).

[98] R. Franz, *AlCrVN - Design of high-temperature low-friction coatings*, PhD thesis, Montanuniversität Leoben (2007).

[99] G. Meier zu Köcker, T. Gross, E. Santner, Wear 179 (1994) 5-10.

[100] E. Vancoille, B. Blanpain, Y. Xingpu, J.-P. Celis, J.R. Roos, J. Mater. Res. 9 (4) (1994) 992-998.

[101] E. Vancoille, J.-P. Celis, J.R. Roos, Wear 165 (1993) 41-49.

[102] J.H. Hsieh, A.L.K. Tan, X.T. Zeng, Surf. Coat. Technol. 201 (2006) 4094-4098.

[103] I. Olefjord, A. Nylund, Surf. Interface Anal. 21 (1994) 290-297.

[104] E. Konca, Y.-T. Cheng, A.M. Weiner, J.M. Dasch, A. Erdemir, A.T. Alpas, Surf. Coat. Technol. 200 (2005) 2260-2270.

[105] H. Mohrbacher, B. Blanpain, J.-P. Celis, J.R. Roos, Wear 180 (1995) 43-52.

[106] B.D. Beake, J.F. Smith, A. Gray, G.S. Fox-Rabinovich, S.C. Veldhuis, J.L. Endrino, Surf. Coat. Technol. 201, (2007) 4585-4593.

[107] H. Ohnuma, N. Nihira, A. Mitsuo, K. Toyoda, K. Kubota, T. Aizawa, Surf. Coat. Technol. 177-178 (2004) 623-626.

[108] M.H. Staia, M. D´Alessandria, D.T. Quinto, F. Roudet, M. Marsal Astort, J. Phys. Condens Matter 18 (2006) 1727-1736.

[109] K. Kutschej, P.H. Mayrhofer, M. Kathrein, P. Polcik, C. Mitterer, Surf. Coat. Technol. 200 (2005) 1731-1737.

[110] U. Helmersson, S. Todorova, S.A. Barnett, J.-E. Sundgren, L.C. Markert, J.E. Greene, J. Appl. Phys. 62 (2) (1987) 481-484.

[111] G. Li, J. Lao, J. Tian, Z. Han, M. Gu, J. Appl. Phys. 95 (1) (2004) 92-96.

[112] Y. Long, F. Giuliani, S.J. Lloyd, J. Molina-Aldareguia, Z.H. Barber, W.J. Clegg, Composites: Part B 37 (2006) 542-549.

[113] H. Ljungcrantz, C. Engström, L. Hultman, M. Olsson, X. Chu, M.S. Wong, W.D. Sproul, J. Vac. Sci. Technol. A 16 (5) (1998) 3104-3113.

[114] A. Madan, I.W. Kim, S.C. Cheng, P. Yashar, V.P. Dravid, S.A. Barnett, Phys. Rev. Lett. 78 (9) (1997) 1743-1746.

[115] Q. Li, I.W. Kim, S.A. Barnett, L.D. Marks, J. Mater. Res. 17 (5) (2002) 1224-1231.

[116] M. Nordin, F. Ericson, Thin Solid Films 385 (2001) 174-181.

[117] M. Larsson, P. Hollman, P. Hedenqvist, S. Hogmark, U. Wahlström, L. Hultman, Surf. Coat. Technol. 86-87 (1996) 351-356.

[118] J. Radanitsch, *Alloying of (Ti,Al)N single and multi-layer thin films*, diploma thesis, Montanuniversität Leoben, in final preparation (2008-2009).

Part II.

Publications related to the topic

List of included publications

I. The influence of bias voltage on structure and mechanical/tribological properties of arc evaporated Ti-Al-V-N coatings,
M. Pfeiler, K. Kutschej, M. Penoy, C. Michotte, C. Mitterer, M. Kathrein,
Surface & Coatings Technology 202 (2007) 1050-1054.

II. The effect of increasing V content on structure, mechanical and tribological properties of arc evaporated Ti-Al-V-N,
M. Pfeiler, K. Kutschej, M. Penoy, C. Michotte, C. Mitterer, M. Kathrein,
Int. Journal of Refractory Metals & Hard Materials (2008) in press.

III. Improved oxidation resistance of TiAlN coatings by doping with Si or B,
M. Pfeiler, J. Zechner, M. Penoy, C. Michotte, C. Mitterer, M. Kathrein,
Surface & Coatings Technology (2008), in submission.

IV. Arc evaporation of Ti-Al-Ta-N coatings: The effect of bias voltage and Ta on high-temperature tribological properties,
M. Pfeiler, G.A. Fontalvo, J. Wagner, K. Kutschej, M. Penoy, C. Michotte, C. Mitterer, M. Kathrein,
Tribology Letters 30(2) (2008) 91-97.

V. On the effect of Ta on improved oxidation resistance of Ti-Al-Ta-N coatings,
M. Pfeiler, C. Scheu, H. Hutter, J. Schnöller, C. Michotte, C. Mitterer, M. Kathrein,
final preparation.

VI. Wavelength modulation of TiAlN - Ti-Al-V-N multilayers by various substrate rotation speeds,
M. Pfeiler, P.H. Mayrhofer, K. Kutschej, M. Penoy, C. Michotte, C. Mitterer, M. Kathrein,
concept for potential publication.

Supervised diploma theses

I. *J. Wagner*, Structural, mechanical and tribological properties of TiAlN and Ti-Al-Ta-N coatings, Leoben, 2007.

II. *J. Zechner*, Oxidation behavior of Ti-Al-Si-N and Ti-Al-B-N coatings, Leoben, 2008.

III. *J. Radanitsch*, Alloying of TiAlN single and multi-layer thin films, Leoben, 2009 (in final preparation).

My contribution to included publications

	Conception and planning[1]	Experiments	Analysis and interpretation	Manuscript preparation[1]
Publication I	100	80	70	100
Publication II	100	80	90	100
Publication III	100	40	90	100
Publication IV	100	70	80	100
Publication V	100	33	60	100
Publication VI	100	70	90	100

[1]Supervision not included

Publication I

Surface & Coatings Technology 202 (2007) 1050-1054

The influence of bias voltage on structure and mechanical/tribological properties of arc evaporated Ti-Al-V-N coatings

by

M. Pfeiler, K. Kutschej, M. Penoy, C. Michotte, C. Mitterer, M. Kathrein

1. Introduction

Although TiAlN is well established as hard coating for cutting applications, the last years revealed an increasing demand for further developments of this coating system by e.g. addition of alloying elements or process optimisation. Most of the time, these approaches aim on the improvement of mechanical properties, oxidation resistance or tribological behaviour, i.e. increasing wear resistance and/or lowering the coefficient of friction [1-4].

A lot of effort has been done in the last years to decrease the coefficient of friction at elevated temperatures. The addition of V to TiAlN by forming a TiAlN/VN multilayer or a Ti-Al-V-N solid solution provides a possible way to decrease the coefficient of friction from 0.8 - 1.0 to reported values of around 0.3 at 700°C. This is caused by the formation of orthorhombic Me_nO_{3n-1} Magnéli phase oxides, (e.g. V_2O_5) which are known to decrease the coefficient of friction due to the presence of easy shearable planes. Additionally, the predominantly formed V_2O_5 offers a low onset of melting around 660°C which further contributes to the drop of the coefficient of friction due to part liquid lubrication. [5,6,26]. Moreover, it has been reported that V enhances the hardness due to incorporation in the face-centered cubic (fcc) TiAlN lattice forming a Ti-Al-V-N solid solution [6].

The bias voltage during the coating process is a highly influential parameter because it controls the energy of the impacting ions. Therefore, it also is a well described tool to influence several coating properties. Petrov et al. reported on the energy of the impinging ions influencing the predominant orientation of TiN and TiAlN [7]. With increasing ion energy, the texture changes from (111) to (200). Moreover, the bombardment causes continuous re-nucleation due to disturbance of the local epitaxial growth. Ljungcrantz et al. reported on the influence of the bias voltage on the residual stresses [8]. At low bias voltages from 0 to -100 V, residual compressive stress increases due to an increase of defect density. At bias voltages of -150 V and above, the ion bombardment induced mobility of atoms was the predominant effect. This causes decreasing residual stresses because of enhanced annihilation of defects. Sato et al. reported that with increasing bias voltage the Al content in TiAlN coatings decreased, whereas residual compressive stresses and hardness increased up to -100 V, and decreased for bias voltages above [9]. Similar results were also published by others [3,10].

The aim of the present work was to deposit V-containing coatings by cathodic arc evaporation in order to investigate the effect of the bias voltage on the Ti-Al-V-N coating system in an industrial scale coating process. While the effect of lubricious oxides on friction in the temperature range between 550 and 700°C is well described [6], we concentrate here on the relation between structure, chemical composition and mechanical properties, i.e. hardness, Young's modulus and wear resistance at room temperature and 500°C.

2. Experimental details

An industrial scale cathodic arc evaporation facility, type Balzers RCS, was used to deposit the coatings. The coating facility has been described more accurately in [11,12]. Powder metallurgically produced targets ($Ti_{16.5}Al_{67}V_{16.5}$) were used to deposit four coatings at bias voltages of -40, -80, -120 and -160 V in an Ar/N_2 atmosphere. For comparison, unalloyed TiAlN coatings were deposited using a $Ti_{33}Al_{67}$ target. The deposition temperature was 450°C for all runs. The coatings were deposited onto three different substrates: Cemented carbide (CC) SNUN cutting inserts (grade S40T) were used for glow discharge optical emission spectroscopy (GDOES), for glancing angle X-ray diffraction (GAXRD) and for the determination of hardness and Young's modulus. Tribological tests were performed on CC discs (Ø 30 × 4 mm, grade TSM33), whereas for the evaluation of residual stresses, single-crystal Si (100) samples (21 × 7 × 0.38 mm) were used.

The resulting layer thickness was assessed by the ball-crater technique (CSM Instruments Calowear). The chemical composition of the coatings was evaluated by GDOES, using a Horiba / Jobin-Yvon JY-10000RT facility. Crystallographic investigations were

performed by GAXRD (Panalytical X´Pert Pro) applying Cu Kα radiation at an angle of incidence of 2°. Hardness and Young's modulus of the coatings were assessed by nano-indentation using a CSIRO ultra micro indentation system (UMIS-2) with a Berkovich indenter. Due to high surface roughness, the samples were polished for 5 min with 1 μm diamond suspension prior to the measurement. Indentations were conducted from 2 to 50mN maximum load. This resulted in maximum penetration depths of 365 nm which was less than 10% of the coating thickness (5.5 - 8 μm) for all coatings. To evaluate hardness and Young's modulus, correction of compliance, initial penetration and contact area were applied to the raw data. Residual stresses were determined by laser-assisted curvature measurement and application of Stoney's formula [13].

The tribological behaviour was investigated by dry sliding tests at room temperature and 500°C on a CSM high-temperature ball-on-disc tribometer. The normal load, sliding speed, pre-heating time, sliding distance and radius of wear track were kept constant at 5 N, 10 cm/s, 90 min, 300 m and 7 mm, respectively. All tests were performed in ambient atmosphere at a relative humidity of 35±5% against an alumina ball (Ø 6 mm). The resulting wear tracks were investigated using a 3D profiling system (Wyco NT1000 white light profilometer). A scanning electron microscope (SEM, ZEISS EVO 50) with energy-dispersive X-ray analysis (EDX, Oxford Instruments Inca) was used to investigate the coating surface and the wear tracks.

3. Results and discussion

Fig.1.1 shows the influence of the bias voltage on the crystallographic structure of Ti-Al-V-N coatings. At -40 V, the deposition resulted in a dual-phase fcc + hcp (hexagonal close-packed) structure. Peaks of the hcp phase can be detected at 32.32, 34.92, 48.62 and 70.03°. With increasing bias voltage, the fraction of the hcp phase decreases until at -160 V a single-phase fcc structure is obtained. The vanishing of the hcp phase might be a result of the Al content decreasing from 65.2 at% at -40 V to 63.3 at% at -160 V. This range of Al content has repeatedly been reported as the region where the hcp phase appears first if the Al content in TiAlN is increased. According to literature, this transition zone, from fcc to fcc + hcp, is located between 63 and 65 at% Al [15,16]. In addition, enhanced ad-atom mobility is induced, caused by the increased energy of the ion bombardment due to the higher bias voltage. Recent calculations of Mayrhofer et al. [15] indicate that the phase stability of fcc TiAlN is determined by the number of Ti-Al bonds in the fcc lattice.

The energy of formation is lowest if the number of Ti-Al bonds is also low. This can be obtained if Ti atoms are predominantly surrounded by Ti atoms and vice versa for

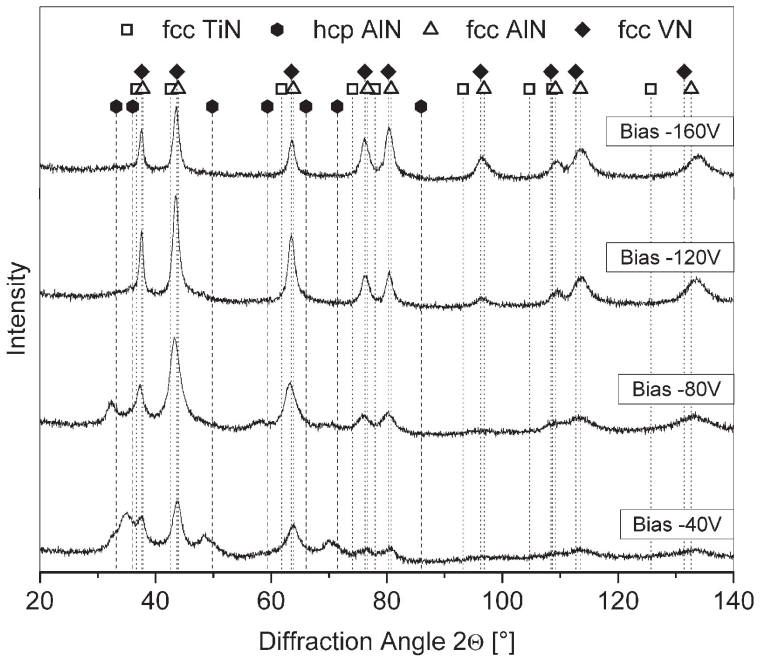

Figure 1.1.: GAXRD patterns of Ti-Al-V-N coatings deposited at different bias voltages.

Al. To ensure this, Al- and Ti-rich regions within the same fcc lattice must be formed. An increased mobility of the ad-atoms might promote the formation of this low-energy configuration with low amount of Ti-Al bonds, leading to an enhanced solubility limit of Al in the fcc TiN lattice. Additionally, collision cascade effects might have a decreasing influence on the survival rate of hcp nuclei on the surface of the growing film. Both effects are assumed to promote the predominant growth of the fcc phase with increasing ion energy, i.e. bias voltage. Furthermore, the increase in compressive stresses with increasing bias voltage can hinder the growth of the less dense hcp phase, compared to the denser fcc phase. A correlation between residual stresses and the presence of hcp phase has also been published by Zhou et al. [17]. Compared to TiAlN, it can be further concluded that V reduces the tendency to form the hcp phase [19,24].

With increasing bias voltage the distribution of orientations becomes more homogeneous, since the peaks at higher angles get more pronounced. According to Petrov et al., this is caused by the higher energy of the impinging ions causing larger defect densities with elevated bias voltages and disturbing the local epitaxial growth of individual grains. Therefore, re-nucleation with random orientation occurs yielding a more homogeneous distribution of orientations [7]. The resulting predominant (100) texture is probably caused by collision cascade effects. According to Dobrev [14], crystals with open channel directions (e.g. 100) have a higher probability of survival caused by the larger penetration

depth of the impacting ions and the energy of the ion is distributed over more atoms. Thus, the ion bombardment induced gain of energy per atom and the destabilising effect of the bombardment is lower.

The dependence of hardness, Young's modulus and residual stresses on the applied bias voltage is shown in Fig.1.2. The residual compressive stress increases from around -0.4 GPa at -40V up to -1.5 GPa at -80 V. However, it remains more or less constant for the higher voltages between -80 and -160V. The increase in residual compressive stress with increasing bias voltage is a well reported phenomenon [10,18]. According to Ljungcrantz et al. it is caused by the increase in defect density due to the ion bombardment. This ion bombardment causes two concurrent effects. First, it increases the defect density. Second, it also increases the ad-atom mobility and diffusivity and thus the ability of annihilation of defects [8]. From -40 to -80 V bias, the process of generating defects seems predominant whereas from -80 to -160 V creation and annihilation of defects seem to balance each other; the residual stresses are not further increased. Similar results were also obtained for TiAlN by Odén et al. [10].

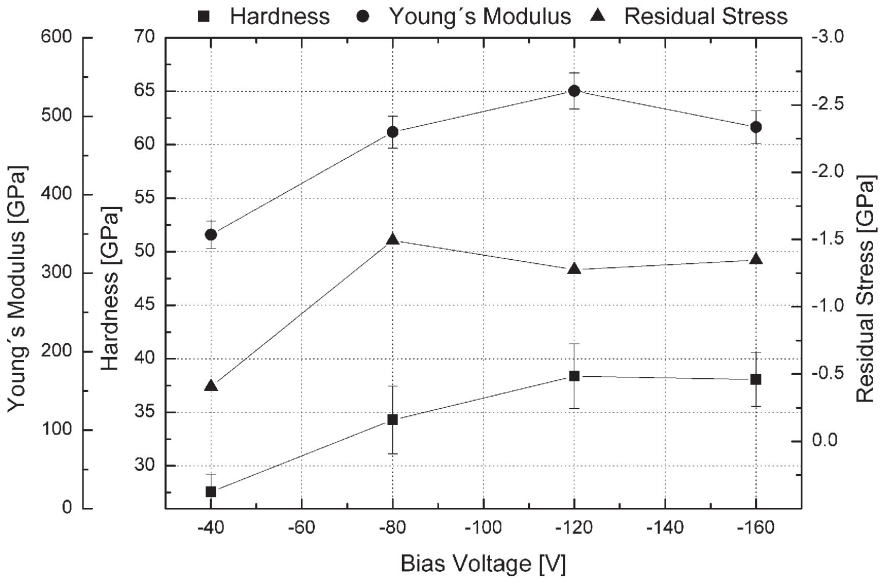

Figure 1.2.: Young´s modulus, hardness and residual compressive stress of Ti-Al-V-N coatings vs. bias voltage.

The hardness of the coatings increases with increasing bias voltage from 27.6 GPa at -40 to 38 GPa at -120 V . Between -120 and -160 V it remains nearly constant at 38 GPa. The dual phase fcc + hcp structure present at low bias voltages exhibits lower hardness values than the single-phase fcc structure formed at high bias voltages (compare

Fig.1.1). Thus, it can be concluded that the increase in hardness is connected with the vanishing of the hcp phase. The rapid decrease in hardness with the appearance of the hcp phase has been published by various authors [17,19,20]. Additionally, the increase of the compressive stresses also contributes to the increase in hardness [3,21].

Hardness and Young's modulus exhibit the same trends with increasing bias voltage. The major increase of the Young's modulus appears between -40 and -80 V (349 to 480 GPa), followed by a smaller increase to -120 V (532 GPa) and a more or less constant value thereafter. Structural changes are the most probable reason for this behaviour. Mayrhofer et al. published calculated bulk and elastic moduli for TiAlN with much lower values for the hcp phase than for the fcc phase [15]. Thus, it can be concluded that also the increase of the Young's modulus is connected with the vanishing of the hcp phase.

Fig.1.3 summarizes with the tribological behaviour of the investigated coatings at room temperature. The coefficient of friction is 0.85 for bias voltages of -40 V and increases slightly up to 1.0 for -160 V, which is in the same range as for unalloyed TiAlN. The wear coefficient is lowest at -40 V (0.37×10^{-14} m^3/Nm) and increases up to 1-1.2×10^{-14} m^3/Nm for the elevated bias voltages, which is about half of the values of unalloyed TiAlN ($\sim$ 2×10^{-14} m^3/Nm).

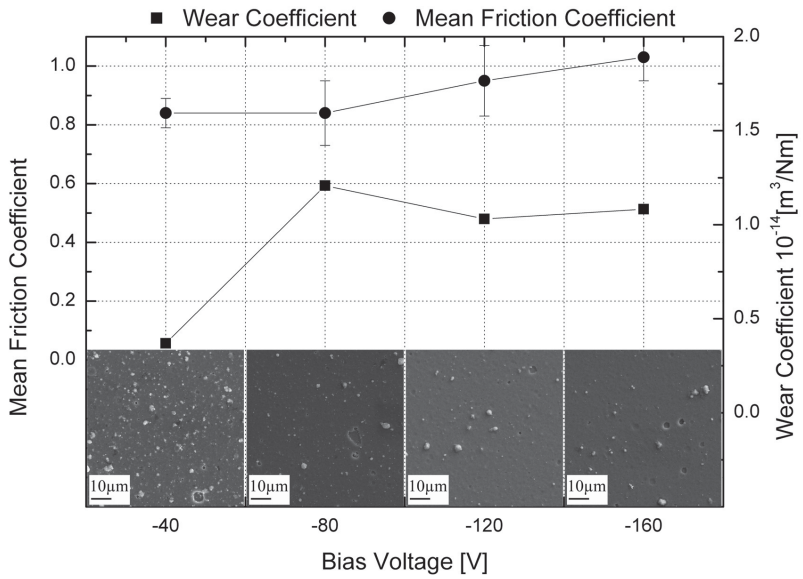

Figure 1.3.: The influence of the bias voltage on the wear and mean friction coefficient of Ti-Al-V-N coatings at room temperature. Inserts: SEM micrographs of the respective coating surfaces in the as-deposited state evidencing the different droplet density.

This result is surprising with respect to the increase in hardness with increasing bias voltage, since higher hardness normally causes less negative wear due to increased abrasion resistance [22]. Here, it is assumed that the difference in the negative wear volume is connected with the interaction of droplets or droplet generated roughness on the surface and the alumina counter body. The droplet density is significantly higher at -40 V than in case of -80, -120 and -160 V (see inserts in Fig.1.3). EDX analysis of the cauliflower featured droplets observed on the coating surface showed the same composition as the matrix, thus similar hardness of these defective surface areas and the undisturbed coating surface is expected. In case of local contacts between the alumina ball and the droplets (or the coating area grown above the droplets), the droplets may act as small cutting edges for the ball. Thus, with higher droplet density a significantly higher abrasion of the alumina counter body occurs until the droplets are flattened and coating and ball get into full contact. Short-distance experiments (20 m, not shown here) resulted in 5 times higher worn ball volume against the coating deposited at -40 compared to -160 V. Thus, after the droplets are flattened, much alumina debris is present for the 40 V coating actually separating ball and coating and distributing the load over more particles. The higher wear of the ball also enlarges the contact area, thus decreases the Hertzian contact pressure. Furthermore, the alumina debris represents softer particles compared to the hard coating surface, which causes less wear of the coating [22]. At elevated bias voltages, a significantly lower amount of droplets is generated; thus no pronounced abrasion of the alumina ball at early stages of the experiment occurs, which debris may protect the surface. Moreover, the load is distributed over a smaller contact area resulting in the high wear volumes shown in Fig.1.3.

The friction coefficients obtained at 500°C are very similar to room temperature since lubricious oxide formation occurs at temperatures above 550°C [19]. 2D cross-sections of the wear tracks after tribological tests at 500°C, gained by optical profilometry are shown in Fig.1.4. The respective wear track of the test is located between x-values of 0.6 and 1.3 mm. From x-values of 0 to 0.6 and 1.3 to 1.9 the unaltered surface of the coating can be seen. Obviously, none of the four coatings showed significant amounts of negative wear after the sliding experiment. For coatings deposited at -40 V, a build-up of material at the edge of the wear track can be seen. This is probably transfer material from the alumina ball, since there is almost no negative wear of the coating detectable. Similar to the room temperature tests, the initial presence of droplets, acting as cutting edges, might be the reason for the increased abrasion of the ball and thus the origin of the transfer material. The depth of all wear tracks is less than 100 nm, thus, essentially only smoothening of the surface roughness occurred. The effect of highly reduced wear at enhanced temperatures has already been described for TiAlN coatings as a result of a protective alumina layer,

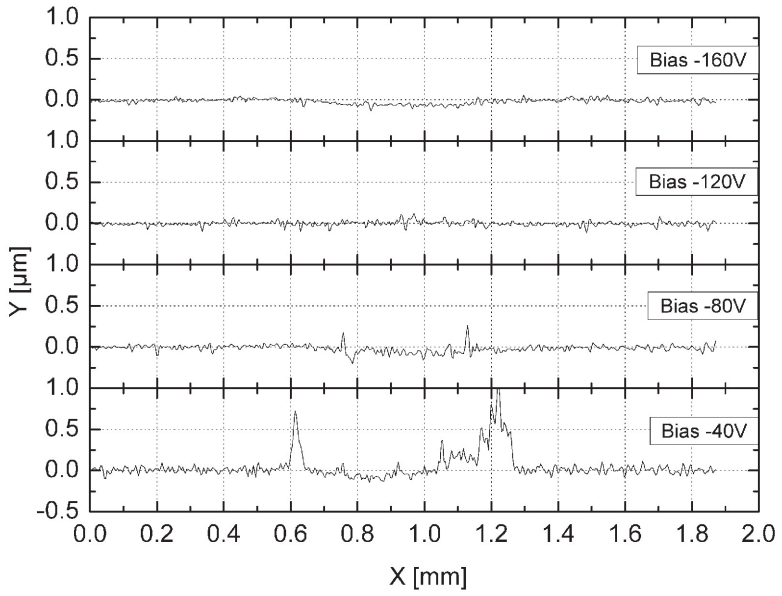

Figure 1.4.: 2D cross-sections of wear tracks after dry sliding experiments against alumina at 500°C for Ti-Al-V-N coatings deposited at different bias voltages.

formed during the experiment [4,19,23,25]. The alumina layer separates efficiently the coating from the ball; thus alumina against alumina sliding occurs, which protects the coating itself of further wear.

4. Conclusions

Four Ti-Al-V-N coatings were deposited by cathodic arc evaporation, using different bias voltages of -40, -80, -120 and -160 V. The structure changed from a dual phase fcc+hcp structure at -40 V to a single-phase fcc structure for coatings deposited at -160 V. This altered structure explains changes of mechanical properties. Hardness and Young's modulus increased up to values of 37 GPa and 532 GPa, respectively, due to vanishing of the hcp phase with increasing bias voltage. Residual compressive stresses increased from -0.4 to -1.3 GPa with increasing bias voltage due to an increased generation of defects by the higher energy of bombarding ions. Wear after room temperature dry sliding tests was affected by the droplet density present on the surface, which decreased with increasing bias voltage. Droplets act as small cutting edges and cause pronounced abrasion of the alumina counter body in early stages of the sliding test leading to less wear of the rougher coating. Wear at 500°C was found to be low for all coatings because of a suspected

formation of a protective alumina layer on the coating during heating and testing.

The results presented here show the potential of V alloying of TiAlN coatings and the major influence of the bias voltage which offers the ability of tailoring the microstructure and thus mechanical and tribological properties.

Acknowledgment

Financial support by the Austrian Kplus Competence Center Programme is gratefully acknowledged.

References

[1] K. Kutschej, N. Fateh, P.H. Mayrhofer, M. Kathrein, P. Polcik, C. Mitterer, Surf. Coat. Technol. 200 (2005) 113.
[2] I.-W. Park, S. R. Choi, J.H. Suh, C.-G. Park, K.H. Kim, Thin Solid Films 447-448 (2004) 443.
[3] M. Ahlgren, H. Blomqvist, Surf. Coat. Technol. 200 (2005) 157.
[4] M. Pfeiler, C. Mitterer, P.H. Mayrhofer, D. Caliskanoglu, W. Koelker, R. Pitonak, in Tooling Materials and their Applications from Research to Market, (N. Rosso, M. Actis Grande, D. Ugues, eds.), Politecnico di Torino, Italy, 2006, Vol. 1, pp. 411-418.
[5] P.H. Mayrhofer, P.Eh. Hovsepian, C. Mitterer, W.-D. Münz, Surf. Coat. Technol. 177-178 (2004) 341.
[6] K. Kutschej, P.H. Mayrhofer, M. Kathrein, P. Polcik, C. Mitterer, Surf. Coat. Technol. 188-189 (2004) 358.
[7] I. Petrov, P.B. Barna, L. Hultman, J.E. Greene, J. Vac. Sci. Technol. A 21 (2003) 117.
[8] H. Ljungcrantz, L. Hultman, J.-E. Sundgren, J. Appl. Phys. 78 (1995) 832.
[9] K. Sato, N. Ichimiya, A. Kondo, Y. Tanaka, Surf. Coat. Technol. 163-164 (2003) 135.
[10] M. Odén, J. Almer, G. Håkansson, Surf. Coat. Technol. 120-121 (1999) 272.
[11] O. Durand-Drouhin, A.E. Santana, A. Karimi, V.H. Derflinger, A. Schütze, Surf. Coat. Technol. 163-164 (2003) 260.
[12] A.E. Santana, A. Karimi, V.H. Derflinger, A. Schütze, Surf. Coat. Technol. 177-178 (2004) 334.
[13] J. Gunnars, U. Wiklund, Mat. Sci. Eng. A 336 (2002) 7.
[14] D. Dobrev, Thin Solid Films 92 (1982) 41.
[15] P.H. Mayrhofer, D. Music, .J.M. Schneider, J. Appl. Phys. 100 (2006) 1.
[16] R. Cremer, K. Reichert, D. Neuschütz, Surf. Coat. Technol. 142-144 (2001) 642.
[17] M. Zhou, Y. Makino, M. Nose, K. Nogi, Thin Solid Films 339 (1999) 203.
[18] A.C. Vlasveld, S.G. Harris, E.D. Doyle, D.B. Lewis, W.-D. Münz, Surf. Coat. Technol. 149 (2002) 217.
[19] K. Kutschej, P.H. Mayrhofer, M. Kathrein, P. Polcik, R. Tessadri, C. Mitterer, Surf. Coat. Technol. 200 (2005) 2358.
[20] A. Kimura, H. Hasegawa, K. Yamada, T. Suzuki, Surf. Coat. Technol. 120-121 (1999) 438.
[21] G. Håkansson, J.-E. Sundgren, D. McIntyre, J.E. Greene, W.-D. Münz, Thin Solid Films 153 (1987) 55.

[22] I.M. Hutchings, Tribology - Friction and Wear of Engineering Materials, Edward Arnold, London, 1992, p.135.
[23] H. Ohnuma, N. Nihira, A. Mitsuo, K. Toyoda, K. Kubota, T. Aizawa, Surf. Coat. Technol. 177-178 (2004) 623.
[24] A.E. Santana, A. Karimi, V.H. Derflinger, A. Schütze, Thin Solid Films 469-470 (2004) 339.
[25] D. McIntyre, J.E. Greene, G. Håkansson, J.-E. Sundgren, W.-D. Münz, J. Appl. Phys. 67 (1990) 1542.
[26] G. Gassner, P.H. Mayrhofer, K. Kutschej, C. Mitterer, M. Kathrein, Tribol. Lett. 17 (2004) 751.

Publication II

Int. Journal of Refractory Metals & Hard Materials (2008)
in press

The effect of increasing V content on structure, mechanical and tribological properties of arc evaporated Ti-Al-V-N coatings

by

M. Pfeiler, K. Kutschej, M. Penoy, C. Michotte, C. Mitterer, M. Kathrein

1. Introduction

Although TiAlN is a highly successful coating due to its excellent mechanical properties and wear resistance [1-3], further demands like increased productivity in cutting processes are the driving force for further developments based on TiAlN coatings.

For high-speed and dry cutting applications, low coefficients of friction or self-lubrication properties in combination with high hardness and wear resistance are required. The addition of V as a TiAlN/VN multilayered structure or as Ti-Al-V-N provides a possible way to decrease the coefficient of friction down to reported values of 0.2-0.3 at temperatures around 700°C [4,5]. This low-friction effect is based on the formation of the lubricious oxide V_2O_5, which exhibits easy shear-able planes and a low melting point. This could enable solid and liquid lubrication effects [6]. Furthermore, it has been reported that the addition of V increases hardness of Ti-Al-V-N due to solid solution hardening of the face-centered cubic Ti-Al-V-N phase [7].

The aim of the present work was to deposit Ti-Al-V-N coatings with various V content by an industrial-scale cathodic arc evaporation process. While the effect of lubricious

oxides on the tribological behaviour of Ti-Al-V-N between 550 and 700°C is well investigated [4,5,7], a study on systematically varied V content and its impact on the coating properties between room temperature (RT) and 500°C is missing. This work adds more knowledge to this field, where in particular, we concentrate on the relation between chemical composition, structure and mechanical properties, i.e. hardness, Young's modulus and wear resistance of Ti-Al-V-N coatings.

2. Experimental

An industrial-scale cathodic arc evaporation facility, type Oerlikon Balzers RCS, was used to deposit the coatings. Four different coatings were produced from powder metallurgically produced targets ($Ti_{33-x}Al_{67}V_x$) with V-contents of x = 0, 16.5, 20 and 25 at% in an Ar/N_2 atmosphere. The bias voltage was -40 V and the deposition temperature was 450°C for all runs. The coatings were deposited onto three different substrates: Cemented carbide (CC) SNUN cutting inserts were used for glow discharge optical emission spectroscopy (GDOES), for glancing angle X-ray diffraction (GAXRD) and for the determination of hardness and Young's modulus. Tribological tests were performed on CC discs (Ø 30 × 4 mm), whereas for the evaluation of residual stresses, single-crystal Si (100) samples (21 × 7 × 0.38 mm) were used.

The resulting layer thickness was assessed by the ball-crater technique (CSM Instruments Calotest). The chemical composition of the coatings was evaluated by GDOES, using a Horiba Jobin-Yvon JY-10000RT facility. Crystallographic investigations were performed by GAXRD (Panalytical X´Pert Pro) applying Cu Kα radiation at an angle of incidence of 2°. Hardness and Young's modulus of the coatings were assessed by nanoindentation using a UMIS ultra-micro indentation system with a Berkovich indenter. Due to high surface roughness in the as-deposited state, the samples were polished for 5 min with 1 μm diamond suspension prior to the measurement. Indentations were conducted from 2 to 50 mN maximum load. This resulted in a maximum penetration depth of 365 nm which was always less than 10% of the coating thickness (4 - 5.3 μm). To evaluate hardness and Young's modulus, correction of compliance, initial penetration and contact area were applied to the raw data. Residual stresses were determined by laser-assisted curvature measurement and application of Stoney´s formula [8].

The tribological behaviour was investigated by dry-sliding tests at RT and 500°C on a CSM high-temperature ball-on-disc tribometer. The normal load, sliding speed, preheating time, sliding distance and radius of wear track were kept constant at 5 N, 10 cm/s, 90 min, 300 m and 7 mm, respectively. All tests were performed in ambient atmosphere at a relative humidity of 35±5% against an alumina ball (Ø 6 mm). Additional tests

have been performed in a modified atmosphere after purging the chamber with argon for several hours until a relative humidity $\leq 2\%$ was reached. The resulting wear tracks were investigated using a 3D profiling system (Wyko NT1000 white light profilometer).

3. Results and discussion

3.1 Microstructure

The results of XRD investigations on Ti-Al-V-N coatings are displayed in Fig. 2.1. It should be noted that we will use the V contents in the target to distinguish the individual coatings. The pattern on the bottom shows results of unalloyed TiAlN, while the other patterns show the influence of increasing V content. All four coatings were found to have a dual-phase structure with face-centred cubic (fcc) and hexagonal close-packed (hcp) phases. With increasing V content, the fcc peaks are shifted to higher angles, which is connected to a smaller unit cell, due to substitution of Ti by V in the fcc TiN based unit cell. Furthermore, the fcc peaks, e.g. the one at $\sim 43°$, become sharper, suggesting an increase in crystallinity. While in the unalloyed TiAlN coating the hcp structure is dominating with a relatively low fcc content, the fraction of the hcp phase decreases with increased addition of V and the system becomes fcc determined. This can be seen especially by the reduced intensities of the hcp peaks at 34.32° and 48.08°.

The reduction of hcp phase with increasing V content can be explained by calculations according to Makino [9]. In this paper a critical Al content was defined, which represents the solubility limit of Al in the respective fcc phase. The published results indicate that fcc VN has a higher solubility of Al. The critical Al content in VN for the fcc/hcp phase transition is predicted at 72.4% Al, while the critical content of Al in fcc TiN should be 65.3% Al, which is in good agreement with experimental data. Consequently, with increasing substitution of Ti by V, the critical Al content increases, the tendency for the fcc/hcp phase transition is reduced and the fraction of hcp phase decreases.

3.2 Mechanical properties

The dependence of residual compressive stress, hardness and Young's modulus on the V content is shown in Fig. 2.2. With increasing V content, the compressive stress is reduced from 690 MPa for unalloyed TiAlN to 330 MPa for 25 at% V. This can be attributed to differences in the lattice mismatch between the fcc phases TiN, AlN and VN. While the lattice mismatch between TiN and AlN is 2.95%, it is only 0.46% between VN and AlN. Therefore, with increasing VN and thus, decreasing TiN content, the overall lattice mismatch decreases resulting in reduced residual stresses.

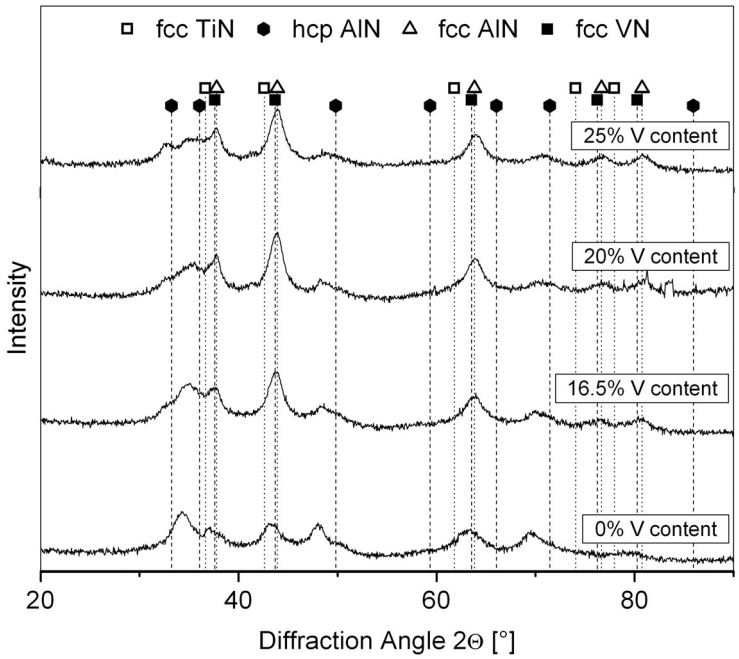

Figure 2.1.: XRD patterns of Ti-Al-V-N coatings with V content ranging from 0 to 25 at%.

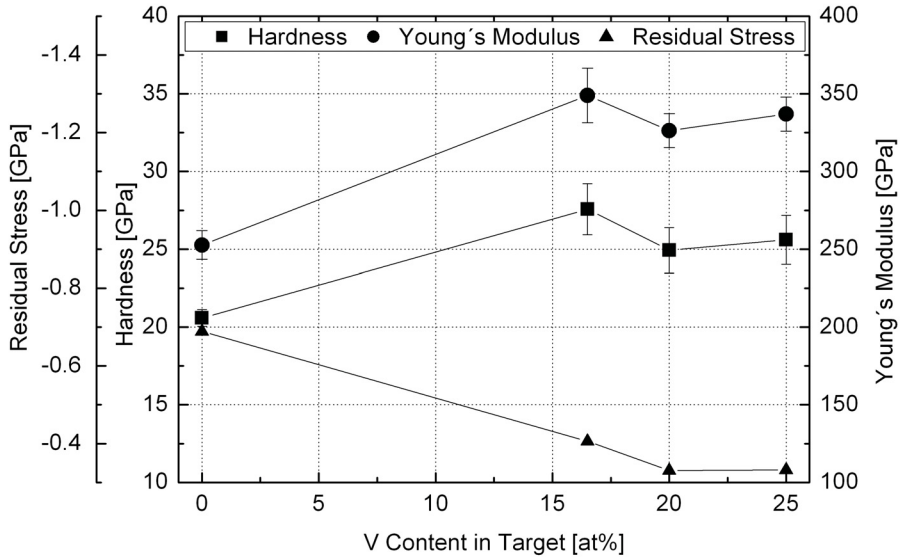

Figure 2.2.: Young's modulus, hardness and residual compressive stress of Ti-Al-V-N coatings vs. V content.

The hardness of the coatings increases from 21 GPa for 0 at% V to 27.5 GPa for 16.5 at% V and slightly decreases for higher V contents. The Young's modulus follows the same trend as the hardness and increases from 250 to 350 GPa. The reduced hcp phase fraction and the lower residual compressive stresses are the most probable reasons for this effect. A reduction of the hcp phase has been frequently reported to increase hardness [10-12]. On the contrary, lower compressive stresses in the coating have been reported to decrease hardness and Young's modulus [10, 13]. This means that two competing effects are present. The decreased fraction of the hcp phase increases hardness, while the decreasing residual stresses reduce the hardness of the coatings. Between 0 and 16.5 at% V, the reduction of hcp phase fraction is the predominant effect which causes a significant hardness enhancement. The slight loss in hardness at higher V content is then caused by the reduced residual compressive stress which seems to be able to balance or even overcome the hardness increasing effect of the hcp phase suppression.

Calculations of bulk and elastic moduli of fcc and hcp phases within the TiAlN system by Mayrhofer et al. indicated much higher values for the fcc phase [14]. Thus, it can be concluded that the behaviour of Young's modulus with increasing V content is also connected to the vanishing of the hcp phase and the reduced residual stresses.

3.3 Tribological properties

The resulting friction coefficients were 0.7 - 0.8 at RT and 0.9 - 1.0 at 500°C for all samples, which corresponds to results published by Kutschej et al. [7]. The results of the wear investigations at RT and 500°C are shown in Figs. 2.3 - 2.5. The 2D cross-sections of the wear tracks after tests at RT are displayed in Fig. 2.3a-d. With increasing V content, decreasing depth of the wear tracks is observed. Two different effects might cause this behaviour. First, for Ti based coatings like TiN and TiAlN, it has been reported that an important tribo-chemical wear mechanism at RT can be TiO_2 (rutile) formation. Meier zu Köcker et al. investigated wear debris after tribological investigations of TiAlN against a TiAlN coated pin and found them to consist of TiO_2 and Al_2O_3 [15]. Vancoille et al. reported on tribological investigations of TiAlN against corundum. The wear debris consisted of a mixed Al-Ti-oxide [16]. With increasing V fraction the reduced content of Ti and thus the less pronounced tribo-chemical formation of rutile-based oxides might be suitable to explain the higher wear resistance, i.e. reduced abrasion with increasing V content.

This tribo-chemical oxide formation is also known to be strongly influenced by humidity. The presence of moisture accelerates the transformation of Ti and TiN to TiO_2, i.e. the rate constant of oxidation is higher [17]. Similar results were also obtained by Konca et al. [18]. They stated that the reduction of oxygen and water vapour in the tribological

contact reduces the amount of wear debris formed.

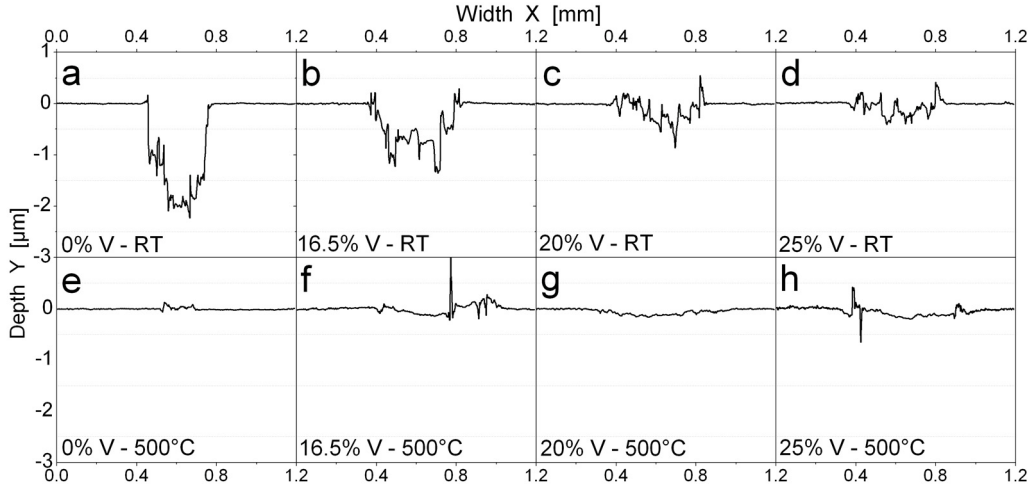

Figure 2.3.: 2D cross-section of wear tracks of Ti-Al-V-N coatings deposited at various V content after tribological tests at (a-d) RT and (e-h) 500°C.

If it is assumed that the controlling parameters in the wear of TiAlN and Ti-Al-V-N coatings at RT are the Ti content and the environment, i.e. presence of oxygen and moisture, a coating with a higher Ti content should suffer higher wear. Furthermore, a reduction of oxygen and/or humidity in the atmosphere during the test should prevent or decrease abrasive wear. This could be confirmed by tests of a $Ti_{40}Al_{60}N$ reference material (see Fig. 2.4a), which resulted in maximum wear of all coatings while in tribological tests of Ti-Al-V-N coatings in Ar atmosphere, wear was almost prevented (see Fig. 2.4b). Thus, it can be concluded that the tribological behaviour of Ti-Al-V-N coatings at RT is determined by tribo-chemical reactions between Ti and the environment.

Furthermore, increased hardness is also reported to lead to better wear resistance [19]. Thus both, the reduced tribo-chemical reactions and the increased hardness with increased V content are responsible for the lower wear coefficients of high V-containing Ti-Al-V-N at RT (see Fig. 2.5).

The results of tribological tests at 500°C, i.e. the 2D cross-sections of the wear tracks, are shown in Fig. 2.3e-h. At 500°C wear is generally low and the wear tracks are very shallow. Without V in the coating, no abrasive loss of material is detectable, which has frequently been reported in literature [11,20]. As the results at RT indicate, this might be connected with the reduced amount of moisture in the tribological contact during sliding at 500°C. Consequently, moisture-related tribo-chemical reactions should be significantly

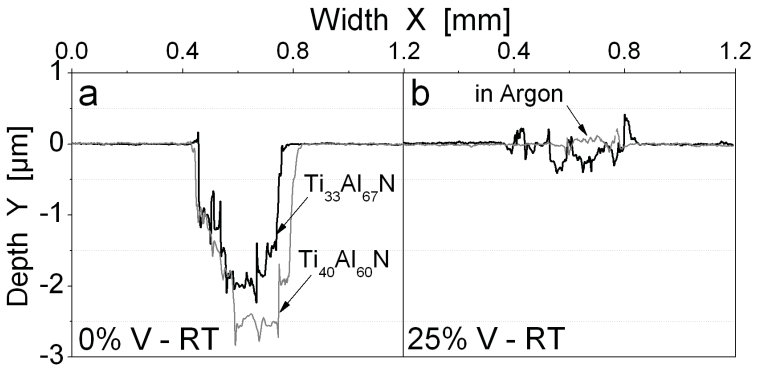

Figure 2.4.: 2D cross-section of wear tracks of Ti-Al-V-N coatings plus additional tests with increased Ti content and in argon atmosphere.

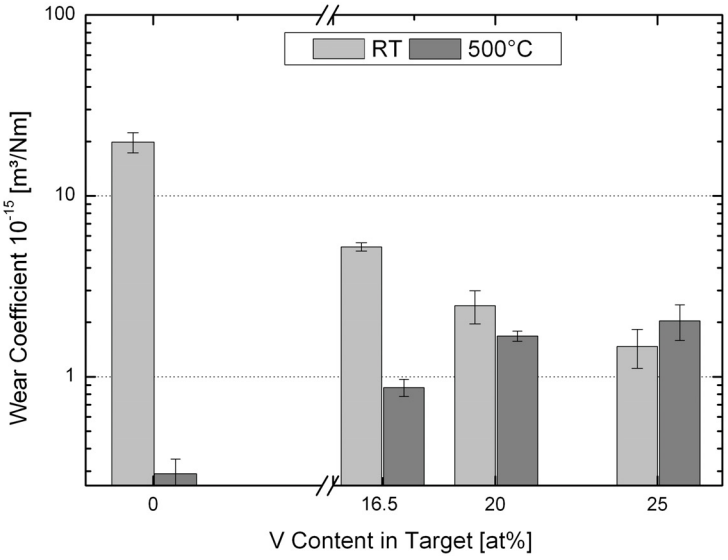

Figure 2.5.: The influence of V content on abrasive wear, tested at RT and 500°C.

decreased, leading to reduced wear. In addition, the higher wear resistance at 500°C, in comparison to RT, might be supported by the reduced fracture probability at elevated temperatures [21]. Vaz et al. stated the presence of a protective Al_2O_3-rich layer in the contact as reason for the prevented abrasion at 500°C [22].

With increased V content a clear trend towards increased wear track width and thus higher wear coefficients can be detected (see Fig. 2.5). The wear resistance at 500°C might be influenced by the reduced coatings resistance to oxidation with increasing V content. Gassner et al. reported on investigations on oxidation of VN coatings, where the onset of oxidation was at 520°C [6]. Similar results were reported of investigations on the oxidation of TiAlN/VN superlattice coatings by Mayrhofer et al. Rapid oxidation was detected by differential scanning calorimetry at temperatures around 550°C, which is related to the formation of V-oxides [4]. In our case, incipient oxidation during the tribological tests at 500°C is observed by intensified coloration of the samples with increasing V content. However, the mentioned temperatures for rapid oxidation are likely to be exceeded in the tribological contact during sliding due to frictional heating and local flash temperatures. Thus, the tribo-chemical formation of V-oxides can also be expected for the Ti-Al-V-N coatings investigated in this work. Since wear increases with increased V content, it can be concluded that the oxides formed in this temperature range are neither protective, nor lubricating. Results from literature on tribology of V and VN indicate that at 500°C the formed oxide layers are too thin to act as a protective layer [23]. The oxidized material is pushed out of the contact and exposes previously un-oxidized coating to the atmosphere again. With increasing V-content, this process is likely to gain importance, which fosters abrasion with increasing V content. Consequently, the wear coefficient increases with increasing V content (see Fig. 2.5).

4. Conclusions

In Ti-Al-V-N coatings deposited by cathodic arc evaporation, increasing V-content reduces the fraction of hexagonal phases in the dual-phase (fcc/hcp) structure. The tribological behaviour at room temperature is determined by tribo-chemical reactions between Ti and the environment. The presence of humidity and Ti especially promotes rutile formation which increases wear. With increasing V content, i.e. decreasing Ti content or in Ar atmosphere, wear is significantly decreased. At elevated temperatures, this effect is of minor importance due to lack of moisture in the tribological contact. Wear at 500°C is generally reduced in comparison to RT and determined by oxidation of V which leads to the formation of not load-bearing oxides which are easily removed during sliding. Thus, wear increases with increasing V content.

The results show that alloying of TiAlN with V improves the resistance to wear at lower temperatures up to high V contents of 25 at%. On the contrary, at 500°C, which is in the range of the onset temperature of oxidation of V, the wear resistance of the coating deteriorates with increasing V content.

Acknowledgment

Financial support by the Austrian Kplus Competence Center Programme is gratefully acknowledged.

References

[1] PalDey S, Deevi SC. Mat. Sci. Eng. A 2003; 342: 58-79

[2] Knotek O, Böhmer M, Leyendecker T., J. Vac. Sci. Technol. A 1986; 4 (6): 2695-2700

[3] Coll BF, Fontana R, Gates A, Sathrum P., Mat. Sci. Eng. A 1991; 140: 816-824

[4] Mayrhofer PH, Hovsepian PEh, Mitterer C. Münz W-D., Surf. Coat. Technol. 2004; 177-178: 341-7

[5] Kutschej K, Mayrhofer PH, Kathrein M, Polcik P, Mitterer C., Surf. Coat. Technol. 2005; 200: 1731-7

[6] Gassner G, Mayrhofer PH, Kutschej K, Mitterer C, Kathrein M., Trib. Lett. 2004; 17: 751-6

[7] Kutschej K, Mayrhofer PH, Kathrein M, Polcik P, Mitterer C., Surf. Coat. Technol. 2004;188-189: 358-363

[8] Gunnars J, Wiklund U., Mat. Sci, Eng. A 2002; 336: 7-21

[9] Makino Y., Surf. Coat. Technol. 2005; 193: 185-191

[10] Pfeiler M, Kutschej K, Penoy M, Michotte C, Mitterer C, Kathrein M., Surf. Coat. Technol. 2007; 202: 1050-4

[11] Kutschej K, Mayrhofer PH, Kathrein M, Polcik P, Tessadri R, Mitterer C., Surf. Coat. Technol 2005; 200: 2358-2365

[12] Ohuma H, Nihira N, Mitsuo A, Toyoda K, Kubota K, Aizawa T., Surf. Coat. Technol. 2004; 177-178: 623-6

[13] Sato K, Ichimiya N, Kondo A, Tanaka Y., Surf. Coat. Technol. 2003; 163-164: 135-143

[14] Mayrhofer PH, Music D, Schneider, JM., J. Appl. Phys. 2006; 100: 1-5

[15] Meier zu Köcker G, Gross T, Santner E., Wear 1994; 179: 5-10

[16] Vancoille E, Celis JP, Roos JR., Wear 1993; 165: 41-9

[17] Mohrbacher H, Blanpain B, Celis JP, Roos JR., Wear 1995; 180: 43-52

[18] Konca E, Cheng Y-T, Weiner AM, Dasch JM, Erdemir A, Alpas AT., Surf. Coat. Technol. 2005; 200: 2260-2270

[19] Hutchings IM. Tribology - Friction and Wear of Engineering Materials, Edward Arnold, London,

(1992) 135

[20] Staia MH, D'Alessandria M, Quinto DT, Roudet F, Marsal Astort M., J. Phys. Condens. Matter 2006; 18: 1727-1736

[21] Beake BD, Smith JF, Gray Al, Fox-Rabinovich GS, Veldhuis SC, Endrino JL., Surf. Coat. Technol. 2007; 201: 4585-4593

[22] Vaz F, Rebouta L, Andritschky M, da Silva MF, Soares JC., Surf.Coat.Tech 1998; 98: 912-7

[23] Fateh N, Fontalvo GA, Gassner G, Mitterer C., Trib. Lett. 2007; 28: 1-7

Publication III

Surface & Coatings Technology (2008)
in submission

Improved oxidation resistance of TiAlN coatings by doping with Si or B

by

M. Pfeiler, J. Zechner, M. Penoy, C. Michotte, C. Mitterer, M. Kathrein

1. Introduction

In the last years, application of wear-resistant hard coatings based on titanium aluminium nitride (TiAlN) has been rapidly growing. TiAlN is highly successful as hard coating for many cutting applications, due to its good wear and oxidation resistance. However, the demand of high-speed cutting and/or minimum lubricant cutting leads to a constant improvement of the coating system and the process it is produced with [1-3]. The addition of further elements in order to gain certain properties can be achieved in different ways, like the deposition of multilayered structures of different transition metal nitrides or as solid solution of the type Ti-Al-X-N [4-6]. Alloying elements like Si or B can lead to the formation of an amorphous Si_3N_4 or BN phase surrounding nanocrystalline TiAlN grains and forming so-called nanocomposites (see [1] and references therein). Carvalho et al. reported on a Ti-Al-Si-N nanocomposite, containing up to 18 at% Si. They detected an amorphous Si_3N_4 phase surrounding nanocrystalline TiAlN grains which enhances mechanical properties [7,8]. The structure of TiAlN/Si_3N_4 coatings was also investigated by Rafaja et al. who reported on arc evaporated Ti-Al-Si-N coatings. The amorphous Si_3N_4 phase which separates the nanocrystalline grains prevents the partial coherency

found between individual grains within clusters of nanocrystalline TiAlN. Once a certain silicon (and aluminium) content is exceeded, the crystallites become non-coherent because the high silicon content hinders the coherency of the crystallites [9]. Since coherency stresses, i.e. intrinsic stresses at the crystallite boundaries, are also described as a possible origin of hardness enhancement, the tissue phase observed can also lead to decreased hardness if a critical thickness is exceeded [10]. Furthermore, for CrAlSiN it was observed that already small amounts of Si change the texture of the coatings. This was related to the amorphous Si_3N_4 phase, which obstructs coherency between neighbouring crystallites during growth [11].

Earlier publications by Vaz et al. indicated also an improvement of the oxidation resistance by the addition of Si to TiAlN [12]. An improvement of the resistance against oxidation of TiN by the addition of Si was already reported in 1995 by Veprek et al. [13]. Furthermore, Veprek et al. found that the addition of Si to TiAlN improves the high temperature stability of the coating. The beneficial effect of Si is connected with the already mentioned amorphous Si_3N_4 tissue, which prevents the decomposition of TiAlN into Ti-rich face-centered cubic (fcc) and Al-rich hexagonal close-packed (hcp) phases, thus avoiding the associated softening of the coating [14].

More recently, the addition of relatively small amounts of Si in the deposition of arc evaporated Ti-Si-N was reported to improve the oxidation resistance, which is connected to a modified oxidation sequence of titanium. After oxidation of Ti-Si-N, the fraction of anatase type TiO_2 increased in the oxide scale at the expense of rutile type TiO_2 with increasing Si content in the coating [15,16].

Likewise, also the addition of B was found to cause a significant improvement of mechanical and tribological properties of Ti-Al-B-N coatings [17,18]. Furthermore, it has been shown that B can lead to a significant improvement of the cutting performance of TiAlN based hard coatings [19]. The oxidation resistance of B-containing coatings, especially TiN/BN nanocomposites, is reported to be only slightly improved in comparison to TiN. This is caused by the lower oxidation resistance of the BN phase accompanied by a loss of B due to oxidation and sublimation of BO_x sub-oxides [20,21].

The aim of the present work was to deposit Ti-Al-B-N and Ti-Al-Si-N coatings by cathodic arc evaporation with doping contents up to 2 at% Si and up to 0.5 at% B in the target.

The influence of relatively high B and Si contents in TiAlN-based nanocomposites is well investigated. Here, we report on the impact of small amounts of Si and B on arc evaporated TiAlN, where in particular we concentrate on the influence of the alloying content on the resistance against oxidation and the individual oxide phases formed.

2. Experimental details

An industrial-scale cathodic arc evaporation facility, type Oerlikon Balzers RCS, was used to deposit the coatings. Five different coatings were produced from powder metallurgically produced targets with target composition (in at%) of $Ti_{33}Al_{67}$, $Ti_{32.5}Al_{67}Si_{0.5}$, $Ti_{31}Al_{67}Si_2$, $Ti_{32.9}Al_{67}B_{0.1}$ and $Ti_{32.5}Al_{67}B_{0.5}$. These compositions will be used in the further text for the coatings deposited. All runs were done in pure N_2 atmosphere at a pressure of 3.2×10^{-2} mbar. The bias voltage was -40 V and the deposition temperature around 450°C. The coatings were deposited onto single-crystal Si (100) samples with the dimensions of 21 × 7 × 0.38 mm. The samples were oxidized in ambient air at 800°C for 30 min and 900°C for 30, 60, and 300 min, using a Carbolite RHF16/15 annealing furnace. The heating rate was set to 10 K/min. After the respective oxidation period, the samples were kept in the furnace for cooling to room temperature.

The crystallographic investigations were performed by glancing angle X-ray diffraction (GAXRD). A Panalytical X'Pert Pro facility was used for the as-deposited samples with an angle of incidence of 2°, while the oxidized samples were investigated using a Bruker D8 Advance diffractometer at an angle of incidence of 1°. In both cases Cu Kα radiation was used. The thickness of the oxide scale after oxidation was evaluated by scanning electron microscopy (SEM) of fracture cross-sections using a Zeiss Evo50 SEM. Energy dispersive X-ray spectroscopy (EDX) was done using an Oxford Instr. INCA facility attached to the SEM. The EDX linescans were performed on polished cross-sections of oxidized samples. The formed oxides were investigated by Raman spectroscopy using a Jobin-Yvon LABRAM confocal Raman spectrometer, which is equipped with a frequency doubled Nd-YAG laser with a power of 100 mW.

3. Results

The results of GAXRD investigations on Ti-Al-Si-N and Ti-Al-B-N coatings can be seen in Fig. 3.1. To illuminate the influence of the respective alloying element, the pattern of undoped Ti-Al-N is shown at the bottom. This reference material exhibits a dual-phase structure with fcc and hcp phases. A comparison of the relative peak intensities of fcc and hcp phases of doped coatings and unalloyed reference material reveals an hcp phase promoting effect of both, Si and B. This can be observed by the increased peak intensities of the hcp (002) and (102) peaks at 32.16° and 48.025°. In comparison to these hcp peaks, the relative intensity of the fcc (111) and (200) peaks at 37.28° and 43.33°, respectively, is reduced if Si or B is added.

This hcp phase promoting effect of Si and B in TiAlN has already been described by

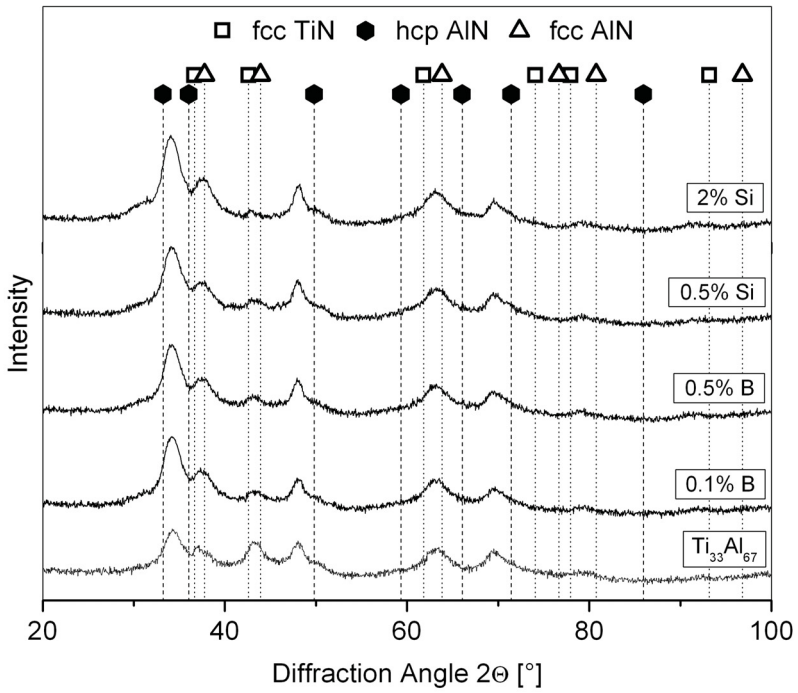

Figure 3.1.: GAXRD patterns of as-deposited Ti-Al-X-N (X=Si, B) coatings with various contents of Si and B.

various authors. Vaz et al. published results of TiAlN and Ti-Al-Si-N [12]. While TiAlN was found to exist in a single-phase fcc structure, the addition of Si results in the formation of a dual-phase structure with fcc and hcp phases. Kutschej et al. published results on Ti-Al-B-N and Ti-Al-Si-N. While the coatings exhibited a dual-phase fcc + hcp structure without Si or B alloying, they found a single-phase hcp structure at Si or B contents of 5 at% in the target [5,22]. Fig. 1 also indicates that there is no significant modification of the peak shape of the fcc and hcp phases due to the doping elements detectable. Thus, a significant decrease of the grain size is not found, fostering the interpretation that a nanocomposite of the TiAlN/Si_3N_4 type [14] is not formed. Instead, it is suggested that the chosen low amounts of Si or B are incorporated in the fcc and hcp phases. However, the presence of small amounts of amorphous Si_3N_4 or BN phases can not be excluded by XRD. Further investigations by TEM are necessary to clarify the nature of Si and B incorporation in the investigated coatings.

The resulting oxide layer thicknesses after oxidation at 800 and 900°C for various times are shown in Fig. 3.2. The given values are mean values of measurements of 5 to 7 positions on the SEM fracture cross-section. After 30 min oxidation at 800°C, no significant influence of the doping elements could be detected. After 30 and 60 min at 900°C, B and especially Si doped coatings show superior resistance to oxidation compared to undoped

TiAlN, where the higher content of the doping elements results in a stronger inhibition of the oxide layer growth. After 300 min at 900°C, TiAlN and Ti-Al-B-N are completely oxidized and the measured oxide scale thicknesses were in the range of the initial thickness of the nitride coating (∼4.5 μm). On the contrary, for Ti-Al-Si-N coatings oxide scales of less than 1 μm thickness were measured which means that more than 80% of the nitride coating remained intact. Again, a higher Si content led to a thinner oxide layer.

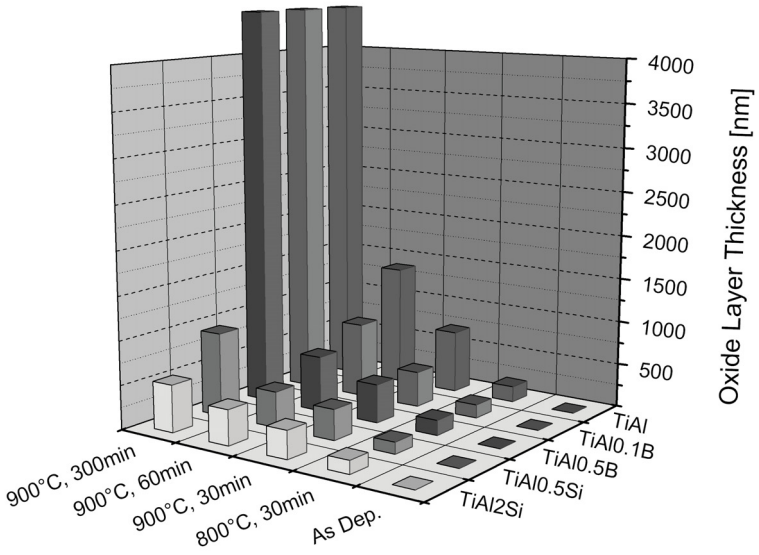

Figure 3.2.: Oxide layer thicknesses of TiAlN and B and Si doped TiAlN coatings after oxidation in ambient air at various oxidation parameters.

The results of the GAXRD investigations after oxidation at 900°C for 60 and 300 min are displayed in Fig. 3.3. For both Ti-Al-Si-N and Ti-Al-B-N, the target composition with the higher content of doping elements, i.e the better oxidation resistance, is given. The pattern of the undoped reference material for both oxidation conditions can be seen at the bottom of the respective GAXRD plot. After oxidation for 60 min, TiAlN shows clear evidence of corundum type α-Al_2O_3 (at 25.64, 35.22, 37.90, 43.34°) and rutile type TiO_2 (at 27.5, 36.12, 39.2, 41.26, 44.16°). No clear indication of anatase type TiO_2 was found, but the peak positions of anatase at 25.5 and 37.9° are overlapped by α-Al_2O_3; thus the presence of anatase can not be excluded. For Ti-Al-B-N and Ti-Al-Si-N, some intensity from the underlying nitride phase can be seen at about 34.5° and 48.3° (compare Fig 1). The intensity of the nitride is reduced compared to Fig. 3.1 due to the oxide layer covering the underlying nitride, the lower angle of incidence used and also due to smaller irradiated area, since the samples were cut into smaller pieces prior to the oxidation treatment.

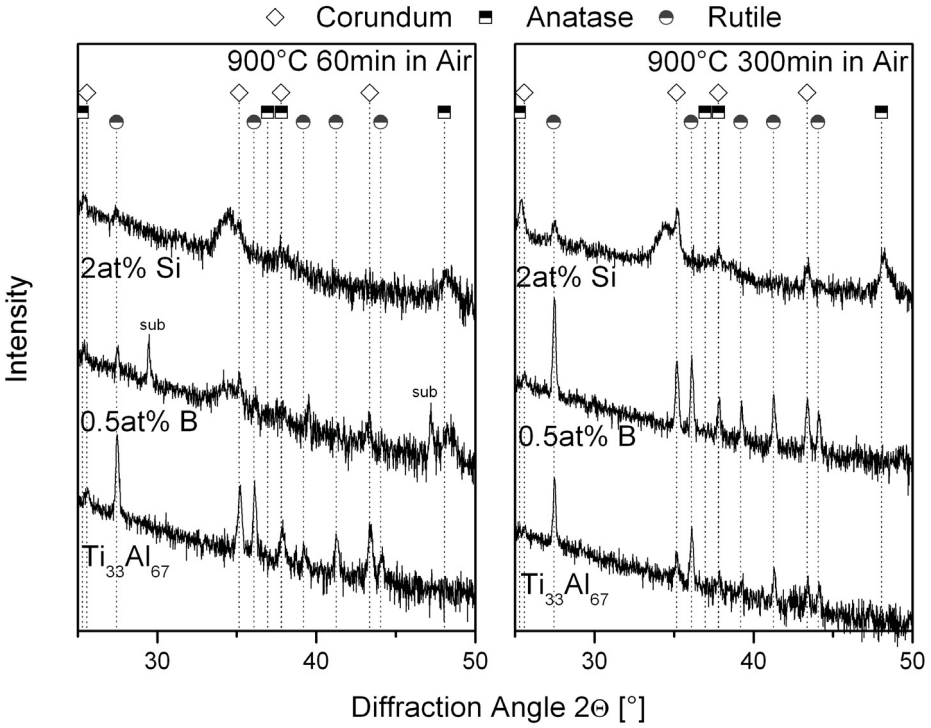

Figure 3.3.: GAXRD patterns of TiAlN and Si and B doped TiAlN coatings after oxidation at 900°C for 60 and 300 min in air.

For Ti-Al-B-N the same types of oxides as for unalloyed TiAlN are detected, but the intensity is significantly lower. This is consistent with the observations concerning the oxide layer thickness (see Fig. 3.2), where the thinner oxide layer leads to reduced intensity for the oxides and enables the detection of the underlying nitride. The presence of anatase can also not be excluded since the most important peak positions of anatase are overlapped by the α-Al_2O_3 or the nitride phases. Ti-Al-Si-N shows only traces of oxides after 60 min at 900°C in air. Most of the oxide peaks mentioned above appear as small peaks with decreased intensity at the respective positions. Between 25 and 30°, two small peaks can be detected as rutile and probably α-Al_2O_3. Concerning the presence of anatase, especially for Ti-Al-Si-N, the peak at 25.36° is shifted and lies between the positions of α-Al_2O_3 (25.57°) and anatase (25.28°), while the other α-Al_2O_3 peaks appear exactly at the expected positions. Since large residual stresses after a heat treatment at 900°C can be excluded as reason for the peak shift, the presence of anatase is likely.

After 300 min at 900°C, TiAlN is completely oxidized, as already mentioned above. The reduced intensity of the formed oxides in comparison to oxidation for 60 min is due to the reduced irradiated area for the XRD investigations, since the samples fractured during the oxidation treatment. Anatase is not found after 300 min; the oxide layer consists of rutile and α-Al_2O_3. Also Ti-Al-B-N is significantly oxidized, as no nitride peaks can be

seen anymore and very sharp oxide peaks appear, in comparison to oxidation for 60 min. The respective oxide peaks can be identified as rutile and α-Al_2O_3. Contrary to TiAlN and B-doped coatings, for Ti-Al-Si-N nitride peaks can still be detected even after 300 min at 900°C. Compared to TiAlN, the rutile peaks are broader which indicates a smaller grain size of the formed oxide. This can be seen for the rutile peak at 27.6°. The peak at 25.36 is again located between the positions of α-Al_2O_3 and anatase, which suggests the presence of both phases. The presence of anatase is also supported by the asymmetric peak at 48.24°, where the position of anatase and hcp nitride is overlapped and the peak is shifted towards the anatase position.

In order to clarify the phase composition of the formed oxides, Raman spectroscopy was conducted, which is known to be a useful tool in the detection of anatase and rutile type titania [16,23]. The results of these investigations can be seen in Fig. 3.4. For TiAlN, after oxidation for 60 min at 900°C, anatase and rutile were detected. After oxidation for 300 min, most of the intensity from anatase has vanished and rutile is the dominant phase. Only small amounts of anatase were detected by Raman spectroscopy. The B doped coatings contain also both types of TiO_2 after oxidation for 60 min, but a higher fraction of anatase is found compared to TiAlN which can be seen by comparing the peak heights of anatase and rutile in the range from 400 to 635 cm^{-1}, where a higher intensity from anatase can be observed. After 300 min, most of the anatase has been transformed into rutile, but again a higher amount of anatase seems to be present compared to TiAlN, since the anatase peaks are sharper for the B-doped coatings. In the case of Ti-Al-Si-N, after 60 min only some increased intensity at anatase peak positions at 196, 369, 514 and 640 cm^{-1} can be found. This is consistent with the SEM and XRD results mentioned above, which also indicated only slight oxidation after 60 min. After 300 min, Ti-Al-Si-N clearly shows peaks which can be related to anatase. Additionally, a small peak which origins from rutile can be seen at 444 cm^{-1}.

The results of investigations by EDX line scans on polished cross-sections of an oxidized Ti-Al-Si-N coating are shown in Fig. 3.5. For clarity, the lines of the individual elements were shifted vertically. Thus, the different intensities between the individual elements are of no significance. Within the upper 500 to 700 nm of the coatings, the high oxygen content and the reduced nitrogen content suggests the presence of the oxide scale. Furthermore, the shape of the Al and Ti signal indicates the presence of an Al- rich top-layer and a Ti- rich layer underneath. On the contrary, Si seems to be rather evenly distributed in the oxide scale, with only slightly decreasing Si contents towards the surface. The same investigations were not possible for B doped coatings, since the contents of B in the coatings are beyond the limit of detection by EDX.

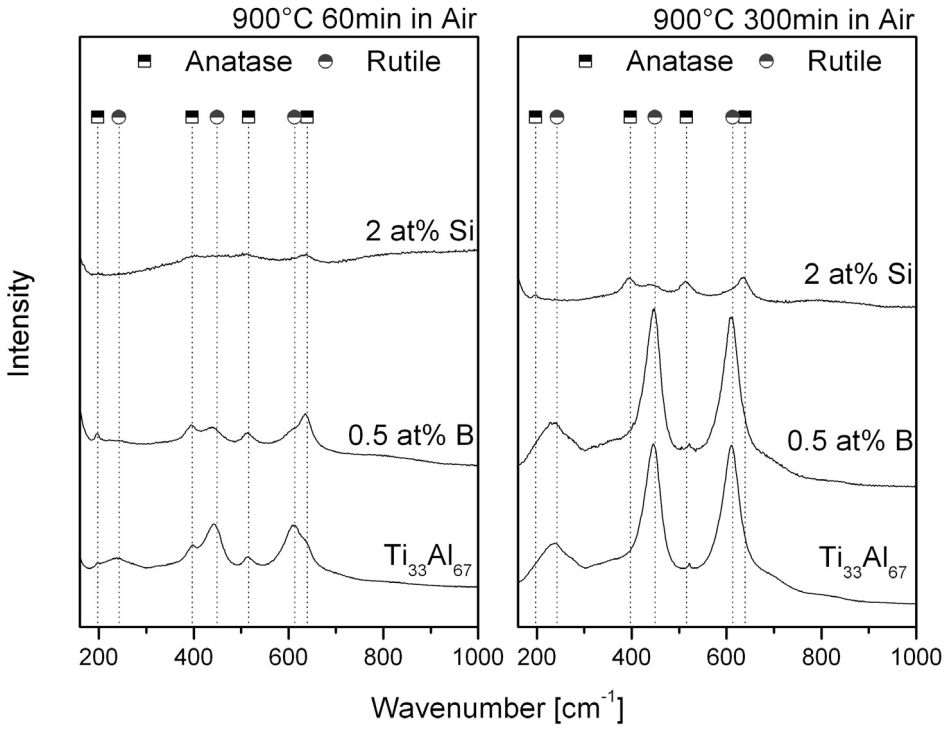

Figure 3.4.: Raman shifts of TiAlN and Si and B doped TiAlN coatings after oxidation at 900°C for 60 and 300 min in air.

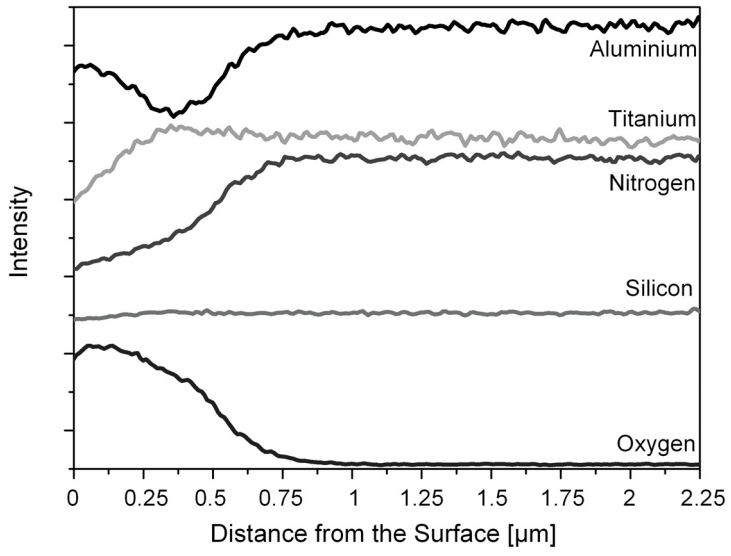

Figure 3.5.: EDX line scan of a Ti-Al-Si-N coating deposited from a target with 2 at% Si after oxidation at 900°C for 300 min.

4. Discussion

The oxidation behaviour of TiAlN coatings is well investigated and reported in literature. According to McIntyre et al. [24], the oxide scale consists of a double layered structure, i.e. an Al-rich top-layer and a Ti-rich sub-layer below. McIntyre et al. attributed the superior oxidation resistance compared to TiN to the upper, dense Al_2O_3 layer, which is expected to hinder the in-diffusion of oxygen [24]. Furthermore, it was reported that the mobile species are Al and O, whereas a limited mobility was detected for Ti. Thus, it was concluded that the oxide scale grows by simultaneous outward diffusion of Al towards the oxide/air interface and inward diffusion of O to the oxide/nitride interface where Ti is oxidized. At temperatures exceeding 800°C, the O transport through the Al-rich oxide is the rate limiting step. After oxidation at 900°C for 40 min, the surface was found to be covered with small crystals which were identified as rutile type TiO_2. The formation of these rutile crystals is postponed if a bias voltage is applied [24]. Vaz et al. reported on thermal oxidation of TiAlN with various Al/Ti ratios. They found that with increasing Al content the thickness of the oxide layer formed at 900°C decreases. The increase of the TiO_2 sub-layer thickness during the oxidation process is accompanied by the development of compressive stress due to large differences of the molar volume between TiO_2 and TiN. These stresses might lead to cracking of the protective Al-rich top-layer and consequently accelerate degradation of the oxidation behaviour. With increasing Al content, the Ti-rich sub-layer was found to grow slower which led to reduced compressive stresses. Thus, the authors attributed the better performance of the coating with higher Al content to the slower growth of the Ti-rich sub-layer and not exclusively to the growing Al-rich top-layer [25]. Furthermore, Vaz et al. reported that the oxidation behaviour deteriorates at very high Al contents and becomes similar to that of hexagonal AlN. The critical concentration coincides with the transition from the fcc to the wurzite structure, i.e. the appearance of hexagonal phases [25].

Rutile is the only stable form of TiO_2, but there are also two metastable forms, brookite and anatase, which transfer into rutile when they are heated. He et al. published results on plasma oxidation of sputtered Ti thin films and found an oxidation sequence, starting with anatase followed by transformation to rutile at around 700°C [26]. Similar results were also reported by Wu et al. on anatase formation in the process of oxidation of TiN films [27]. According to Gribb and Banfield, who published experiments on nanocrystalline titania, anatase transforms into rutile during coarsening after exceeding a certain grain size, which was determined to be around 14 nm. Once the phase transformation into rutile is completed, rutile was found to coarsen much faster than anatase did before the transformation [28]. These results were also theoretically confirmed by thermodynamical analysis by Zhang et al. [29]. Consequently, it can be summarized that the failure of

TiAlN coatings due to oxidation is probably related to the formation of rutile in the lower Ti-rich sub-layer of the oxide scale. This rutile formation is connected with the generation of compressive stresses, which might crack the dense and protective Al-rich top-layer, leading to intensified oxidation and finally failure of the coating. The formation of rutile is likely to follow nucleation and growth of anatase grains up to a critical grain size of about 14 nm [28]. After that, anatase starts to transform to rutile, which is followed by pronounced grain coarsening of the rutile phase once the transformation is completed.

In comparison to TiAlN, Ti-Al-Si-N and Ti-Al-B-N coatings show an increased content of hcp phase, which would predict a decreased resistance to oxidation [25]. Obviously, the addition of Si and B has further benefits, which are able to overcome the drawback of increased hcp phase. For the investigated Ti-Al-Si-N and Ti-Al-B-N coatings, a significantly higher amount of anatase was found after oxidation which was also connected to a thinner oxide layer. The addition of Si or B might hinder growth of anatase grains, indicated by a retarded anatase - rutile transformation and a higher fraction of anatase after the oxidation treatment. This might also be the reason for the reduced grain size of the detected rutile phases. Slower grain growth of anatase leads to a delayed transformation into rutile and consequently reduced time for rutile coarsening. Smaller rutile grains and/or a reduced thickness of the lower Ti-rich sub-layer in the oxide scale cause reduced compressive stresses [25] which could crack the protective top-layer. Thus, the protective integrity of the initially formed oxide scale can be maintained longer, leading to the better oxidation performance of the Si and B-doped coatings. Similar results were also published Pilloud et al. who reported on improved oxidation resistance of TiN by Si addition [16]. With increasing Si content, the oxide was found to contain a higher fraction of anatase in comparison to rutile, which is also accompanied by a decreased thickness of the oxide scale. The growth of TiO_2 grains was suggested to be inhibited by formation of an amorphous Si-based phase, which covers the Ti-rich grains. Since B can also form amorphous tissue phases [30], a similar explanation is also possible for Ti-Al-B-N. For longer oxidation treatments, the loss of B due to formation and sublimation of BO_x sub-oxides might be the reason for the deteriorated performance of B-doped coatings, in comparison to Ti-Al-Si-N [21].

Another possible explanation is that Si and B could act as reactive elements for rutile, similarly to the effect of Y on phase transformation in alumina, as described by Jedlinski [31]. He suggested chemical doping of the lattice and/or the consumption of the intrinsic oxygen vacancies as possible effects that lead to a retarded phase transformation. Furthermore, Y in Ti-Al-Y-N coatings has been described to segregate at the grain boundaries during oxidation. This blocks grain boundary out-diffusion of metal and in-diffusion of oxygen ions causing improved oxidation resistance [32]. Such effects could also explain

the retarded phase transformation of anatase into rutile and thus be the origin of the improved oxidation resistance of Ti-Al-Si-N and Ti-Al-B-N coatings.

5. Conclusion

Cathodic arc evaporated Ti-Al-N coatings doped with small amounts of B or Si, respectively, exhibit a dual-phase structure with cubic and hexagonal phases. The formation of hexagonal phases was found to increase in comparison to TiAlN reference material, but no significant decrease in grain size or indications for the formation of a TiAlN/Si_3N_4 nanocomposite were detected. Despite the higher content of hcp phase, the addition of B and Si was found to increase the coatings resistance to oxidation, where in particular Si significantly decreased the thickness of the formed oxide scale. The oxide scale was found to consist of an Al-rich top-layer and a Ti-rich sub-layer underneath. Corundum type Al_2O_3 and anatase type as well as rutile type TiO_2 phases were detected in the oxide scale. The improved oxidation resistance of Ti-Al-Si-N and Ti-Al-B-N is accompanied by a higher fraction of the metastable anatase TiO_2 type to the expense of the stable rutile TiO_2 type. This suggests the conclusion that the alloying elements modify the oxidation sequence of titanium. The results show that doping of TiAlN with small amounts of B and Si significantly improves the oxidation resistance, where especially Si is found to be a highly effective doping element.

Acknowledgment

Financial support by the Austrian Federal Government and the Styrian Provincial Government, represented by Österreichische Forschungsförderungsgesellschaft mbH and Steirische Wirtschaftsförderungsgesellschaft mbH, within the research activities of the K2 Competence Centre on "Integrated Research in Materials, Processing and Product Engineering", operated by the Materials Center Leoben Forschung GmbH under the frame of the Austrian COMET Competence Centre Program, is gratefully acknowledged.

References

[1] S. Veprek, M.J.G. Veprek-Heijman, Surf. Coat. Technol. 202 (2008) 5063-5073.
[2] S. PalDey, S.C. Deevi, Mater. Sci. Eng. A342 (2003) 58-79.
[3] O. Knotek, M. Böhmer, T. Leyendecker, J. Vac. Sci. Technol. A4 (6) (1986) 2695-2700.
[4] P.H. Mayrhofer, P.Eh. Hovsepian, C. Mitterer, W.-D. Münz, Surf. Coat. Technol. 177-178 (2004) 341-347.
[5] K. Kutschej, N. Fateh, P.H. Mayrhofer, M. Kathrein, P. Polcik, C. Mitterer, Surf. Coat. Technol.

200 (2005) 113-117.
[6] M. Pfeiler, G.A. Fontalvo, J. Wagner, K. Kutschej, M. Penoy, C. Michotte, C. Mitterer, M. Kathrein, Tribol. Lett. 30 (2) (2008) 91-97.
[7] S. Carvalho, L. Rebouta, E. Ribeiro, F. Vaz, M.F. Denannot, J. Pacaud, J.P. Riviere, F. Paumier, R.J. Gaboriaud, E. Alves, Surf. Coat. Technol 177-178 (2004) 369-375.
[8] S. Carvalho, E. Ribeiro, L. Rebouta, C. Tavares, J.P. Mendonca, A. Caetano Monteiro, N.J.M. Carvalho, J.Th.M. De Hosson, A. Cavaleiro, Surf. Coat. Technol. 177-178 (2004) 459-468.
[9] D. Rafaja, A. Poklad, V. Klemm, G. Schreiber, D. Heger, M. Sima, M. Dopita, Thin Solid Films 514 (2006) 240-249.
[10] D. Rafaja, A. Poklad, V. Klemm, G. Schreiber, D. Heger, M Sima, Mat. Sci. Eng. A462 (2007) 279-282.
[11] M. Dopita, D. Rafaja, Ch. Wüstefeld, M. Ruzicka, V. Klemm, D. Heger, G. Schreiber, M. Sima, Surf. Coat. Technol. 202 (2008) 3199-3207.
[12] F. Vaz, L. Rebouta, M. Andritschky, M.F. da Silva, J.C. Soares, Surf. Coat. Technol. 98 (1998) 912-917.
[13] S. Veprek, S. Reiprich, L. Shizi, Appl. Phys. Lett. 66 (1995) 2640.
[14] S. Veprek, H.-D Männling, M. Jilek, P. Holubar, Mat Sci Eng. A366 (2004) 202-205.
[15] P. Steyer, D. Pilloud, J.F. Pierson, J.-P. Millet, M. Charnay, B. Stauder, P. Jacqout, Surf. Coat. Technol. 201 (2006) 4158-4162.
[16] D. Pilloud, J.F. Pierson, M.C. Marco de Lucas, A. Cavaleiro, Surf. Coat. Technol. 202 (2008) 2413-2417.
[17] M.A. Baker, S. Klose, C. Rebholz, A. Leyland, A. Matthews, Surf. Coat. Technol. 151-152 (2002) 338-343.
[18] C. Rebholz, J.M. Schneider, A.A. Voevodin, J. Steinebrunner, C. Charitidis, S. Logothetidis, A. Leyland, A. Matthews, Surf. Coat. Technol. 113 (1999) 126-133.
[19] M. Kathrein, C. Michotte, M. Penoy, P. Polcik, C. Mitterer, Surf. Coat. Technol. 200 (2005) 1867-1871.
[20] P. Karankova, M.G.J. Veprek-Heijman, M.F. Zawrah, S. Veprek, Thin Solid Films 467 (2004) 133-139.
[21] S. Veprek, M.G.J. Veprek-Heijman, P. Karvankova, J. Prochazka, Thin Solid Films 476 (2005) 1-29.
[22] K. Kutschej. P.H. Mayrhofer, M. Kathrein, C. Michotte, P. Polcik, C. Mitterer, in Proceedings of the 16th International Plansee Seminar (G. Kneringer, P. Rödhammer, H. Wildner, eds.), Plansee, Reutte, Austria, 2005 Vol. 2, 774-788.
[23] J. Wagner, C. Mitterer, M. Penoy, C. Michotte, W. Wallgram, M. Kathrein, in Proc. 16th International Plansee Seminar, (G. Kneringer, P. Rödhammer, H. Wildner, eds.), Plansee, Reutte, Austria, 2005, Vol. 2, 917-931.
[24] D. McIntyre, J.E. Greene, G. Hakansson, J.-E. Sundgren, W.-D. Münz, J. Appl. Phys. 67 (3) (1990) 1542-1553.
[25] F. Vaz, L. Rebouta, M. Andritschky, M.F. da Silva, J.C. Soares, J. Europ. Cer. Soc. 17 (1997) 1971-1977.
[26]G. He, Q. Fang, L. Zhu, M. Liu, L. Zhang, Chem. Phys. Lett. 395 (2004) 259-263.
[27] S.X. Wu, Y.J. Liu, X.J. Xing, X.L. Yu, L.M. Xu, Y.P. Yu, S.W. Li, J. Appl. Phys.103 (2008) 063517.
[28] A.A. Gribb, J.F. Banfield, Am. Mineral., 82 (1997) 717-728.
[29] H. Zhang, J.F. Banfield, J. Mater. Chem., 8 (9) (1998) 2073-2076.
[30] P.H.Mayrhofer, C. Mitterer, J.G. Wen, J.E. Greene, I. Petrov, Appl. Phys. Lett. 86 (13) (2005)

131909.
[31] J. Jedlinski, Oxid. Met., 39 (1/2) (1993) 55-60.
[32] M.I. Lembke, D.B. Lewis, W.-D. Münz, J.M. Titchmarsh, Surf. Eng, 17 (2) (2001) 153-158.

Publication IV

Tribology Letters 30(2) (2008) 91-97

Arc evaporation of Ti-Al-Ta-N coatings: The effect of bias voltage and Ta on high-temperature tribological properties

by

M. Pfeiler, G.A. Fontalvo, J. Wagner, K. Kutschej, M. Penoy, C. Michotte, C. Mitterer, M. Kathrein

1. Introduction

During the last three decades, wear protective coatings like TiN and its evolutionary development Ti-Al-N became well known and highly successful on the market due to their excellent mechanical properties and wear resistance [1-3]. However, further demands like increased productivity in cutting applications require further optimisation of the coating system and the process it is produced with. Alloying of Ti-Al-N with Ta has shown to be beneficial in cutting tests. Ta-alloyed coatings show an increase of the maximum milling time of approximately 20% compared to conventional Ti-Al-N [4]. Furthermore, it has been shown that Ta promotes the formation of the face-centered cubic (fcc) phase at the expense of the hexagonal phase which was reported to result in increased mechanical and wear properties at elevated temperatures [5]. More generally, also the application of a bias voltage is a suitable tool for influencing nucleation, growth and crystal structure and, thus, the properties of a coating, due to the possibility to control the energy of the impacting ions. The ion bombardment during growth causes continuous re-nucleation due to disturbance of the local epitaxial growth which can lead to a modified texture [6].

At low bias voltage levels (-0 − -100V), the residual compressive stress increases with increasing bias voltages due to a higher defect density, which is also connected with an increase in hardness. At higher bias voltages, the ion bombardment induced mobility of atoms, which promotes the annihilation of defects, reduces the residual stresses and consequently the hardness also drops [7-10]. Recent results show that an increased bias voltage can be used to suppress the formation of undesired hexagonal close-packed (hcp) phases in Ti-Al-N based coatings, e.g. Ti-Al-V-N [11].

Although some general trends for affecting the fcc/hcp phase transformation in Ti-Al-N based coatings by alloying with e.g. V, Si, and B [12-14] are described in literature, only little is known on Ta-alloying and, in particular for Ti-Al-Ta-N coatings, on the tribological mechanisms present at various temperatures and the influence of bias voltage on their tribological response. This study adds more knowledge to this field and provides a possible explanation for the improved cutting performance of Ta-alloyed coatings [4]. In particular, we report on the influence of bias voltage and the role of Ta-alloying on the tribology at room temperature, 500°C, 700°C, and 900°C, the structure in the as-deposited state and the oxidation behaviour of Ti-Al-Ta-N.

2. Experimental details

An industrial-scale cathodic arc evaporation facility (Oerlikon Balzers RCS) was used to deposit the coatings from powder metallurgically produced targets ($Ti_{38}Al_{57}Ta_5$ and $Ti_{40}Al_{60}$). The coatings were deposited at bias voltages of -40, -80, -120, and -160 V in pure N_2 atmosphere at a pressure of 3.2×10^{-2} mbar. The deposition temperature was 450°C for all runs. The deposition time was 95 min at a deposition rate of 40 - 45 nm/min. The coatings were deposited onto three different substrates: Cemented carbide (CC) SNUN cutting inserts (grade S40T) were used for glow discharge optical emission spectroscopy (GDOES) and for glancing angle X-ray diffraction (GAXRD). Tribological tests were performed on polished CC discs (Ø 30×4 mm, grade TSM33), whereas for the oxidation experiments single-crystal Si (100) samples (21 × 7 × 0.38 mm) were used.

The resulting layer thickness was assessed by the ball-crater technique (CSM Instruments Calowear). The chemical composition of the coatings was evaluated by GDOES, using a Horiba / Jobin-Yvon JY-10000RT facility. Crystallographic investigations of the as-deposited coatings were performed by GAXRD (Panalytical X'Pert Pro) at an angle of incidence of 2°, while oxidized samples were investigated using a Siemens D500 Diffractometer with Bragg-Brentano configuration. In both cases Cu Kα radiation was used. The oxidation experiments were performed in ambient air at temperatures between 700 and 900°C. The samples were heated up at a heating rate of 10 K/min, kept at constant

temperature for 10 min (900°C for 10 min and 300 min) and cooled down in the chamber to ambient temperature. The tribological behaviour was investigated by dry sliding tests at room temperature, 500, 700, and 900°C on a CSM high-temperature ball-on-disc tribometer. The normal load, sliding speed, pre-heating time, sliding distance, and radius of wear track were kept constant at 5 N, 10 cm/s, 90 min, 300 m, and 7 mm, respectively. Standard tests were performed in ambient atmosphere at a relative humidity of 35±5% against an alumina ball (Ø 6 mm). Alumina was chosen as counter material because of its chemical inertness up to high temperatures. Additional tests were performed in Ar (99.999% purity) and synthetic air (80% N_2, 20% O_2), after purging the chamber for 4 hours with the respective gas, at a relative humidity of around 2%. The resulting wear tracks were investigated using 3D profiling systems (Wyco NT1000 Interferometer and Nanofocus μSurf Profiler). A scanning electron microscope (SEM, ZEISS EVO 50) with energy-dispersive X-ray analysis (EDX, Oxford Instruments Inca) was used to investigate the coating surface as well as oxidized surfaces and fracture cross-sections.

3. Results and Discussion

3.1 Microstructure

The results of XRD investigations on Ti-Al-Ta-N coatings in the as-deposited state are displayed in Fig. 4.1. To illuminate the influence of Ta in the coating, the XRD pattern of unalloyed Ti-Al-N deposited at -40V bias is displayed at the bottom. Both Ti-Al-N and Ti-Al-Ta-N coatings, grown at -40V bias, show a dual-phase structure containing fcc and hcp phases. Comparing the peak intensities of Ti-Al-N and Ti-Al-Ta-N for this bias voltage reveals a suppressing effect of the hcp phase by Ta. This can be observed by the reduced peak intensity of the hcp (002) peak at 34.77°. Furthermore, the fcc peaks of the Ti-Al-Ta-N coating are shifted towards lower angles which is connected with a lattice widening due to solid solution of the larger Ta atom in the fcc lattice.

With bias voltage increasing up to -80V for Ti-Al-Ta-N, the hcp phase is suppressed and the systems transforms into a single-phase fcc structure. The vanishing of the hcp phase might be a result of enhanced ad-atom mobility during deposition which is induced by the increased energy of the ion bombardment due to the higher bias voltage. Recent calculations of Mayrhofer et al. [15] indicate that the phase stability of fcc Ti-Al-N is determined by the number of Ti-Al bonds in the fcc lattice. The energy of formation is lowest if the number of Ti-Al bonds is also low. This can be obtained if Ti atoms are predominantly surrounded by Ti atoms and vice versa for Al. To ensure this, Al- and Ti-rich regions within the same fcc lattice must be formed. An increased mobility

of the ad-atoms might promote the formation of this low-energy configuration with low amount of Ti-Al bonds, leading to an enhanced solubility limit of Al in the fcc TiN lattice. Additionally, collision cascade effects might have a decreasing influence on the survival rate of hcp nuclei on the surface of the growing film [6]. Both effects are assumed to promote the predominant growth of the fcc phase with increasing ion energy, i.e. bias voltage. Furthermore, an increase in compressive stresses with increasing bias voltage could hinder the growth of the less dense hcp phase, compared to the denser fcc phase [16]. Such an increase in residual compressive stress with increasing bias voltage has been reported by various authors. [11,17,18]. A correlation between residual stresses and the presence of hcp phase has also been published by Zhou et al. [19].

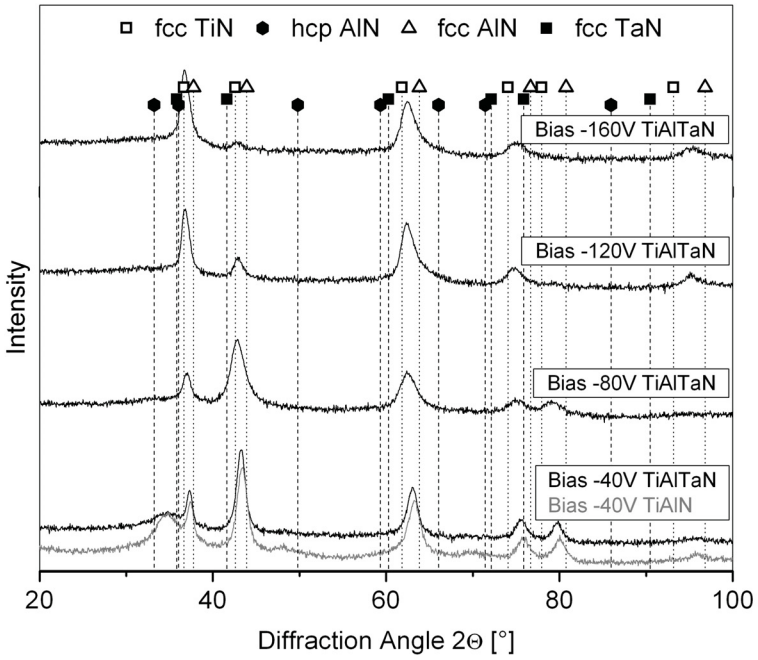

Figure 4.1.: XRD patterns of Ti-Al-Ta-N and Ti-Al-N coatings deposited at various bias voltages.

Finally, the Al content which is decreasing from 62.7 at% at -40 V to 61.2 at% at -160 V bias may also contribute to the vanishing of the hcp phase. The wurtzite-type hcp phase of Ti-Al-N origins from hcp AlN; thus, a decrease in Al content also decreases the tendency to form hcp phases. According to literature, the transition zone, from a single-phase fcc to a dual-phase fcc + hcp structure, is located between 60 and 65 at% Al [19,20]. This effect of suppression of hcp phase with increasing bias voltage has also been observed and described for V alloyed Ti-Al-N coatings [11].

With increasing bias voltage, the predominant orientation of the fcc phase changes from

(200) to (111). Texture crossovers with changing process parameter such as ion energy, ion/neutral ratio, N_2 partial pressure or coating thickness are well reported phenomena [6,21,22]. According to ab initio studies by Gall et al. this might be connected with different surface diffusion energies of adatoms on the respective (111) and (001) lattice sites [23]. This could favour a preferential growth of grains where adatoms are stronger bonded and surface diffusion is hindered. The increased energy of the impacting ions with increased bias could influence the adatom mobility.

3.2 Tribological Behaviour between Room Temperature (RT) and 700°C

The results of tribological tests of Ti-Al-N deposited at a bias voltage of -160 V at RT, 500, and 700°C can be seen in Fig. 4.2. Pronounced abrasion can be detected at RT, while at 500 and 700°C no significant loss of material has been observed; only flattening of the surface occurred. A comparison of these results to Ta-alloyed coatings also deposited at -160V and tested under the same conditions (see Fig. 4.3) displays no change in the tribological response due to Ta-alloying in the investigated temperature range. This is also valid for the other bias voltages (not shown here). Therefore, we focus on the results of Ta-alloyed coatings, which are summarized in Fig. 4.3. There, the rows show the influence of the changing testing temperature, whereas the columns present the influence of the different bias voltages.

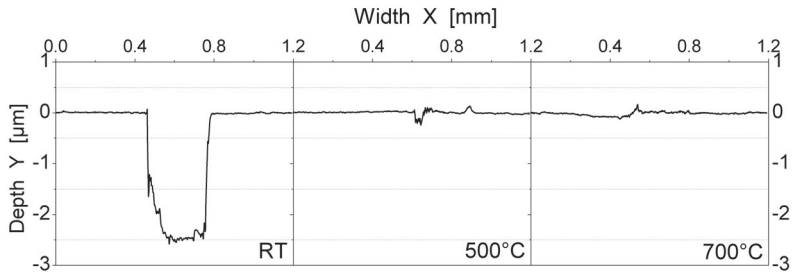

Figure 4.2.: 2D cross-sections of wear tracks obtained on Ti-Al-N coatings deposited at -160 V bias voltage after tribological tests at RT, 500, and 700°C.

For tests conducted at RT in ambient atmosphere (see Fig. 4.3a-c), no influence of the bias voltage on the wear behaviour can be detected. Severe wear occurred in all cases and similar wear track depths can be measured; thus the variation of the bias voltage showed no influence on the tribological behaviour at RT. Additional test under synthetic air and Ar (see Fig. 4.3a), which resulted in significantly reduced wear, revealed the

important role of moisture and O_2 during sliding. If both, moisture and O_2 are removed by purging with Ar to a relative humidity of 2%, wear is significantly decreased. The same is valid if only moisture is removed by purging with synthetic air (80% N_2, 20% O_2). Thus, the presence of moisture in the tribological contact is determinant for wear at RT in ambient air. Tribo-chemical reactions between the coating and O_2 and/or moisture of the environment control the wear behaviour.

The important role of the moisture on tribology of Ti-Al-N based coatings in different atmospheres has been previously discussed by other authors. Wear decreases significantly with decreasing humidity, elevated temperature or under inert gas atmosphere [24,25]. This behaviour might be connected with the effect of hydration of Al_2O_3 in a humid environment according to Olefjord and Nylund [26]. They found that pre-oxidized Al continues to oxidize in humid atmospheres due to hydration of previously formed Al_2O_3. So the oxide layer itself becomes thinner and further oxidation occurs. This is not the case for dry atmospheres.

The tribological behaviour of the investigated coatings is strongly related to the presence of moisture at room temperature. The continuous formation of Al_2O_3 in the sliding contact, which is likely to be promoted by moisture, presumably promotes the easy removal of material by abrasion. Other possible influences like bias voltage or Ta-alloying have not been detected or seem to be negligible.

At 500°C (Fig. 4.3d-f), no loss of material is detectable; however, the bias voltage during deposition affects the tribological behaviour of the coating. The sample deposited at -40 V bias voltage shows a wear track width of about 1000 μm which decreases at higher bias voltages to 300 μm (-160 V). The respective width of the wear tracks corresponds exactly to the diameter of the wear scar on the Al_2O_3 ball. The reason for this effect may be the difference in droplet-generated surface roughness in the as-deposited state, which is presented in Fig. 4.4.

The samples deposited at -80, -120, and -160 V exhibit a significantly lower amount of macro-particles on the surface compared to samples deposited at -40 V. The same effect and its influence on tribology has been described earlier for Ti-Al-V-N coatings [11]. It has been concluded, that droplets act as sharp tips which cause severe abrasion of the ball during the first few revolutions. Thus, the load is distributed to a higher apparent area of contact during the further test, thus decreasing wear. This effect does not cause any significant abrasion of the coating at 500°C. A possible explanation is the change of the ambient atmosphere. Especially the absence of humidity at 500°C might play an important role, as described above. In addition, the higher wear resistance at 500°C might be further increased by the increased toughness of the coating. Investigations of Ti-Al-N coatings at 25-500°C revealed that the fracture probability at elevated temperatures is

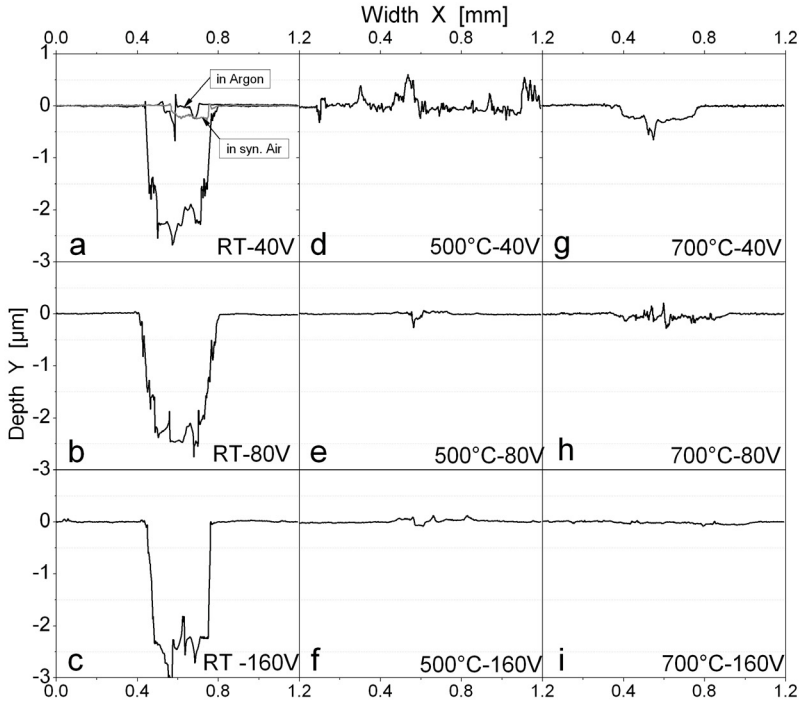

Figure 4.3.: 2D cross-sections of wear tracks obtained on Ti-Al-Ta-N coatings deposited at various bias after tribological tests at RT, 500, and 700°C (plus additional RT test in Ar and synthetic air for -40V bias).

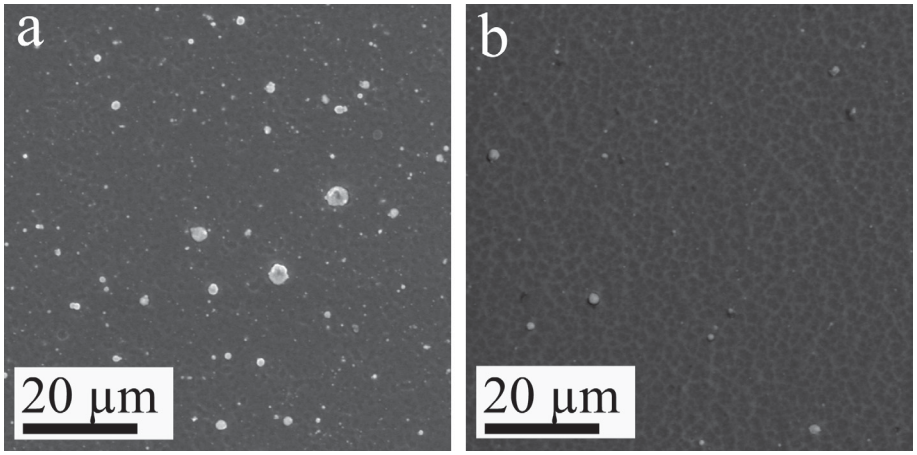

Figure 4.4.: SEM micrographs of the surface of Ti-Al-Ta-N coatings deposited at -40 (a) and -160 V (b) bias voltage.

significantly reduced [27]. Additionally, the formation of a protective Al_2O_3-rich layer in the sliding contact may also contribute to the prevention of abrasion [14].

After tribological tests at 700°C (Fig. 4.3g-i), a loss of material was found for -40 V, while for elevated bias voltages, especially -160 V, only flattening of the surface occurred. This can be explained by the change in oxidation resistance according to Vaz et al. Within their investigation on oxidation of Ti-Al-N, a protective layered Al_2O_3 - TiO_2 structure at temperatures between 750°C and 900°C has been found, which vanished with the transition from the fcc to the hcp structure [14].

Applying a bias voltage of -40 V results in a dual-phase fcc + hcp structure (see Fig. 4.1) which should have lower resistance to oxidation. The Al_2O_3 ball continuously removes the formed oxide on the coating surface during sliding and exposes un-oxidized coating to the atmosphere. The influence of bias voltage on the oxidation resistance was investigated by SEM fracture cross-sections of samples deposited at -40 V (i.e. a coating with dual-phase fcc + hcp structure) and -80 V (single-phase fcc). After oxidizing for 5 h at 900°C in ambient air, an oxide layer of around 450 nm thickness for the -40 V sample has been observed (Fig. 4.5a) while the oxide layer is 350 nm thick for -80 V (Fig. 4.5b). Thus, a higher resistance to oxidation of the single-phase fcc structure, deposited at -80V bias, can be assumed.

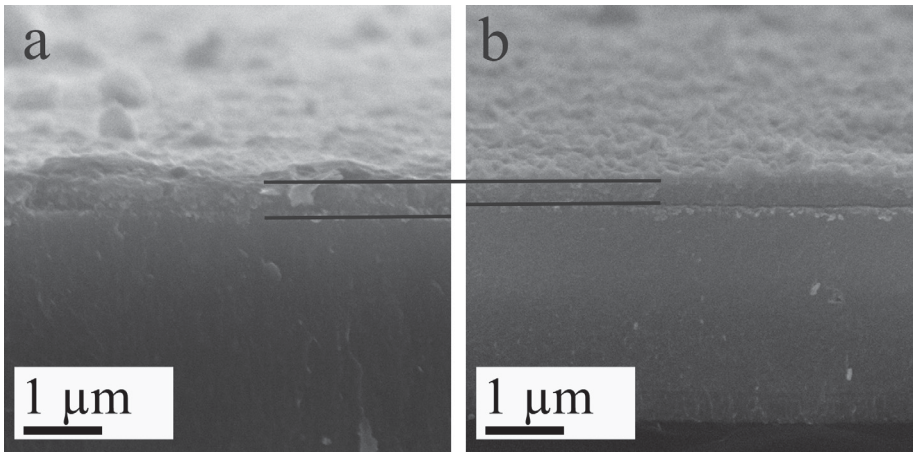

Figure 4.5.: SEM micrographs of cross-sections of Ti-Al-Ta-N coatings deposited at (a) -40 and (b) -80 V after oxidizing at 900°C for 300 min in air (guide lines show the position of the surface and the oxide-nitride interface).

3. Tribological behaviour at 900°C

To elucidate differences in the high-temperature tribological properties further, Ti-Al-Ta-N and Ti-Al-N coatings, both deposited at -40 V bias, were tribologically tested at 900°C in ambient air. For Ti-Al-Ta-N, the planned sliding distance of 300 m was reached

without obvious coating failure, while the Ti-Al-N was completely destroyed after 60 m. SEM investigations of fracture cross-sections on the Ta-alloyed coatings revealed a thin oxide layer of about 200 nm thickness on top of the underlying nitride outside of the wear track (Fig. 4.6a). In EDX investigations, neither W nor Co nor C was detected in the coating. Thus, the interface to the CC substrate remained intact.

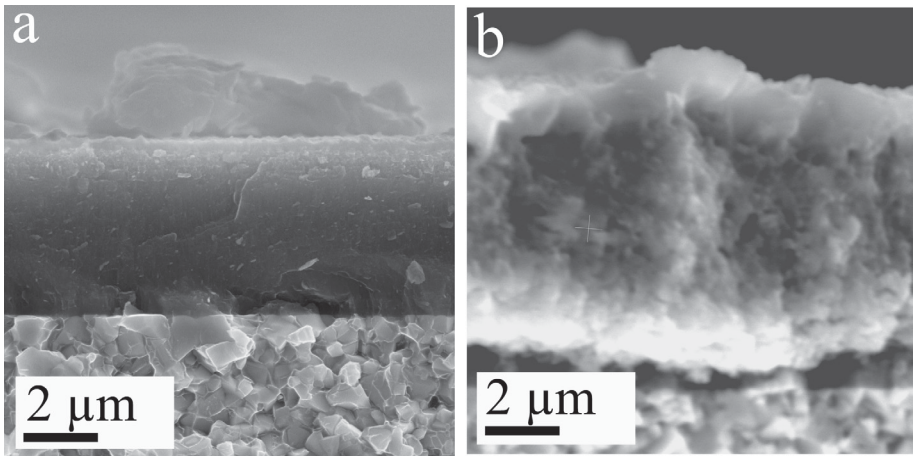

Figure 4.6.: SEM micrographs of Ti-Al-Ta-N (a) and Ti-Al-N (b) coatings after tribological tests at 900°C (Ti-Al-N failed after 20% of sliding distance).

Contrary to the Ta-alloyed coating, it is assumed that Ti-Al-N was already fully oxidized during the heating-up step of the tribometer test. Consequently, diffusion and oxidation of the substrate occurred, which resulted in massive delamination of the coating (see Fig. 4.6b) and finally caused the early failure of the sample during testing. This has been confirmed by EDX analysis of a remaining coating fragment which showed contents of W and Co from the substrate material and a high amount of O.

The corresponding wear track of the Ti-Al-Ta-N coating can be seen in Fig. 4.7. An investigation of the wear track of Ti-Al-N was not possible, since only fragments of the coating survived the test. For Ti-Al-Ta-N, no obvious abrasion, but a build-up of material in the range of 15 μm height has been detected by profilometry and SEM. The micrographs indicate that the substrate material has risen under the sliding ball. EDX analysis of the wear track showed only Co and O on the surface, while in the region below the track only W and O were detected. Ti and Al were not found in that region but only in wear debris next to the track. Obviously, no coating is left in the wear track and the CC substrate expanded due to oxidation of W and Co, which caused the rising of the material under the tribo-contact. Nevertheless, apart from the wear track itself, the nitride coating is still intact (see Fig. 4.6a for higher magnification). The higher flash temperatures in the contact during sliding, which are likely to exceed 1000°C [28], are suspected to cause severe oxidation and finally the failure of the coating. However,

it is not clear if the oxidized coating was worn away and exposed the substrate to the atmosphere or if cracking and in-diffusion of oxygen caused oxidation of the interface and the substrate and, consequently, failure due to loss of adhesion.

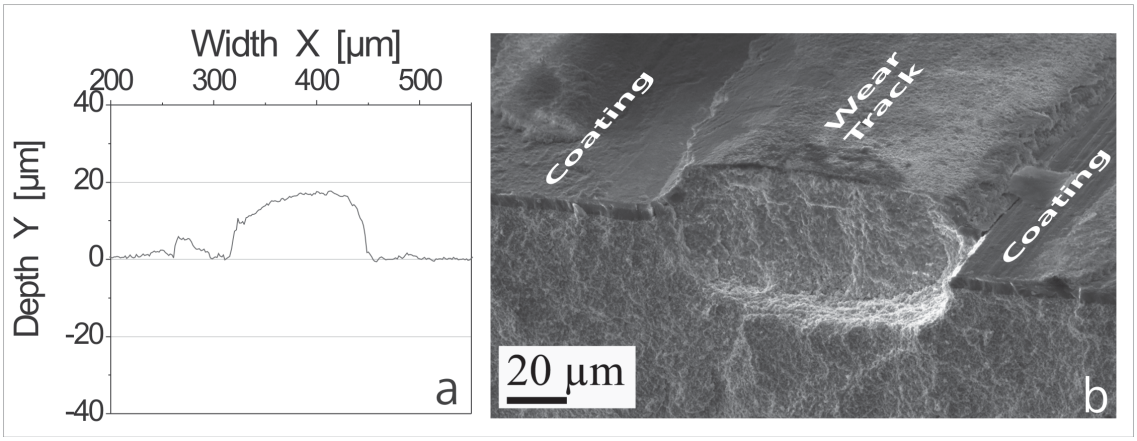

Figure 4.7.: Resulting wear track after tribological tests of Ti-Al-Ta-N coatings at 900°C, (a) 2D cross-section, (b) SEM cross-section.

To shed more light on the oxidation resistance of Ta-alloyed coatings without interference of the CC substrate, additional oxidation experiments of Ti-Al-Ta-N and Ti-Al-N on Si substrates at 700, 800, and 900°C have been performed. The samples have been heated up in air and kept on temperature for 10 min and 300 min (900°C only). Afterwards, the samples were investigated by XRD (see Fig. 4.8).

No oxide peaks have been detected in case of Ti-Al-Ta-N coatings after annealing at 700 and 800°C. After 10 min at 900°C, some minor evidence of oxidation can be detected. Even after 300 min. at 900°C, only slight oxidation of the Ta-alloyed coating is observed. Nevertheless, also peaks which origin from the nitride coating can be seen (around diffraction angles of 35-37°, 43°, and 62-63°). This is corroborated by the fracture cross-section of the Ta-alloyed coating shown in Fig. 4.5a. On the contrary, Ti-Al-N is oxidized completely (see Fig. 4.8).

4. Conclusion

For Ti-Al-Ta-N coatings deposited by cathodic arc evaporation, the increasing bias voltage promotes a transformation from a dual-phase structure containing cubic and hexagonal phases to a single-phase cubic structure. The tribological behaviour at room temperature is predominantly determined by the presence of moisture which supports tribo-reactions that increase wear. In the absence of moisture at elevated temperatures, no loss of material is detectable. Furthermore, the formation of a protective oxide layer and the increase in

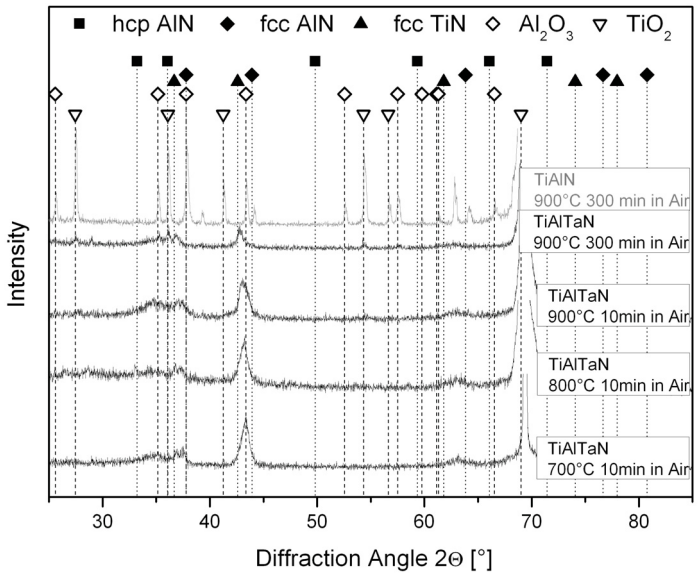

Figure 4.8.: XRD patterns after oxidation experiments of Ti-Al-Ta-N and Ti-Al-N coatings (bias voltage -40 V) annealed at 700, 800, and 900°C for 10 and 300 min.

toughness with increased temperature might contribute as well to reduce wear. Droplet-generated surface roughness, which decreases with bias voltage, is also a determinant factor of the tribological response at elevated temperatures. Once a critical temperature is exceeded, the resistance to oxidation of the coatings, which was found to be connected with the coatings microstructure, determines the wear behaviour at high temperatures. The incorporation of Ta in Ti-Al-N coatings significantly increases the resistance to oxidation of the coatings. Since oxidation resistance plays a determinant role in high-temperature tribological applications, Ta alloyed Ti-Al-N coatings show enhanced wear resistance at high temperatures.

Acknowledgments

Financial support by the Austrian Kplus Competence Center Programme is gratefully acknowledged. Marisa Rebelo de Figueiredo from the Christian Doppler Laboratory for Advanced Hard Coatings, University of Leoben, Austria is acknowledged for experimental support on tribological tests in various atmospheres.

References

[1] PalDey, S., Deevi, S. C.: Mat. Sci. Eng. A 342 58-79 (2003)
[2] Knotek, O., Böhmer, M., Leyendecker, T.: J. Vac. Sci. Technol. A4 (6) 2695-2700 (1986)
[3] Coll, B. F., Fontana, R., Gates, A., Sathrum, P.: Mat. Sci. Eng. A140, 816-824 (1991)
[4] Kathrein, M., Michotte, C., Penoy, M., Polcik, P., Mitterer C.: Surf. Coat. Technol. 200 1867-1871 (2005) [5] Kutschej, K., Mayrhofer, P. H., Kathrein, M., Michotte, C., Polcik, P., Mitterer, C.: Proceedings of the 16th International Plansee Seminar 2005, Plansee Holding AG, Reutte, Tyrol, Austria, Editors: G. Kneringer, P. Roedhammer, H. Wildner , Volume 2, 774-788 (2005)
[6] Petrov, .I., Barna, P. B., Hultman, L., Greene, J. E.: J. Vac. Sci. Technol. A 21, 117-128 (2003)
[7] Ljungcrantz, H., Hultman, L., Sundgren, J.-E.: J. Appl. Phys. 78, 832-837 (1995)
[8] Sato, K., Ichimiya, N., Kondo, A., Tanaka, Y.: Surf. Coat. Technol. 163-164, 135-143 (2003)
[9] Ahlgren, M., Blomqvist, H.: Surf. Coat. Technol. 200, 157-160 (2005)
[10] Durand-Drouhin, O., Santana, A. E., Karimi, A., Derflinger, V. H., Schütze, A.: Surf. Coat. Technol. 163-164, 260-266 (2003)
[11] Pfeiler, M., Kutschej, K., Penoy, M., Michotte, C., Mitterer, C., Kathrein M.: Surf. Coat. Technol. 202, 1050-1054 (2007)
[12] Kutschej, K., Mayrhofer, P. H., Kathrein, M., Polcik, P., Mitterer, C.: Surf. Coat. Technol. 188-189, 358-363 (2004)
[13] Kutschej, K., Fateh, N., Mayrhofer, P. H., Kathrein, M., Polcik, P., Mitterer, C.: Surf. Coat. Technol. 200, 113-117 (2005)
[14] Vaz, F., Rebouta, L., Andritschky, M., da Silva, M. F., Soares, J. C.: Surf.Coat.Tech 98, 912-917 (1998)
[15] Mayrhofer, P. H., Music, D., Schneider, J. M.: J. Appl. Phys. 100, 1-5 (2006)
[16] Mayrhofer, P. H., Hoerling, A., Karlsson, L., Sjoelen, J., Larsson, T., Mitterer, C., Hultman, L.: Appl. Phys. Lett. 83, 2049-2051 (2003)
[17] Odén, M., Almer, J., Håkansson, G.: Surf. Coat. Technol. 120-121, 272-276 (1999)
[18] Vlasveld, A. C., Harris, S. G., Doyle, E. D., Lewis, D. B., Münz, W.-D.: Surf. Coat. Technol. 149, 217-224 (2002)
[19] Zhou, M., Makino, Y., Nose, M., Nogi, K.: Thin Solid Films 339, 203-208 (1999)
[20] Cremer, R., Reichert, K., Neuschütz, D.: Surf. Coat. Technol. 142-144, 642-648 (2001)
[21] Knuyt, G., Quaeyhaegens, C., D'Haen, J., Stals, L. M.: Surf. Coat. Technol. 76-77, 311-315 (1995)
[22] Iordanova, I., Kelly, P. J., Mirchev, R., Antonov, V.: Vacuum 81, 830-842 (2007)
[23] Gall, D., Kodambaka, S., Wall, M. A., Petrov, I., Greene, J. E.: J. Appl. Phys. 93, 9086-9094 (2003)
[24] Meier zu Köcker, G., Gross, T., Santner, E.: Wear 179, 5-10 (1994)
[25] Konca, E., Cheng, Y.-T., Weiner, A. M., Dasch, J. M., Erdemir, A., Alpas, A. T.: Surf. Coat. Technol. 200, 2260-2270 (2005)
[26] Olefjord, I., Nylund, A.: Surf. Interface Anal. 21, 290-297 (1994)
[27] Beake, B. D., Smith, J. F., Gray, Al., Fox-Rabinovich, G. S., Veldhuis, S. C., Endrino, J. L.: Surf. Coat. Technol. 201 (2007) 4585
[28] Rabinowicz, E.: Friction and Wear of Materials, John Wiley and Sons Inc., New York, London, Sydney, 86-90 (1995)

Publication V

in final preparation

On the effect of Ta on improved oxidation resistance of Ti-Al-Ta-N coatings

by

M. Pfeiler, C. Scheu, H. Hutter, J. Schnöller, C. Michotte, C. Mitterer, M. Kathrein

1. Introduction

The current trend in machining industry to high speed and high feed rate cutting in combination with minimum use of coolants and lubricants leads to a constant increase of the working temperatures and consequently thermal and thermo-oxidative loading on cutting tools. Therefore, materials applied in such machining operations need to exhibit high hot hardness and a high resistance to oxidation. Although the well established and highly successful titanium aluminium nitride (TiAlN) hard coatings fulfil these requirements in general [1,2], recent developments show promising improvements [3-6]. The alloying of TiAlN with Ta has shown to be beneficial in cutting, where the maximum milling time was increased significantly [7]. Kutschej et al. reported on improved mechanical and tribological properties of Ti-Al-Ta-N, which was connected to a promoting effect of Ta on face centered cubic (fcc) at the expense of the hexagonal close packed (hcp) phases [8]. Recently, we have shown that the improved performance of Ti-Al-Ta-N could be connected to a significantly better tribological behaviour at high temperatures, exceeding 900°C. The results also indicate a higher resistance to oxidation of Ti-Al-Ta-N in comparison to TiAlN [9].

Various concepts are available in literature, which are suitable to explain the effect of

different alloying elements on the oxidation resistance [4, 10-12]. However, the potential of Ta incorporation for oxidation tuning and the function of Ta in the oxidation process of TiAlN have not yet been studied in detail. Thus, the aim of the present work was to deposit Ti-Al-Ta-N coatings by cathodic arc evaporation and to investigate the impact of Ta on the oxidation behaviour systematically. In particular, we concentrate on the morphology of the oxide layer, the various formed oxides and the distribution of the chemical elements in the oxide scale. The obtained results should provide information to develop an explanation of the origin of the excellent oxidation resistance of the investigated material.

2. Experimental details

An industrial-scale cathodic arc evaporation facility, type Oerlikon Balzers RCS, was used to deposit the coatings from powder metallurgically produced targets with target composition (in at%) of $Ti_{40}Al_{60}$ and $Ti_{38}Al_{57}Ta_5$. These compositions will be used in the further text for the coatings deposited. All runs were done in pure N_2 atmosphere at a pressure of 3.2×10^{-2} mbar. The bias voltage was -40 V and the deposition temperature around 450°C. The coatings were grown, after depositing a 300 nm thin TiN interlayer, onto single-crystal Si (100) samples with the dimensions of 21 × 7 × 0.38 mm. The samples were oxidized in ambient air at 800°C for 30 min and 900°C for 30, 60, and 300 min, using a Carbolite RHF16/15 annealing furnace. The heating rate was set to 10 K/min. After the respective oxidation periods, the samples were kept in the furnace for cooling to room temperature.

The crystallographic investigations were performed by glancing angle X-ray diffraction (GAXRD). The as-deposited and oxidized samples were investigated using a Bruker AXS D8 Advance diffractometer at an angle of incidence of 1° with Cu Kα radiation. Secondary ion mass spectroscopy (SIMS) was conducted using an ION TOF-SIMS.5 facility. Depth profiling was performed in the so-called dual beam mode [13]. As primary ion species for the generation of the secondary ions, Bi^+ (energy: 25 keV), produced by a liquid metal ion gun (LMIG), was used. For crater erosion in the negative secondary ion mode, Cs^+, for crater erosion in the positive secondary ion mode, $O_2{}^+$ was used.

Scanning electron microscopy (SEM) was done using a Zeiss Evo50 with an attached Oxford Instruments INCA energy dispersive X-ray spectroscopy (EDX) detector. The SEM-EDX line-scans were performed on polished cross-sections of oxidized samples. After sputtering a thin layer of Au on the surface, a Ni plating was deposited onto the oxidized samples in order to protect the oxide scale during polishing and to improve edge resolution. Transmission electron microscopy (TEM) was conducted using a FEI Titan microscope,

operated at 300 keV, and a JEOL 2011 microscope, operated at 200 keV. The samples for TEM were prepared by cross-sectional tripod polishing followed by Ar-ion milling using a Gatan PIPS 691 device.

3. Results

After the oxidation treatment, the samples were broken and cross-sectional fracture surfaces were investigated by SEM. The measured oxide scale thickness vs. the oxidation treatment is shown in Fig.5.1. Obviously, a significant improvement of the oxidation resistance can be observed for Ta-alloyed coatings. Even after short times of 30 min at peak temperature, the oxide scale on Ti-Al-Ta-N measures only 60% of the scale observed on TiAlN. After 60 min at 900°C in ambient air, the thickness of the oxide scale was decreased to only 12-15% in comparison to TiAlN. After 300 min, the whole TiAlN coating of $\sim$4 μm thickness was oxidized, while on Ti-Al-Ta-N, the oxide was less than 500 nm thick. Thus, approximately 85% of the original nitride coating is still intact, while the reference material already failed.

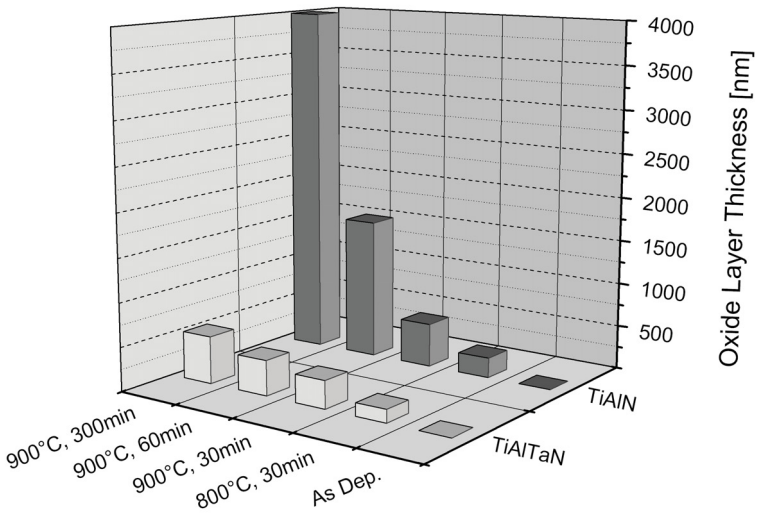

Figure 5.1.: Oxide layer thickness of TiAlN and Ti-Al-Ta-N after oxidation in ambient air at various oxidation parameters.

The results of GAXRD investigations on Ti-Al-Ta-N and TiAlN reference material after oxidation can be seen in Fig. 5.2, where vertical drop lines indicate the standard position of possible oxide and nitride phases. At the bottom, the pattern of as deposited Ti-Al-

Ta-N is given, which displays a dual phase structure, with hcp (2Θ = ~34.5°) and fcc phases (at 37.26, 43.18 and 62.96°). The fcc and hcp nitride peaks shift with increasing time and oxidation temperature towards the standard peak positions of fcc TiN and hcp AlN, respectively. This indicates the beginning of the decomposition of the metastable Ti-Al-Ta-N into the stable TiN and AlN phases [2] during the oxidation treatment.

After an oxidation treatment for 30 min at 800°C, no oxide peaks can be seen while after 30 min at 900°C, additional peaks which origin from the rutile-type TiO_2 can be observed at 2Θ = 27.52, 36.18, 39.26, 41.22 and 54.32°. Furthermore, some intensity stemming from corundum-type α-Al_2O_3 at 2Θ ~35.28, 43.36 and 57.64° can be detected. After 300 min, all the observed oxide peaks gain intensity and can be clearly identified which can be explained by the presence of a thicker oxide scale caused by longer oxidation times (compare Fig. 5.1). Besides the Ti and Al based oxides, no Ta-based oxides, like Ta_2O_5 were observed, which indicates the incorporation of Ta in the observed oxides. However, after 300 min at 900°C the dominant phases, with respect to detected intensity in the XRD pattern, are the nitride phases, which is consistent with the significantly thinner oxide layers observed for Ti-Al-Ta-N (compare Fig. 5.1).

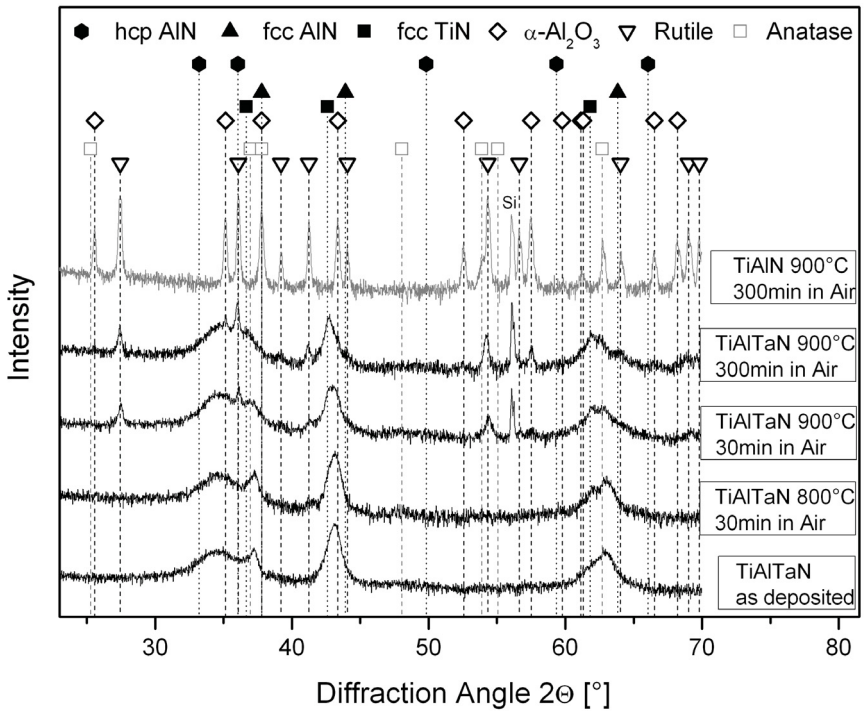

Figure 5.2.: GAXRD patterns of Ti-Al-Ta-N and TiAlN coatings oxidized at various conditions.

Contrary to that, the TiAlN coating is completely oxidized which is shown by clear and sharp peaks of α-Al_2O_3, rutile-type TiO_2 and no remaining nitride phase detectable. In

addition, the metastable anatase type TiO_2 is detected at 54.02 and 62.78°. This oxide phase is probably also present in the Ti-Al-Ta-N coatings, but due to the significantly thinner oxide scale, too less material is probed to detect anatase by XRD in this coating.

In order to investigate the composition of the oxide scale qualitatively, cross-sectional SEM-EDX line scans were performed (Fig. 5.3). Fig. 3a shows an SEM overview (back scattered electron mode) of a polished cross-section trough the oxidized nitride coating. The EDX profile for Ti-Al-Ta-N, oxidized at 900°C for 300 min, can be seen in Fig. 3b. A comparison of the oxygen and the nitrogen signal suggests that the oxide scale is in the range of 400 to 500 nm thick, which is consistent with Fig. 1. In the oxide layer, the elemental distribution differs significantly from that in the nitride coating. At the surface, the Al concentration is significantly increased, which indicates an Al-rich top-layer with almost no detected concentration of Ta and Ti. The results also suggest the existence of an Al-depleted sub-layer. In this zone, a slight enrichment of Ti and Ta with respect to the nitride coating can be detected. The observed stronger increase of Ta near the oxide-nitride interface might be related to the overlapping of Ta and Si peaks in the EDX spectrum. Since Si is the substrate material of the investigated samples, the Ta content might be influenced by Si and thus, overestimated.

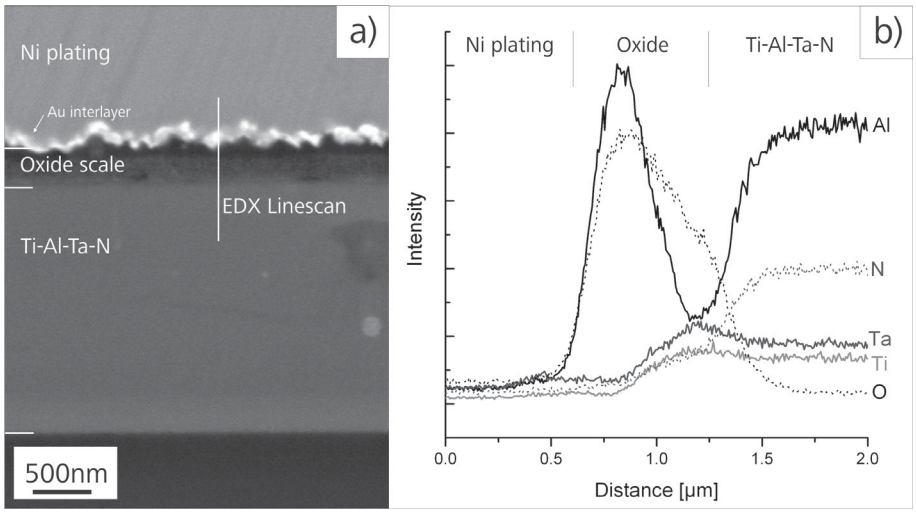

Figure 5.3.: a) Back scattered SEM cross-section of Ti-Al-Ta-N oxidized at 900°C for 300 min, b) SEM-EDX line scan over the oxide scale.

In order to get a deeper insight on the distribution of the elements in the oxide scale, SIMS investigations were conducted. The depth profile of oxidized Ti-Al-Ta-N can be seen in Fig. 5.4. The measurements were conducted in the negative secondary ion mode, which allows the detection of negatively charged molecules like TiO, AlO, TaO or N-compounds. Fig. 5.4 displays the intensity (logarithmic scale) for selected ions vs. sputter time. After 450 to 500 sec, the oxide scale is sputtered through and the nitride coating is reached. This

can be seen by a significant increase in AlN and TaN, accompanied by a decrease of the O-containing ions. After 2200 - 2300 s the interface to the Si substrate is reached, which can be seen in a dramatic drop for the nitrides and rise of the Si signals. Si also exhibits an increased content in the region of the oxide-nitride interface, but is not detected at the surface.

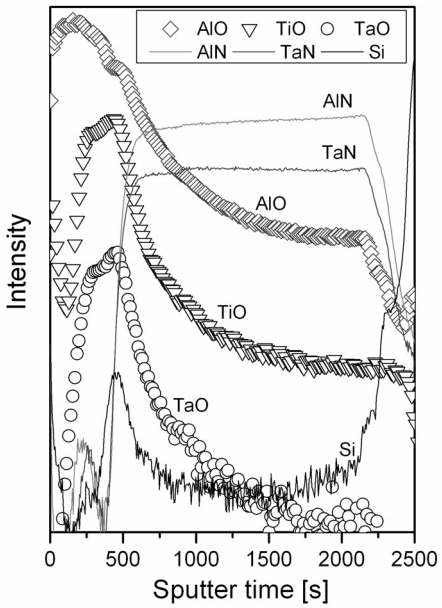

Figure 5.4.: SIMS depth profile (negative secondary ion mode, logarithmic intensity scale) of Ti-Al-Ta-N oxidized at 900°C for 300 min.

The AlO signal reaches a maximum close to the surface of the sample, while the content of TiO and TaO is found highest in an underlying sub-layer from which it decreases significantly towards the surface for both compounds.

Fig. 5.5 displays SIMS depth profiles of Ti-Al-Ta-N coatings in the as deposited and the oxidized state. The investigations were conducted in positive secondary ion mode, thus positive secondary ions are detected. For clarity, the spectra of the individual elements are shifted vertically, thus differences concerning intensity are of no significance. The higher noise level of the Si and the Ta signal is due to the generally lower content and the logarithmic scale. In the as deposited state, all elements are homogeneously distributed in the film. The increased Ti content at high sputter times (around 2600 sec) is caused by the TiN interlayer, which is deposited prior to the deposition of the Ti-Al-Ta-N layer.

After oxidation, the Al content at the top of the sample is maintained while Ti and in particular Ta are found depleted at the surface. Al shows a zone of reduced content

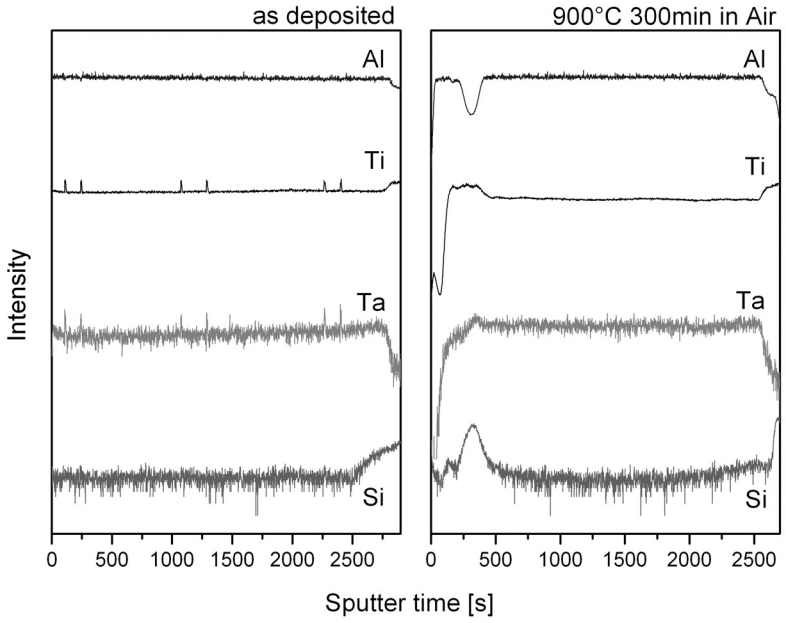

Figure 5.5.: SIMS depth profile (positive secondary ion mode, logarithmic intensity scale) of Ti-Al-Ta-N as deposited and oxidized at 900°C for 300 min.

underneath the Al-rich top-layer. This zone of reduced Al content coincides with a region of Ti enrichment. Within this zone of Ti enrichment, the Ta content decreases slightly towards the surface. Once the Al-rich top-layer is reached, Ta disappears completely.

Summarizing the results of SEM-EDX profiles and SIMS investigations, it can be concluded that the oxide scale of Ti-Al-Ta-N consists of an Al-rich top-layer and a Ti-rich sub-layer. Ta is only detected in the Ti-rich sub-layer. None of the methods used showed a significant content of Ta in the surface-near Al-rich layer. Considering the logarithmic scale and the small number of counts detected for Si in general, the Si peak at the interface between nitride and oxide is of minor importance and this increased Si content is too low to explain the improved oxidation resistance. Moreover, since the TiN diffusion barrier between Si and the nitride coating was found to be intact after the oxidation, the most probable origin is diffusion on fast paths by droplet generated voids. EDX analyses of polished cross-sections have been done at positions where large droplets were found near the nitride-substrate interface. The results revealed a significantly higher Si content around these droplets and within the cauliflower-like coatings structures grown on top of these initial droplets. Thus it is possible that Si can diffuse quickly along the voids to the surface in early stages of the oxidation experiment. A similar effect has already been described for Co in arc evaporated TiAlN coatings on cemented carbide by Hörling et al.

[14].

The results of TEM investigations of Ti-Al-Ta-N oxidized at 900°C for 300 min are shown in Fig. 5.6. The bright field TEM (BF-TEM, Fig. 5.6a) shows an overview of the oxidized coating. Furthermore, the positions of further investigations (Figs 5.6b-d) are marked. Fig. 5.6a confirms the suspected thickness of the oxide scale in the range of 400 nm. Furthermore it can be seen, that the oxide scale appears in a dense layer on top and a less dense, porous structure at the interface between oxide and nitride coating. Scanning TEM (STEM) in connection with qualitative, high spatial resolution EDX data, using a spot of around 1 nm diameter, confirmed the results concerning the distribution of the elements mentioned above. In addition, within the oxide scale three different zones or layers can be distinguished in the high-angle annular darkfield (HAADF) image (Fig. 5.6b). First, the Al-rich top-layer without detectable amount of Ta, which appears as dense. Second, the underlying Ti-rich layer with a remarkable Ta content can be found. This Ti-Ta-rich sub-layer can be subdivided into a compact and dense layer at the interface to the Al-rich top-layer and a porous zone at the nitride-oxide interface.

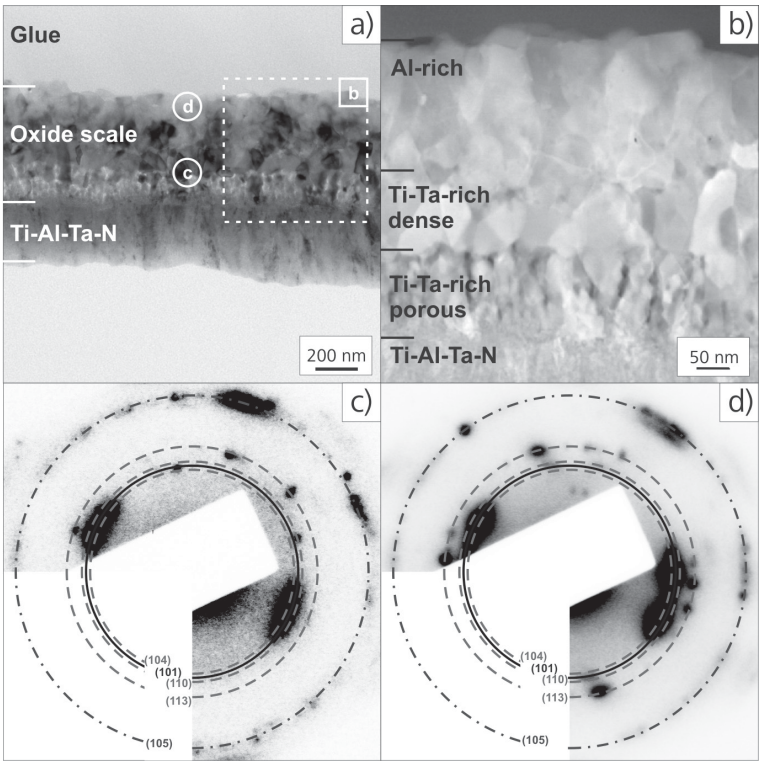

Figure 5.6.: (a) BF-TEM overview, (b) higher magnification HAADF-STEM image of a Ti-Al-Ta-N coating oxidized at 900°C for 300 min and SAED patterns of (c) Ti-Ta rich sub-layer and (d) Al-rich top-layer (dashed lines give positions of α-Al_2O_3, solid line of rutile TiO_2 and dash-dot line of anatase TiO_2.

Furthermore, the EDX measurements, using a small spot, suggest a slightly higher Ta

content in the porous zone in comparison to the dense Ti-rich zone. This is consistent with the SIMS results mentioned earlier (compare Fig. 5.5). The selected area electron diffraction (SAED) patterns were taken at similar regions as indicated in Fig. 5.6a. The pattern of the Ti-rich sub-layer (Fig. 5.6c) shows the existence of (101) rutile-type (solid line) as well as (105) anatase-type TiO_2 (dash-dotted line). In addition, (11-23) and (11-20) corundum-type α-Al_2O_3 (dashed lines) were identified. Due to overlapping positions of (101) planes of rutile and α-Al_2O_3, the presence of (10-14) planes of α-Al_2O_3 can not be excluded. The SAED pattern of the Al-rich layer (Fig. 5.6d) shows increased intensity of (11-23) planes of α-Al_2O_3. In comparison to Fig. 5.6c, another broad spot is detected which is most probably (10-14) α-Al_2O_3. Anatase and rutile can also be identified similarly to Fig. 5.6c. These results are consistent with the observations concerning the chemical composition, which predict a higher content of Al-based oxides in the surface near top-layer.

In both patterns, no signs of Ta-based oxides like Ta_2O_5 can be detected. Since Ta is in the oxide layer only detected in connection with Ti, the formation of a solid solution of Ta in TiO_2, forming a (Ta, Ti)O_2 phase is suggested, where Ta substitutes for Ti in the rutile lattice. The formed oxide is then referred to as Strueverite or tantalian rutile. Even if the conditions of the oxide formation might be different, the existence of this mineral in nature indicates the possibility of Ta being incorporated into rutile [15,16]. Strueverite exhibits the same crystal lattice and the same space group (P42/mnm) as rutile (compare JCPDS 01-081-0912, $TiTaO_4$). However, taking the low Ta content into account, the incorporation of Ta should cause only a moderate peak shift in comparison to pure rutile which is not detectable by XRD or SAED.

4. Disucssion

The oxidation behaviour of TiAlN coatings is well investigated and reported in literature. According to McIntyre et al. [10], the oxide scale consists of a double layered structure, i.e. an Al-rich top-layer and a Ti-rich sub-layer below. Similar results were also published by Ichmura et al. [17]. According to Hofmann, the formation of the Al_2O_3 top-layer can be explained by its higher oxide formation free enthalpy [18]. McIntyre et al. attributed the superior oxidation resistance compared to TiN to the upper, dense Al_2O_3 layer, which is expected to hinder the in-diffusion of oxygen [10]. Furthermore, it was reported that the mobile species are Al and O, whereas a limited mobility was detected for Ti. Thus, it was concluded that the oxide scale grows by simultaneous outward diffusion of Al towards the oxide/air interface and inward diffusion of O to the oxide/nitride interface where Ti is oxidized. At temperatures exceeding 800°C, the O transport through the Al-rich oxide

is the rate limiting step. After oxidation at 900°C for 40 min, the surface was found to be covered with small crystals which were identified as rutile type TiO_2. The formation of these rutile crystals is postponed if a negative bias voltage is applied [10].

Vaz et al. reported on thermal oxidation of TiAlN with various Al/Ti ratios. They found that with increasing Al content the thickness of the oxide layer, formed at 900°C, decreases. The increase of the TiO_2 sub-layer thickness during the oxidation process is accompanied by the development of compressive stress due to large differences of the molar volume between TiO_2 and TiN. These stresses might lead to cracking of the protective Al-rich top-layer and consequently accelerate degradation of the oxidation behaviour. With increasing Al content, the Ti-rich sub-layer was found to grow slower which led to reduced compressive stresses. Thus, the authors attributed the better performance of Al-rich coatings to the slower growth of the Ti-rich sub-layer and not exclusively to the growing Al-rich top-layer. Furthermore, Vaz et al. reported that the oxidation behaviour deteriorates at very high Al contents and becomes similar to that of hexagonal AlN. The critical concentration coincides with the transition from the fcc to the wurzite structure, i.e. the appearance of hcp phases [19].

Consequently, it can be summarized that the failure of TiAlN coatings due to oxidation is probably related to the formation of rutile in the lower Ti-rich sub-layer of the oxide scale. This rutile formation is connected with the generation of compressive stresses, which might crack the dense and protective Al-rich top-layer, leading to intensified oxidation and finally failure of the coating.

Alloying elements like Y have shown the ability to significantly improve the resistance to oxidation of TiAlN. Lembke et al. reported that the benefit of Y is connected with its preferential diffusion to the column boundaries where it blocks diffusion paths [4]. According to Rovere et al., Y can act as a reactive element and provide additional sites for heterogeneous nucleation of the oxide scale, which consequently accelerates the formation of stable α-Al_2O_3 and might be one of the reasons for the outstanding oxidation resistance of CrAlYN [11]. Very recently, reports on the influence of Si or B doping on the oxidation resistance of TiAlN were published [6]. B and Si are reported to modify the oxidation sequence of Ti, which is suspected to lead to a slower formation of rutile in the coating. It was concluded that the thus slower accumulation of harmful compressive stresses in the Ti-rich sub-layer leads to the improved oxidation behaviour.

Reddy et al. published results on oxidation of a ternary TiAlTa alloy. They mentioned that the free energy of formation of Ta_2O_5 is lowest compared to Al_2O_3 and TiO_2 [20] which questions the ability of Ta to act similar to Y, as described by Rovere et al. [11]. However, Reddy et al. reported that the addition of Ta to TiAl leads to increased resistance to oxidation. It was suspected that Ta might favour the formation of α-Al_2O_3.

Furthermore, Ta^{5+} might dope the TiO_2 lattice which decreases the number of oxygen vacancies and/or titanium interstitials in the TiO_2 lattice [20]. Similar effects have already been described for Nb by Leyens where Nb influences the mass transport in TiO_2 by reducing the oxygen vacancy concentration [21]. Ta exhibits the same valency as Nb (5+) and, as mentioned before, a significant solubility of Ta in rutile is likely [15,16]. Thus, Ta might hinder the O mass transport in TiO_2 by doping the TiO_2 lattice and reducing the concentration of oxygen vacancies. This is also supported by our results, where Ta is mainly found in regions where Ti is present as well. According to McIntyre et al., O transport to the oxide-nitride interface is the rate limiting step in the investigated temperature range [10]. Thus, Ta might hinder the O-mass transport in rutile, leading to decreased oxidation of Ti at the oxide-nitride interface and thus a slower formation of rutile. The slower formation of rutile would result in a slower accumulation of compressive stresses, which could crack the protective α-Al_2O_3 top layer. Thus, the protective integrity of the oxide scale can be maintained longer, compared to unalloyed TiAlN, leading to the higher resistance of Ti-Al-Ta-N coatings against oxidation.

In addition, we have already shown that the alloying of TiAlN with Ta leads to a stabilisation of the fcc phase to the expense of hcp phases [9] According to Vaz et al., a decreased content of hcp phase should also contribute to an improved resistance to oxidation [19]. Our findings are in good agreement with results reported in literature since the oxide scale consists of an Al-rich top-layer and a Ti-rich sub-layer. However, the alloying element Ta is not present in both layers in the oxide scale, but only in the Ti-rich sub-layer detectable. To the authors best knowledge, improved oxidation resistance of TiAlN based coatings by modification of the rutile-type sub-layer represents a new approach and is previously unpublished. The origin of the porous oxide layer between nitride and the dense upper oxide layers (see Fig. 5.6b) could not be clarified unambiguously. One possibility is that contrary to the in-diffusion of oxygen, the out-diffusion of metallic ions, i.e. Al ions is not hindered. Thus, the outward flux would be larger than the inward flux which would necessarily lead to the formation of pores and/or voids. However, further investigations are necessary, to explain the formation of the porous zone in detail.

5. Conclusion

Ti-Al-Ta-N coatings, deposited by cathodic arc evaporation, exhibit a significantly higher resistance to oxidation in comparison to TiAlN. The thickness of the oxide scale after oxidation treatment was found to be decreased by a factor of up to 8. The oxide scale of an oxidized Ti-Al-Ta-N coating contains α-Al_2O_3 as well as rutile- and anatase-type

TiO_2, but no evidence of Ta-based oxides were found. Furthermore, the oxide scale was found to consist of an Al-rich top-layer without detectable amounts of Ta. Underneath, a Ti-Ta-rich sub-layer was detected, suggesting that Ta is incorporated in the TiO_2 lattice. The Ti-Ta-rich sub-layer exhibits a dense structure at the interface to the Al-rich layer but was found to be porous at the interface to the nitride coating. The improved oxidation resistance is explained by doping of rutile-type TiO_2 with Ta^{5+} which reduces the amount of O-vacancies and thus the mass transport of O in rutile to the oxide-nitride interface. The slower oxidation of Ti leads to the excellent oxidation behaviour of this type of coatings. This is the reason for the improved performance of Ti-Al-Ta-N coatings in cutting applications.

Acknowledgments

Financial support by the Austrian Federal Government and the Styrian Provincial Government under the frame of the Austrian COMET Competence Centre Program is gratefully acknowledged.

M. Pfeiler is grateful to Mr. Florian Rovere (University of Leoben) for valuable discussions on reactive element effects and Dr. Gerardo Fontalvo (University of Leoben) for helpful discussions. Furthermore, the technical assistance of Steffen Schmidt for TEM investigations is gratefully acknowledged.

References

[1] O. Knotek, W.-D. Münz, T. Leyendecker, J. Vac. Sci. Technol. A 5 (4) 1987 2173-2179.
[2] P.H. Mayrhofer, A. Hörling, L. Karlsson, J. Sjölen, T. Larsson, C. Mitterer, L. Hultman, Appl. Phys. Lett. 83 (10) (2003) 2049-2051.
[3] F. Vaz, L. Rebouta, M. Andritschky, M.F. da Silva, J.C. Soares, Surf. Coat. Technol. 98 (1998) 912-917.
[4] M.I. Lembke, D.B. Lewis, W.-D. Münz, J.M. Titchmarsh, Surf. Eng., 17 (2) (2001) 153-158.
[5] S. Veprek, H.-D. Männling, M. Jilek, P. Holubar, Mater. Sci. Eng. A366 (2004) 202-205.
[6] M. Pfeiler, J. Zechner, M. Penoy, C. Michotte, C. Mitterer, M. Kathrein, Surf. Coat. Technol. 2008, in submission.
[7] M. Kathrein, C. Michotte, M. Penoy, P. Polcik, C. Mitterer, Surf. Coat. Technol. 200 (2005) 1867-1871.
[8] K. Kutschej, P.H. Mayrhofer, M. Kathrein, C. Michotte, P. Polcik, C. Mitterer, in: Kneringer, G., Roedhammer, P., Wildner, H. (eds.) Proceedings of the 16th International Plansee Seminar 2005, vol. 2, pp. 774-788. Plansee Holding AG, Reutte, Tyrol, Austria (2005).
[9] M. Pfeiler, G.A. Fontalvo, J. Wagner, K. Kutschej, M. Penoy, C. Michotte, C. Mitterer, M. Kathrein, Tribol. Lett. 30 (2) (2008) 91-97.
[10] D. McIntyre, J.E. Greene, G. Hakansson, J.-E. Sundgren, W.-D. Münz, J. Appl. Phys. 67 (3) (1990)

1542-1553.
[11] F. Rovere, P.H. Mayrhofer, A. Reinholdt, J. Mayer, J.M. Schneider, Surf. Coat. Technol. 202 (24) (2008) 5870-5875.
[12] P. Steyer, D. Pilloud, J.F. Pierson, J.-P. Millet, M. Charnay, B. Stauder, P. Jacquot, Surf. Coat. Technol. 201 (2006) 4158-4162.
[13] J. Schnöller, R. Wiesinger, C. Kleber, U. Hilfrich, M. Schreiner, H. Hutter, J. Anal. Bioanal. Chem., 390(6), (2008) 1543-1549.
[14] A. Hörling, L. Hultman, M. Oden, J. Sjölen, L. Karlsson, J. Vac. Sci. Technol. A 20 (5) (2002) 1815-1823.
[15] P. Cerny, M. Novak, R. Chapman, Mineral Petrol 52 (1-2) (1995) 61-73.
[16] A.K. Rub, M. Stemprok, M.G. Rub, Mineral Petrol 63 (3-4) (1999) 199-222.
[17] H. Ichimura, A. Kawana, J. Mater. Res. 8 (5) (1993) 1093-1100.
[18] S. Hofmann, Thin Solid Films, 193-194 (1990) 648-664.
[19] F. Vaz, L. Rebouta, M. Andritschky, M.F. da Silva, J.C. Soares, J. Europ. Cer. Soc. 17 (1997) 1971-1977.
[20] R.G. Reddy, Y. Li, M.F. Arenas, High Temperature Materials and Processes 21 (4) (2002) 195-205.
[21] C. Leyens, Oxidation behaviour of titanium alloys and titanium aluminides, in Titanium and Titanium Alloys, C. Leyens, M. Peters, Editors, Wiley-VCH (2003) 207-209.

Publication VI

Concept for potential publication

Wavelength modulation of TiAlN - Ti-Al-V-N multilayers by various substrate rotation speeds

by

M. Pfeiler, P.H. Mayrhofer, K. Kutschej, M. Penoy, C. Michotte, C. Mitterer, M. Kathrein

1. Introduction

Ti-Al-V-N has been recently introduced as a possible candidate for further development of TiAlN based hard coatings. The incorporation of V as TiN/VN multilayer or Ti-Al-V-N coating can lead to potential low friction and enhanced wear behaviour [1-3]. Additionally, it has been shown that V as a substitutional atom in the TiAlN solid solution has an fcc stabilizing effect, which can increase coating hardness and Young's modulus [4,5] Also the suppressing of hcp phase in the Ti-Al-V-N system by increased bias voltage can significantly improve the mechanical properties [6]. Multilayered structures were intensively investigated and hardness enhancement of up to 25 GPa was initially reported in TiN/VN superlattices. As the wavelength of the multilayer was decreased, the hardness increased with a maximum hardness at a wavelength of roughly 10 nm [7]. The hardening effect was attributed to the so-called superlattice effect and is based on differences in the shear modulus between the individual layer materials leading to differences in the dislocation line energy. Increasing hardness with decreasing multilayer period was also observed by Li et al. [8]. Long et al. [9] reported recently that this superlattice effect is not generally observed. Huge hardness enhancements of up to 25 GPa are not consistent with the idea of increased dislocation line energy. Consequently, no significant variation of hardness

with the wavelength of the multilayer has been found. However, a smaller increase of ∼5 GPa might be observed and connected with differences in shear modulus. Ljungcrantz et al. [10] reported on nanoindentation and abrasive wear tests of TiN/NbN multilayers with various wavelengths of multilayers. No significant influence on hardness and wear resistance was observed. Hardness and wear of the multilayer was in between the values of the single layer materials. Furthermore, it has been shown that multilayered coatings can also show the effect of epitaxial stabilization of phases. This so-called template effect enables the stabilization of fcc AlN by a fcc template layer, although hcp AlN is thermodynamically favoured and fcc AlN is normally unstable at pressures below 22 bar [11]. Similar observations are also reported by other authors [12,13]. The aim of the present work was to deposit TiAlN / Ti-Al-V-N multilayers with various multilayer wavelengths by an industrial scale cathodic arc evaporation process. The multilayer wavelength was modulated by changing the rotation speed of the substrate carousel. Here we report on the hardness increase from Ti-Al-V-N single layers to TiAlN / Ti-Al-V-N multilayers, where in particular we concentrate on the fcc stabilizing effect by the use of $Ti_{50}Al_{50}N$ as a fcc template and its influence on the resulting mechanical and tribological properties by suppressing the hcp phase. Furthermore, the influence of multilayer wavelength on hardness and wear resistance was investigated.

2. Experimental details

An industrial scale cathodic arc evaporation facility, type Oerlikon Balzers RCS, was used to deposit the coatings. Powder metallurgically produced targets with compositions (in at.%) $Ti_{16.5}Al_{67}V_{16.5}$ and $Ti_{50}Al_{50}$ were used to deposit multilayered coatings. Due to the use of two Ti-Al-V and two TiAl targets and the substrate rotation, coatings with compositional modulations could be synthesized. The multilayer was toped with a 150 nm thick, decorative TiN layer. The deposition runs were conducted at four different rotation speeds between 0.75 and 3 rev/min, resulting in different multilayer wavelengths, in pure N_2 atmosphere at a pressure of 3.2×10^{-2} mbar. The bias voltage was -40 V for all runs. For comparison, $Ti_{16.5}Al_{67}V_{16.5}N$ single layer coatings were deposited at -40 V and -120 V bias voltage, respectively. The coatings were deposited onto cemented carbide (CC) SNUN cutting inserts, CC discs (Ø 30 × 4 mm) and single-crystal silicon (100) samples. The SNUN samples were used for glancing angle X-ray diffraction (GAXRD) and for nanoindentation. Tribological tests were performed on CC discs whereas for transmission electron microscopy (TEM) investigations single-crystal silicon (100) samples (21 × 7 × 0.38 mm) were used. Crystallographic investigations were performed by GAXRD (Panalytical X´Pert Pro) applying Cu Kα radiation at an angle of incidence of 2°. Hardness

and Young's modulus of the coatings were assessed by nanoindentation using a UMIS ultra micro indentation system with a Berkovich indenter. Due to high surface roughness, the samples were polished for 5 min with 1 μm diamond suspension prior to the measurement. To evaluate hardness and Young's modulus, correction of compliance, initial penetration and contact area were applied to the raw data. The tribological behaviour was investigated by dry sliding tests at room temperature, 500 and 700°C on a CSM high-temperature ball-on-disc tribometer. The normal load, sliding speed, pre-heating time, sliding distance, and radius of wear track were kept constant at 5 N, 10 cm/s, 90 min, 300 m, and 7 mm, respectively. All tests were performed in ambient atmosphere at a relative humidity of 35 $\pm$ 5% against an alumina ball (Ø 6 mm). The resulting wear tracks were investigated using a 3D profiling system (Wyco NT1000 white light profilometer). Transmission electron microscopy (TEM) and selected area electron diffraction (SAED) investigations were conducted using a Philips CM12 facility, operated at 120 keV. The samples were prepared by cross-sectional tripod polishing followed by Ar-ion milling using a Gatan PIPS 691 device.

3. Results and Discussion

The results of the XRD investigations can be seen in Fig. 6.1. The pattern on the bottom is the Ti-Al-V-N single layer deposited at -40 V bias. This coating exhibits a dual phase structure and contains both fcc and hcp crystals. Due to the incorporation of Al and V in the lattice, the fcc peaks of the Ti-Al-V-N phase are shifted towards higher angles of 2Θ, while hcp peaks are shifted to lower angles. By raising the bias voltage up to -120 V, the coating can be deposited as a single phase fcc structure (see Fig. 6.1). Thus, increasing the bias voltage hinders the formation of hcp phases and promotes a single phase fcc structure, which has been already reported earlier [6]. The upper three patterns in Fig. 6.1 show the TiAlN / Ti-Al-V-N multilayer coatings deposited at various rotation speeds of the substrate carousel. In none of the patterns, hcp phases can be detected. Thus, the TiAlN layer acts as a fcc template, which enables growth of a single phase Ti-Al-V-N layer at low bias voltages due to epitaxial stabilization of the fcc crystals as mentioned above. The TiN top-layer is also detected in the XRD pattern and appears at TiN standard positions. Due to the topmost position of the TiN-layer and the glancing angle measurements, the TiN phase appears dominant with respect to intensity. As mentioned before, the underlying multilayer of TiAlN and Ti-Al-V-N is shifted from the fcc TiN standard positions due to incorporation of the alloying elements, resulting is a reduced lattice parameter. The variation of rotation speed does not have a significant influence on the crystal structure. This indicates that the fcc stabilizing effect of the TiAlN layer is

also working for the lowest rotation speed which causes the highest multilayer wavelength.

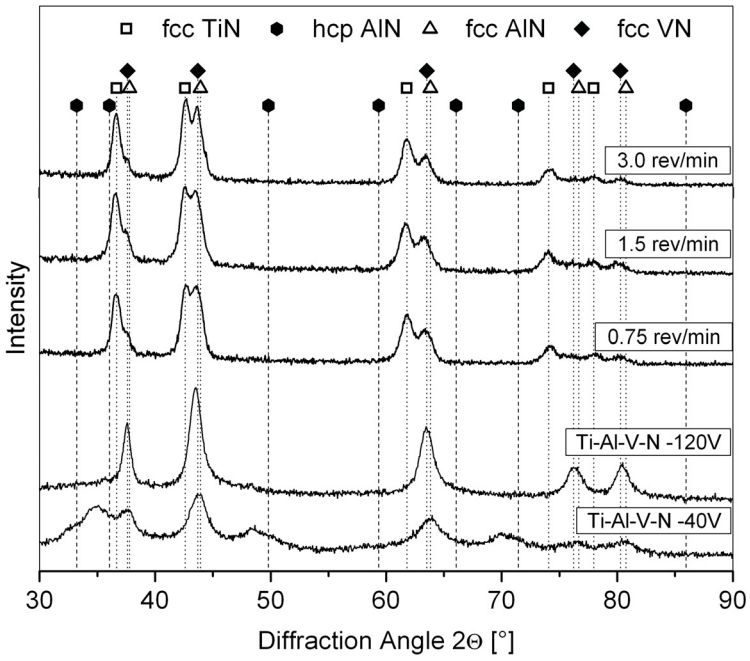

Figure 6.1.: XRD patterns of Ti-Al-V-N single layers deposited at -40 and -120 V bias voltage and TiAlN / Ti-Al-V-N multilayers deposited at -40 V and various rotation speeds.

In order to support the XRD investigations, TEM investigations were conducted. The TEM investigations revealed a good correlation between the rotation speed of the substrate carrousel and the resulting multilayer wavelength. The lowest rotation speed of 0.75 rev/min resulted in a multilayer wavelength of 40 - 45 nm (Fig. 6.2a). The additional layers within the layered structure are caused by the double rotation of the substrate carousel. The standard rotation speed of 1.5 rev/min resulted in 19 - 25 nm multilayer wavelength (Fig. 6.2b) and the highest rotation speed (3 rev/min) yielded a periodicity in the range of 10 nm (Fig 6.2c). However, due to the compositional similarity, the phase contrast between the two layers is not pronounced, making it rather difficult to distinguish between TiAlN and Ti-Al-V-N layers. Nevertheless, brighter and darker layers are observable. Therefore, to guide the eye the periodicity of the multilayer was marked in Fig. 6.2 by black lines.

The SAED pattern of the multilayer deposited at the lowest rotation speed can be seen in Fig. 6.3. All rings were identified as fcc rings of the NaCl structure of TiN. No intensities indicative for hexagonal phases were detected. Thus, the SAED pattern support the XRD results shown in Fig. 6.1, confirming the stabilization of the fcc Ti-Al-

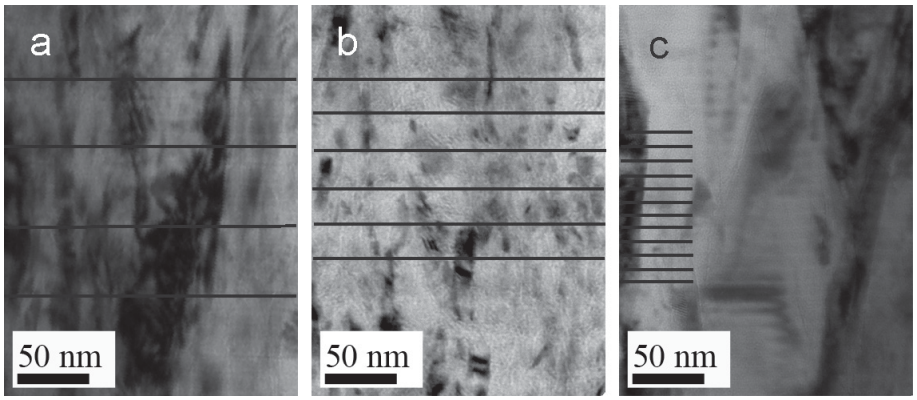

Figure 6.2.: TEM bright field cross sectional images of TiAlN / Ti-Al-V-N multilayers grown at a bias voltage of -40 V and various rotation speeds a) 0.75 rev/min, b) 1.5 rev/min, c) 3rev/min.

V-N phase by use of a fcc TiAlN template also at the rather high multilayer wavelength of 40-45 nm.

The results of nanoindentation of TiAlN / Ti-Al-V-N multilayers grown with various wavelengths are shown in Fig. 6.4. Prior to the nanoindentation tests, the TiN top-layer was removed by polishing with a 1 μm diamond suspension. The values for the multilayers are given together with the values for the single layer Ti-Al-V-N coating deposited at -40 V, which shows a dual phase fcc+hcp structure and the single fcc phase film grown at -120 V (see Fig. 6.1). The hardness and Young's modulus is highest for the multilayers but there is only little influence of wavelength on the hardness values. All four rotation speeds lead to comparable mechanical properties. The measured hardness and Young´s modulus values for the multilayers are significantly increased compared to the single layer deposited at -40 V, but similar to the single layer grown at -120 V. Thus, in comparison to the -40 V coatings, the increased bias voltage levels the multilayer effect on hardness and modulus. This suggests that an important effect of the hardness enhancement for dual phase fcc+hcp structures is the suppressing of the formation of the hcp phase. This is in good agreement by results published in literature [14-17]. For the single layer, a second important contribution is the higher residual compressive stress, which is also known to increase hardness [18]. This means that for the multilayers (deposited at -40 V) another contribution for the hardness enhancement must be present. The higher amount of interfaces and grain boundaries caused by the interrupted growth due to nucleation of the second layer might be a suitable origin of the higher hardness [19].

The wear coefficient determined by ball-on-disc testing against alumina balls at room temperature, 500 and 700°C can be seen in Fig. 6.5. For these tribological tests, the TiN toplayer was not removed, but is not expected to play a dominant role under the selected wear conditions. For all test conditions, abrasive wear, i.e. loss of coating material, was

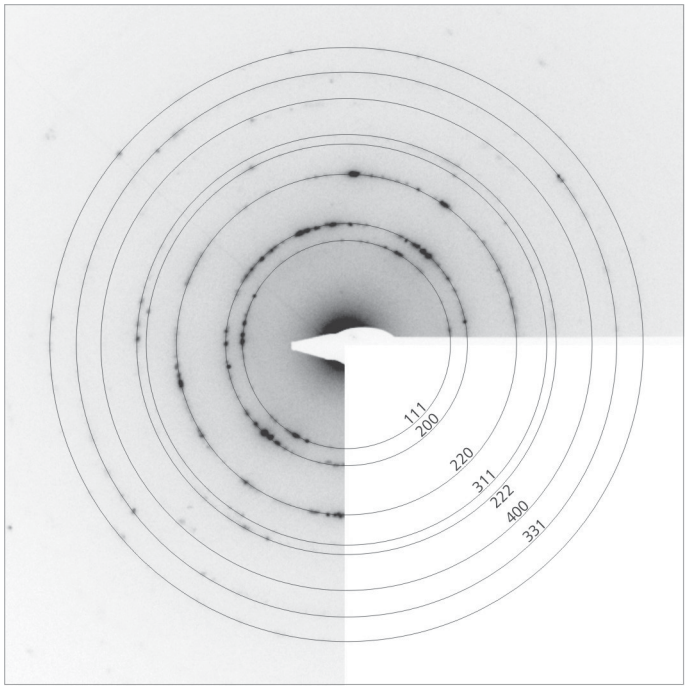

Figure 6.3.: SAED pattern of the TiAlN / Ti-Al-V-N multilayer grown at a bias voltage of -40 V and a rotation speed of 0.75 rev/min.

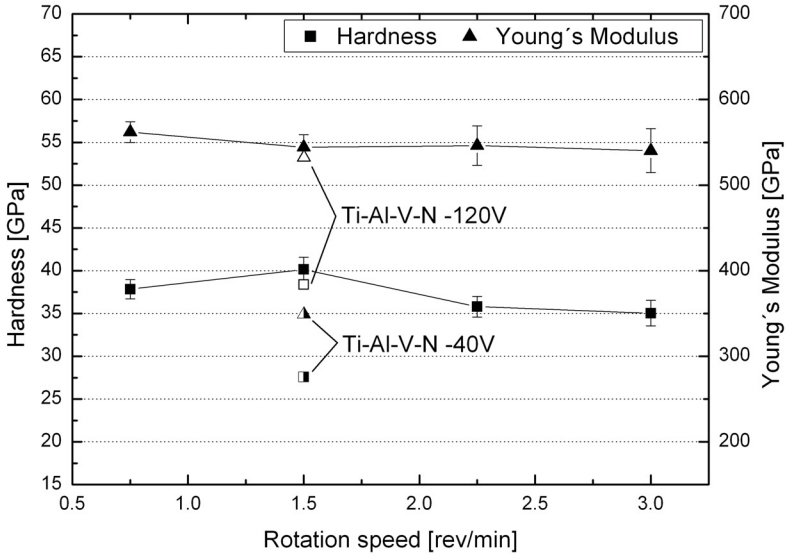

Figure 6.4.: Hardness and Young´s modulus of TiAlN / Ti-Al-V-N multilayers grown with various wavelengths at a bias voltage of -40V (black symbols). For comparison values for Ti-Al-V-N single layer coatings grown at 1.5 rev/min at -40V and -120V bias respectively are given.

dominating. At room temperature, the results are independent from the wavelength of the multilayers, especially if the large error bars are considered. That suggests that mainly the chemical composition and the hardness determines the tribological behaviour and not the layered structure. This is supported by recent publications which indicate that wear of TiAlN based hard coatings at room temperature is governed by the tribo-chemical oxidation of Ti to the rutile modification of TiO_2 [4, 20].

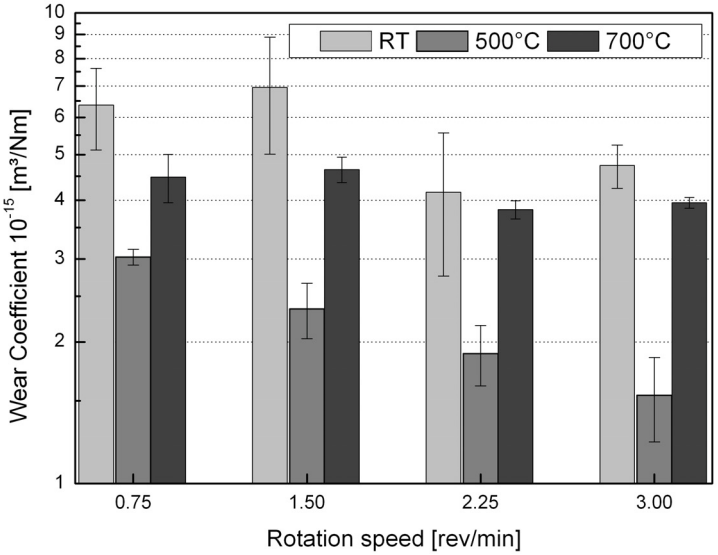

Figure 6.5.: Wear coefficients of ball on disc sliding test of TiAlN / Ti-Al-V-N multilayers at RT, 500°C and 700°C.

At 500°C, a clear trend towards reduced wear with higher rotation speeds can be seen (6.5). The abrasive wear coefficient decreases with increasing rotation speed from 3 to 1.5×10^{-15} m^3/Nm. The wear behaviour at elevated temperatures is controlled by the coatings' resistance to high temperature oxidation. V-containing coatings start to oxidize between 520 and 550°C [2,21], which is accompanied by out-diffusion of V and formation of V-oxides. These temperatures can easily be reached in the tribological contact due to frictional heating and local flash temperatures. Thus, the oxidation of V during tests at 500°C can be assumed. The formed oxides are neither protective nor lubricating and might be easily removed by the sliding ball. This exposes unoxidized material to the atmosphere again and causes further oxidation and wear. If the V-containing layers are separated by TiAlN layers in the multilayer architecture, the out-diffusion of V might be hindered and the wear process proceeds slower. A higher rotation speed during deposition leads to more diffusion barriers, which block out-diffusion more efficiently, thus reducing the wear

coefficient. At 700°C, the wear rate is again independent from the rotation speed (see Fig. 6.5). This could be explained by the strong and fast diffusion and oxidation of V at this temperature, which cannot be hindered efficiently by the TiAlN layers. Furthermore, due to the frictional heat the TiAlN layer might also start to oxidize since the onset of oxidation for TiAlN is between 700 and 800°C [22]. However, in comparison to single layer coatings, the multilayers survived the tribological test, which can also be attributed to the TiAlN template layers acting as diffusion barrier.

4. Conclusion

TiAlN / Ti-Al-V-N multilayered coatings were grown on cemented carbide and silicon (100) substrates by cathodic arc evaporation. The wavelength of the multilayer was modified by varying the rotation speed of the substrate carousel during deposition. The use of a fcc TiAlN template enables the epitaxial fcc stabilization of the originally dual phase fcc+hcp Ti-Al-V-N structure. The stabilization effect can be realised up to high multilayer wavelengths exceeding 40 nm. This leads to improved hardness and Young´s modulus due to hindered formation of hcp phases, without the necessity of high bias voltages. The mechanical properties were found to be independent of the substrate rotation speed. Wear at room temperature was found unaffected by the varied multilayer wavelength. The wear at 500°C was improved with increasing rotation speed, which is connected with a higher amount of TiAlN layers acting as diffusion barrier for the harmful V out-diffusion. This barrier function is also found at 700°C, although at a reduced scale and independent from the multilayer wavelength. The results show that the application of a fcc template layer leads to a significant improvement of the properties of Ti-Al-V-N coatings, without necessarily applying high bias voltages and thus creating high compressive stresses.

Acknowledgments

Financial support by the Austrian Federal Government and the Styrian Provincial Government under the frame of the Austrian COMET Competence Centre Program is gratefully acknowledged.

References

[1] K. Kutschej, P.H. Mayrhofer, M. Kathrein, P. Polcik, C. Mitterer, Surf. Coat. Technol. 188-189 (2004) 358-363.
[2] P.H. Mayrhofer, P.Eh. Hovsepian, C. Mitterer, W.-D. Münz, Surf. Coat. Technol. 177-178 (2004)

341-347.
[3] M. Kathrein, C. Michotte, M. Penoy, P. Polcik, C. Mitterer, Surf. Coat. Technol. 200 (2005) 1867-1871.
[4] M. Pfeiler, K. Kutschej, M. Penoy, C. Michotte, C. Mitterer, M. Kathrein, Int. J. Refract. Met. Hard Mater. (2008) doi:10.1016/j.ijrmhm.2008.06.008.
[5] P.H. Mayrhofer, D. Music, J.M. Schneider, J. Appl. Phys. 100 (2006) 1.
[6] M. Pfeiler, K. Kutschej, M. Penoy, C. Michotte, C. Mitterer, M. Kathrein, Surf. Coat. Technol. 202 (2007) 1050-1054.
[7] U. Helmersson, S. Todorova, S.A. Barnett, J.-E. Sundgren, L.C. Markert, J.E. Greene, J. Appl. Phys. 62 (2) (1987) 481-484.
[8] G. Li, J. Lao, J. Tian, Z. Han, M. Gu, J. Appl. Phys. 95 (1) (2004) 92-96.
[9] Y. Long, F. Giuliani, S.J. Lloyd, J. Molina-Aldareguia, Z.H. Barber, W.J. Clegg, Composites: Part B 37 (2006) 542-549.
[10] H. Ljungcrantz, C. Engström, L. Hultman, M. Olsson, X. Chu, M.S. Wong, W.D. Sproul, J. Vac. Sci. Technol. A 16 (5) (1998) 3104-3113.
[11] A. Madan, I.W. Kim, S.C. Cheng, P. Yashar, V.P. Dravid, S.A. Barnett, Phys. Rev. Lett. 78 (9) (1997) 1743-1746.
[12] G. Li, J. Lao, J. Tian, Z. Han, M. Gu, J. Appl. Phys. 95 (1) (2004) 92-96.
[13] Q. Li, I.W. Kim, S.A. Barnett, L.D. Marks, J. Mater. Res. 17 (5) (2002) 1224-1231.
[14] M. Zhou, Y. Makino, M. Nose, K. Nogi, Thin Solid Films 339 (1999) 203-208.
[15] A. Kimura, H. Hasegawa, K. Yamada, T. Suzuki, Surf. Coat. Technol. 120-121 (1999) 438-441.
[16] Y. Tanaka, T.M. G¨ur, M. Kelly, S.B. Hagstrom, T. Ikeda, K. Wakihira, H. Satoh, J. Vac. Sci. Technol. A 10 (4) 1749-1756.
[17] K. Kutschej, P.H. Mayrhofer, M. Kathrein, P. Polcik, R. Tessadri, C. Mitterer, Surf. Coat. Technol. 200 (2005) 2358-2365.
[18[P.H. Mayrhofer, F. Kunc, J. Musil, C. Mitterer, Thin Solid Films 415 (2002) 151-159.
[19] S. PalDey, S.C. Deevi, Mat. Sci. Eng. A342 (2003) 58-79.
[20] M. Pfeiler, G.A. Fontalvo, J. Wagner, K. Kutschej, M. Penoy, C. Michotte, C. Mitterer, M. Kathrein, Tribol. Lett. 30 (2) (2008) 91-97.
[21] G. Gassner, P.H. Mayrhofer, K. Kutschej, C. Mitterer, M. Kathrein, Tribol. Lett. 17 (2004) 751-756.
[22] O. Knotek, W.-D. Münz, T. Leyendecker, J. Vac. Sci. Technol. A 5 (4) (1987) 2173-2179.